Microbe radionuclides interactions, the implication in nuclear fuel storage pond management

A thesis submitted to the University of Manchester for the degree of

Doctor of Philosophy in the Faculty of Science and Engineering

2021

Kejing Zhang

School of Earth and Environmental Sciences

Content

List of Figures and Tables **4**
Abstract **9**
Declaration **10**
Copyright Statement **11**
Acknowledgements **12**
The Author **14**
Chapter 1 Project context and thesis structure **15**
1.1 Project context **15**
1.2 Thesis Structure. **16**
1.3 Author contributions **17**
Chapter 2 Introduction **19**
2.1 The Nuclear fuel cycle **21**
2.1.1 The fuel cycle 21
2. 1.2 First Generation Magnox Storage Pond (FGMSP) at Sellafield 25
2.2. Microorganisms in nuclear storage facilities **27**
2.2.1 Microbes in spent nuclear fuel ponds 27
2.2.2 Microbial diversity in FGMSP 28
2.3 Interactions of microorganisms and radionuclides **29**
2.3.1 Interaction between microbes from SNFPs and radionuclides 32
2.3.2 Interaction between microbes and Cs 34
2.4 Bloom control methods **35**
2.4.1 Nutrients Removal 36
2.4.2 Oxidation and Photocatalysts 36
2.4.3 Sonication, UV and Flushing 38
2.5. Potassium in Microorganisms **39**
2.5.1 Roles of potassium in bacteria 39
2.5.2 Potassium transport system 40
2.6 Aims and objectives **41**
2.6.1 Aims 42
2.6.2 Objectives 42
2.7 Reference **44**
Chapter 3 Methodology **56**
3.1 Measurement of *Pseudanabaena catenata* growth **56**
3.2 Cell morphology **57**

3.3 Scanning transmission X-ray microscope **57**
3.3.1 Description of STXM 57
3.3.2 Near Edge X-ray Absorption Fine Structure (NEXAFS) 58
3.4 Inductively coupled plasma mass spectrometry (ICP-MS) **61**
3.5 16S rRNA Gene Sequencing **61**
3.6 Molecular biology- Cell lysis, Protein Extraction, Identification and Quantification **63**
3.6.1 Cell lysis 63
3.6.2 Protein Extraction 64
3.6.3 Protein Identification and Quantitation 64
3.6.4 Workflow of proteomics study in this project 65
3.7 References **69**
Chapter 4 The interplay between Cs, K and the cyanobacterium *Pseudanabaena catenata*, the fate of Cs and its impact on cell growth and protein expression **72**
Abstract **72**
4.1 Introduction **73**
4.2 Materials and Methods **75**
4.2.1 Culturing of *P.catenata* 75
4.2.2 Growth measurement, cell morphology and water chemistry 76
4.2.3 Scanning transmission X-ray microscopy (STXM) 76
4.2.4 LC-MS sample preparation, protein identification and quantification 77
4.3 Results and Discussion **79**
4.3.1 Impact of Cs and K on cell growth and morphology 79
4.3.2 Fate of Cs in *P. catenata* culture 81
4.3.3 Impact of Cs and K on *P. catenata* protein expression 84
4.4 Conclusion **94**
4.5 References **96**
4.6 Appendix **104**
Chapter 5 KOH versus NaOH, the inhibited effect on the growth of cyanobacteria *Pseudanabaena catenata*: Implications for control of P. catenata dominated blooms in FGMS115
Abstract **115**
5.1 Introduction **117**
5.2 Materials and Methods **119**
5.2.1 Batch Culture Experiment 119
5.2.2 Chemostat Experiment 120
5.2.3 DNA extraction and 16S rRNA gene sequencing 120
5.2.4 Protein extraction, Identification and Quantification 122

5.3 Results **124**
5.3.1 The effect of KCl and NaCl on the Growth of *P. catenata* in Batch Culture 124
5.3.2 The effect of KOH and NaOH on the Growth of the *P. catenata* in a Chemostat System 126
5.4 Discussion **136**
5.5 Conclusion **140**
5.6 References. **141**
5.7 Appendix **148**
Chapter 6 Discussion **151**
Appendices **155**
A1 The fate of Sr in alkaline cultures of the cyanobacterium *Pseudanabaena catenata* **155**
Abstract **155**
A1.1 Introduction **156**
A1.2 Methods **159**
A.1.2.1 Culturing of *Pseudanabaena catenata* with Sr 159
A1.2.2 Optical density, chlorophyll-a concentration, and pH measurements 160
A1.2.3 Assessment of Sr behaviour 161
A 1.2.4 PHREEQC modelling 163
A1.3 Results **163**
A1.3.1 The effect of Sr on the growth of the *P. catenata* culture 163
A1.3.2 Sr removal from solution 165
A1.3.3 Sr saturation calculations 166
A1.3.4 Determining the fate of Sr in the *P. catenata* culture 166
A1.4 Discussion **172**
A1.5 References **176**

List of Figures and Tables

Chapter 2 Introduction.....19
Table 2.1 Legacy sites in the UK (NDA,2002) 21
Figure 2. 1 Nuclear fuel cycle from uranium mining to disposal (WNA, 2021).....24
Figure 2.2 Process of fuel fabrication (WNA, 2021).....25
Figure 2.3 Microbial community comparison of FGMSP samples based on 16S rRNA gene sequences, samples were collected between August 2014 and September 2017 (Foster *et al,* 2020) 30
Chapter 3 Methodology.....56
Figure 3.1 Schematic scanning x-ray transmission microscope (STXM) (Koprinarov and Hitchcock, 2000).....58
Figure 3.2 X-ray absorption edges of carbon, nitrogen and oxygen (Koprinarov and Hitchcock, 2000) 59
Figure 3.3 NEXAFS spectra of common polymers. PC, polycarbonate; PET, poly (ethylene terephthalate); PPTA, poly (p-phenylene terephthalamide); PAR, polyacrylate; PS, polystyrene; SAN, styrene-acrylonitrile; Nylon-6, poly(ε-caprolactam); PP, polypropylene; PE, polyethylene (Koprinarov and Hitchcock, 2000).....60
Figure 3.4 16S RNA gene of *Escherichia coli* showing nine variable regions 62
Figure 3.5 Schematic of the protocol for protein extraction using S-trap coloumn (Protifi, 2021) 64
Figure 3.6 Schematic of LC-MS system (Chemyx, 2021).....65
Figure 3.7 Workflow for proteomics study.....66
Chapter 4 The interplay between Cs, K and the cyanobacterium *Pseudanabaena catenata*, the fate of Cs and its impact on cell growth and protein expression.....72
Figure 4.1 (A) Growth curves of *P. catenata* cultures obtained by plotting the mean values of the optical density at 600 nm. Cultures were spiked with 0.5 mM CsCl, 1 mM CsCl, 2.5 mM KCl, 5 mM KCl and 1 mM Cs + 2.5 mM K, or were untreated (Control). Error bars show the standard deviation. (B) Representative cells observed under light microscopy, x1000 amplification. Samples were taken after 10 days incubation.....81
Figure 4.2 (A) STXM elemental maps of *P. catenata* cells. Proteins (Blue): 288.2 eV; Cs (Red): 735.0 eV (a) *P. catanata* cell from the control sample (b) Heteromorphic *P. catanata* cell from the 1 mM Cs sample. (c) Normal shape *P. catanata* cell from the 1 mM Cs sample. (d) *P. catanata* cell from the 1 mM Cs + 2.5 mM K sample (B) STXM-based NEXAFS spectra

corresponding to R1 - R5 showing in the elemental map. (a) NEXAFS carbon spectra. (b) NEXAFS caesium spectra.....83
Figure 4.3 Comparative proteomic analysis between treatment groups. (A) Venn diagram summary the number of labelled proteins in the total proteins data base. (B) Hierarchical clustering showing the changes in abundances of the identified proteins. Missing values were imputed from normal distribution. The protein abundances were normalized by z-score (the mean of each protein was subtracted; the results were then divided by the standard deviation). Z-scores were used for hierarchical clustering into heat map. The nearness of two items was defined by Euclidean distance. The distance between 2 clusters was defined by average distances between 2 single items. (C)Histogram of down-regulated proteins. (D) Histogram of up-regulated proteins. Differentially expressed proteins were evaluated by using multiple-sample test. Proteins with p< 0.05 and log2 folder change >1.5 or < - 1.5 were considered as significantly differentially expressed proteins. Significantly differentially expressed proteins were then categorized to KEGG for the histogram of up- / down- regulated proteins.....87
Figure 4.4 Schematic of photosynthesis pathway regulated by Cs and K treatment. The results were obtained by plotting the log2 fold change of the quantified proteins identified in the KEGG database. Up-regulated proteins are shown in red colour and down-regulated proteins are shown in green colour in the boxes representing each protein. Each box is divided into 5 segments, the 5 segments from left to right correspond to the expression of proteins in the 0.5 mM Cs, 1 mM Cs, 1 mM Cs + 2.5 mM K, 2.5 mM K and 5 mM K treatments respectively. 90
Figure 4.5 Schematic of the two-component system regulated by Cs and K treatment. The results were obtained by plotting the log2 fold change of the quantified proteins identified in the KEGG database. Up-regulated proteins are shown in red colour and down-regulated proteins are shown in green colour in the boxes representing each protein. Each box was divided into 5 segments, the 5 segments from left to right correspond to the expression of proteins in the 0.5 mM Cs, 1 mM Cs, 1 mM Cs + 2.5 mM K, 2.5 mM K and 5 mM K treatments respectively. 94
Appendix 4.1 Chemical composition of BG-11 medium 104
Appendix 4.2 Cells in 1 mM Cs group observed under light microscopy, x1000 amplification. Samples were taken after 10 days incubation.....105
Appendix 4.3. (A) concentration of K in supernatant. (B) concentration of Cs in supernatant 105
Appendix 4.4. Enrichment results of the differentially expressed pathways.....106
Appendix 4.5 (A) Grouped abundance values of kdpD proteins (B) Grouped abundance values

of kdpA proteins 107
Appendix 4.6 (A) Grouped abundance values of nblS proteins (B) Grouped abundance values of sasA proteins..... 108
Appendix 4.7 (A) Grouped abundance values of TrkA proteins (B) Grouped abundance values of TrkB proteins..... 109
Appendix 4.8 Schematic of enriched pathways regulated by Cs and K treatment. The results were obtained by plotting the log2 fold change of the quantified proteins identified in the KEGG database. Up-regulated proteins are shown in red colour and down-regulated proteins are shown in green colour in the boxes representing each protein. Each box was divided into 5 segments, the 5 segments from left to right correspond to the expression of proteins in the 0.5 mM Cs, 1 mM Cs, 1 mM Cs + 2.5 mM K, 2.5 mM K and 5 mM K treatments respectively. 114
Chapter 5 KOH versus NaOH, the inhibited effect on the growth of cyanobacteria *Pseudanabaena catenata*: Implications for control of P. catenata dominated blooms in FGMS 115
Figure 5.1. Growth curves obtained by plotting the mean value of the optical density measured at 600 nm wavelength. Error bars are defined by standard deviation. (A) OD_{600} of *P. catenata* cultures spiked with 1 mM, 2.5 mM, 5 mM and 10 mM KCl. (B) OD_{600} of *P. catenata* cultures spiked with 1 mM, 2.5 mM, 5 mM and 10 mM NaCl. 125
Figure 5.2 Growth curves of the chemostat cultures obtained by measuring the optical density at 600 nm wavelength. Cultures were initially flushed by standard BG-11 medium, from the time point marked “flush”, 3 treatments were given to the cultures. Control culture was continuously flushed with a standard BG-11 medium. The KOH and NaOH cultures were continuously flushed with modified BG-11 medium containing either 10 mM KOH or 10 mM NaOH, respectively. The pH of the medium was adjusted to 11 with HCl. 127
Figure 5.3 Genus-level microbial community comparison of *P. catenata* cultures flushed with standard BG-11 medium, KOH buffered BG-11 medium and NaOH buffered BG-11 medium based on 16S rRNA gene sequences. Samples were collected at day 17, 26, 38 and 53. Day 17 is the start point of changing flushing medium to KOH/NaOH buffered medium. Sequences that cannot be identified to genus level were resolved to the last matched taxonomic level of identification G- Genus, F-Family, O-orde, C-Class. 128
Figure 5.4 Microbial diversity comparison based on protein abundances. Percentage of each microorganism was obtained by using the total protein abundances of each organism divided by the total identified protein abundances of each sample. 131

Figure 5.5. Comparison of dynamic proteomic changes across time points. (a) Principal component analysis plot based on the abundance values of all identified proteins. Results were cut off by Benjamini-Hochberg FDR 0.05. Squares represents control samples. Circles represents KOH buffered medium flushed samples. Diamonds represents NaOH buffered medium flushed samples. Colour code: Green- day 17, Blue- day 26, Red- day 38. (b) Hierarchical clustering showing the changes in abundances of the identified proteins. Missing values were imputed from normal distribution. The protein abundances were normalized by z-score (the mean of each protein was subtracted; the results were then divided by the standard deviation). Z-scores were used for hierarchical clustering into heat map. The nearness of two items was defined by Euclidean distance. The distance between 2 clusters was defined by average distances between 2 single items. 134
Figure 5.6 Numbers of up-regulated or down-regulated proteins in the KOH and NaOH group relative to the Control group. Abundance ratios of the KOH and NaOH group to the Control group at selected time points were used to evaluate the regulation of protein expression (e.g., regulation of a specific proteins in the KOH group at day 26 was evaluated by the ratio of protein abundance of this protein in the KOH group to its abundance in the control group at day 26). The ratios were log2 transformed. Proteins with log2 fold change values > 2 or < -2 were classified into up-regulated or down regulated proteins. (a) Down-regulated proteins in KOH group. (b) Up-regulated proteins in KOH group. (c) Down-regulated proteins in NaOH group. (d) Up-regulated proteins in NaOH group. 135
Appendix 5.1 Chemical composition of BG-11 medium 148
Appendix 5.2 Concentration of K/Na in the culture measured by ICP-MS. 1 mM samples were taken routinely, samples were centrifuged and the supernatant were using for quantification of the K/Na concentrations in the culture (a) Concentration of potassium in culture across time (mM), (b) Concentration of sodium in culture across time (mM) 149
Appendix 5.3 Enrichment results, FDR 0.05 149
Appendix 5.4 Up-regulated proteins in KOH group. Protein classification was based on KEGG. Proteins were filtered by Log2 folder change > 2 149
Appendix 5.5 cultures were flushed with standard BG-11 medium, KOH suspended BG-11 medium, NaOH suspended BG-11 medium from left to right 150
A1 The fate of Sr in alkaline cultures of the cyanobacterium *Pseudanabaena catenata* 155
Figure A1.1: Growth curves of *P. catenata* with and without the addition of Sr: a) optical density at 600 nm; b) Chl-a concentrations (μgL^{-1}); c) pH; d) percentage of Sr in solution

measured by ICP-AES. Error bars are the standard deviation of 3 replicates. 165
Figure A1.2: TEM images and EDS data taken from samples of *P. catenata* cultures incubated with $SrCl_2$ at day 20, washed twice. EDS data corresponds to the numbers on TEM images, site of scans indicated by red circle. All scale bars represent 2 μm.....169
Figure A1.3: XRD analysis of a bulk sample of *P. catenata* culture incubated with Sr. Red dots indicate the presence of calcian strontianite [(Sr 0.85, Ca 0.15) (CO_3)] 170
Figure A1.4: Sr K-edge EXAFS experimental data (black line). Theoretical best fit (red line) calculated using Artemis (Ravel and Newville, 2007) 172
Supplementary Table 1: PHREEQC thermodynamic calculations of Sr (1 mM) saturation in BG11 medium at pH 7.2 and pH 10. 183
Supplementary Figure 1: Percentage of Sr in solution of sterile BG11 medium. Error bars denote standard deviation of three replicates.....184
Supplementary Figure 2: TEM image and EDS data taken from a sample of *P. catenata* culture day 20, washed twice. EDS data taken from the electron dense feature of highlighted with the red circle. Peaks indicate the presence of P; the Cu peaks are due to the Cu-TEM grids. 185
Supplementary Figure 3: TEM image and EDS data taken from a sample of *P. catenata* culture incubated with $SrCl_2$ at day 20, washed twice. EDS data collected from within the region indicated by red circle. The peaks do not show the presence of Sr associated with the cell (away from the polyphosphate features), the Cu peaks are due to the Cu-TEM grid. 185

Word count: 42974

Abstract

The First Generation Magnox Storage Pond (FGMSP) at the Sellafield Nuclear Facility in the UK is in active use on site, and will shortly be undergoing decommissioning. High levels of radioactivity and alkaline pH at 11.4 provide extreme conditions in the pond. Despite such an extreme environment, seasonal blooms are frequently reported. The blooms restrict the visibility of pond water, which significantly hinders the maintenance and decommissioning operations. Previous investigations on the bloom identified that the dominant bloom organism was a cyanobacterium affiliated with a *Pseudanabaena* species. A mixed laboratory culture of *Pseudanabaena catenata* with a similar microbial community to the pond sample, was used to investigate the adaptive responses to the abundant radionuclide Cs. The investigation found that *P. catenata* can uptake Cs using the K transport system. A high K^+ affinity Kdp-ATPase system was switched off by 1 mM of Cs. A moderate K^+ affinity Trk system was highly stimulated by Cs which may increase the uptake of Cs^+/K^+ and stimulated a series of metabolic pathways, such as photosynthesis. Uptake of Cs induced common response proteins and proteins relate to nutrient limitation. In addition, Cs can be accumulated by *P. catenata* and concentrated in discrete zones. High concentration of K^+ significantly reduced the growth of *P. catnata*. A chemostat experiment indicated that KOH performed better than NaOH in controlling the growth of the *P. catanata* dominated culture and so can be suggested as an alternative to the use of NaOH in the pond system to control the bloom and simultaneously maintain the alkaline conditions of pond water.

Declaration

No portion of the work referred in the thesis has been submitted in support of an application for another degree or qualification of this or any other university or other institute of learning.

Copyright Statement

Acknowledgements

I would like to thank my supervisors Jon Lloyd, Jon Pittman for their continued support and advice over the course of this PhD. Their patience and encouragement have allowed me to develop as a scientist and as a person, for which I will always be very grateful.

I would like to thank to Dr Lynn Foster, who guide me in my MSc and promoted me to make the decision of being a PhD.

I would like to thank the University of Manchester, for giving me the opportunity to undertake this research project and providing me such a period of unforgettable experience.

I would like to thank Christopher Boothman for all of his help and support with all the questions and requests that I have had over the 5 years.

I would like to thank Victoria Coker, who provide me the chance to experience the STXM.

I would like to thank Araki, Tohru, the stuff in Diomond Light Source who helped me on the STXM experiment.

Thanks to David Knight, Ronan O'cualain and Stacey Warwood, the stuffs in life science core facility who helped me carried out the proteomics work.

I would like to thank Ilya Strashnov for the ICP-MS analysis.

Thank you to the Geomicro group, everyone has always been so helpful and friendly, always

ready to help and offer support or advice, I have been very lucky to be part of an amazing research group. Thank you to Naji Bassil and Dawn Buchanan for all your help with me.

I would like to say thanks to my girlfriend, who will be my wife in a month. Thank you for loving me 10 years.

I have to say the biggest thank you to my parents, who have supported and respected my every decision. You taught me how to speak, how to walk and how to be a person.

Finally, I want to say thanks to myself, for making the decision of being a PhD and not giving up.

The Author

The author graduated from the HuBei University of Technology in 2014 with BSc degree in Environmental Engineering and a MSc degree from the University of Manchester in Pollution and Environmental Control.

Chapter 1 Project context and thesis structure

1.1 Project context

The Sellafield site is the largest nuclear site in the UK. Several spent nuclear fuel ponds (SNFPs) are in the facility and the ponds are in different stages of decommissioning. The First Generation Magnox Storage Pond (FGMSP) built in the late 1950s were occupied as a storage site for the Magnox nuclear power stations. Due to the long-term storage, the fuel rods and the claddings have corroded. The decommissioning work of the FGMSP is a priority. The pond was abundant with Sr and Cs. The pH of the pond was maintained at 11.4 to minimize the corrosion of stored fuels and claddings. The FGMSP is an open-aired pond, and so many environmental factors, for example, seabird guano, giving ingress of carbon and nitrogen could affect the pond system. Therefore, despite the extreme conditions of the pond with regard to high pH and radioactivity, seasonal microbial blooms were frequently reported. The bloom reduced the visibility of the pond which disrupted the pond management and decommissioning progress. The triggers for the bloom event were unknown and the adaptive mechanisms of microorganisms to this extreme condition was not clear.

Previous PhD projects had identified that the dominant microorganism in the pond was a cyanobacterium of *Pseudanabaena* sp. In order to develop control methods for the bloom, understanding its physiology in this experiment is essential. Previous work has identified the response of *Pseudanabaena* to radiation and the interaction between *Pseudanabaena* and Sr. The main aim of this work is to understand the interactions between *Pseudanabaena* and another pond abundant radionuclide Cs, and investigating a bloom control method for *Pseudanabaena* dominated microbial bloom in the pond. The output of this work could contribute to understand the mechanism of microorganism adaptation to Cs abundant environments and provide alternative choice for the Sellafield in bloom control.

1.2 Thesis Structure.

The majority of this thesis is made up of two research papers. The research chapters start with a general introduction to the scientific knowledge of the research area, including the information of the First Generation Magnox Storage Pond (FGMSP) at Sellafield Site, the microbial blooms in SNFPs and the interaction between microorganisms and radionuclides (Cs), methods to control the growth of bloom dominated microorganisms. The end of the thesis is made up of a conclusion which contain a discussion of the outcomes and future work.

Chapter 1: Project context and thesis structure

Chapter 2: Introduction: provides information on the nuclear fuel cycle, spent nuclear fuel ponds (SNFPs), the formation of microbial blooms in the ponds and the microorganisms that have been identified. An overview of known information about microorganism radionuclide interactions and bloom control methods in SNFPs. The aims and objectives of this work

Chapter 3: General methodology: provides detailed information about the theoretical and practical details of the techniques used in this project.

Chapter 4: Research chapter "The interplay between Cs, K and the cyanobacterium *Pseudanabaena catenata*, the fate of Cs and its impact on cell growth and protein expression" In this study, I incubated *P.catenata* in a series of cultures with increasing concentrations of K and/or Cs. I monitored the growth of the cultures by optical density, the cell morphology by light microscopy, the distribution of Cs by Scanning transmission X-ray microscopy (STXM) and used LC-MS based proteomic techniques to identify the impact of Cs on *P. catenata* protein expression level.

Chapter 5: Research chapter "KOH versus NaOH, the inhibited effect on the growth of

cyanobacteria *Pseudanabaena catenat*a: Implications for control of *P. catenata* dominated blooms in FGMS" A chemostat experiment was carried out to simulate the pond system in the FGMSP. The culture was continuously flushed with KOH or NaOH. Optical density was recorded to compare the inhibitory effect on *P.catenata* growth, 16S rRNA gene sequencing and proteomic techniques were applied to analyze the change of microbial community and protein expression.

Chapter 6: Discussion

1.3 Author contributions

Chapter 4: The interplay between Cs, K and the cyanobacterium *Pseudanabaena catenata*, the fate of Cs and its impact on cell growth and protein expression

Kejing Zhang	**Principal author; experimental work; data analysis**
Lynn Foster	**Provided amino acid database for proteomics analysis**
Naji Bassil	**Enrichment analysis for differentially expressed proteins**
Jon K Pittman	**Concept development; manuscript review**
Jonathan R Lloyd	**Concept development; extensive manuscript review**

Chapter 5: KOH versus NaOH, the inhibited effect on the growth of cyanobacteria *Pseudanabaena catenat*a: Implications for control of *P. catenata* dominated blooms in FGMS

Kejing Zhang	**Principal author; experimental work; data analysis**
Lynn Foster	**Provided amino acid database for proteomics analysis**
Christopher Boothman	**16S rRNA gene sequencing analysis**
Jon K Pittman	**Concept development; manuscript review**
Jonathan R Lloyd	**Concept development; extensive manuscript review**

A1 The fate of Sr in alkaline cultures of the cyanobacterium *Pseudanabaena catenata*

This is a published work. The work was written and published during my PhD, I collected the data for this project during my MSc project and drafting led by lead author Lynn Foster

Chapter 2 Introduction

Energy demand increases with the development of human society. A person in an industrial country consumes about 150 – 350 gigajoules of energy per year (WNA, 2021). The world population are currently 7.6 billion and predicted to reach 9.8 billion by 2050 (UN DESA, 2017). With the increases of human population, the impact on energy demand is foreseen. Currently, 80% of the world energy comes from fossil fuels, such as oil, natural gases and coal. Theoretically, the resources of fossil fuels are sufficient to support the consumption of energy for more than a century. However, there are many environmental problems associated with the increasing extraction and burning of them. Therefore, more intensive utilization of non-carbon energy resources like nuclear power is required to decrease the dependence on fossil fuels (WNA, 2021). The basis of nuclear power reaction is a chain reaction of uranium fission which yields a large amount of energy. Typically, one tonne of natural uranium can produce 44 million kwh of electricity, which equals to the production of burning 850,000 m^3 or 20,000 tonnes coal. Currently, there are over 430 commercial nuclear power reactors are working and they generate 10% of the world's electricity (Ewing, 2015).

Radioactive wastes are generated at all stages of nuclear fuel cycle, include inherently radioactive materials, and materials contaminated by radioactivity. The areas where nuclear power and particularly nuclear weapons were developed, such as the USA, UK, France and the former Soviet Union (FSU) are facing the challenges from nuclear legacy. In terms of the UK, nuclear legacies cover nearly 85% of total nuclear liabilities. As shown in Table 2.1, this includes: 1) the Magnox fleet of nuclear power stations built during the 1960s- 1970s and operated by British Nuclear Fuels plc (BNFL). 2) Facilities and plants for Magnox fuel reprocessing and all materials and wastes associated with the reprocessing at Sellafield site. 3)

Nuclear facilities and plants which were established during the 1940s-1960s to support the research programmes of the Government and operated by BNFL and the United Kingdom Atomic Energy Authority (UKAEA), and all materials, wastes and spent fuel produced in those programmes (NDA, 2002).

The facilities and structures at nuclear power generating and reprocessing sites should be demolished and decontaminated when the sites reached the end of their working lives. The process of demolishment and decontamination is referred to as decommissioning (NDA, 2002). For safety reason, decommissioning is not carried out instantly after the facilities were shut down. In addition to the contaminated surfaces of the plant, the components which have been exposed to neutron irradiation will be radioactive as well. These materials may include 137Cs, 63Ni, 60Co, 55Fe and 14C, wherein, 55Fe and 60Co are highly radioactive due to the gamma rays that they produce (WNA, 2017). Thus, decommissioning is not allowed to be immediately carried out after shut down. New structures or facilities may be built during decommissioning but they will ultimately be decommissioned as well once not required. The decommissioning process can last for 100 years, depending on the type of plants and facilities involved. Apart from the long-time scale, the cost of decommissioning is huge. It is assessed that more than £115 billion is required for UK alone and the work is expected to be completed around 2135(NDA, 2002). Wherein, the cost of work in Sellafield site is estimated around £85 billion and this part of work is expected to be finished around 2120 (NDA, 2015). The First Generation Magnox Storage Pond (FGMSP) is one of the older spent nuclear fuel ponds (SNFPs) at Sellafield site. Due to the long-term operation, the cladding has corroded. The decommissioning and retrieval of waste from older legacy storage ponds, such as FGMSP is a priority at the Sellafield site.

Table 2.1 Legacy sites in the UK (NDA,2002)

BNFL	**Sellafield**	**Operational and decommissioning – fuel reprocessing and storage and management of nuclear wastes and materials. Also includes the Calder Hall Magnox station**
	Capenhurst Works	**Decommissioning/waste management and storage**
	Springfields Works	**Operational – fuel manufacture and nuclear services**
	Drigg Storage Site	**Low Level Waste disposal**
UKAEA	**Dounreay**	**Decommissioning**
	Windscale	**Decommissioning**
	Harwell	**Decommissioning**
	Winfrith	**Decommissioning**
Magnox	**Wylfa**	**Operational**
	Oldbury	**Operational**
	Sizewell A	**Operational**
	Dungeness A	**Operational**
	Hinkley Point A	**Defuelling and decommissioning**
	Bradwell	**Defuelling and decommissioning**
	Hunterston A	**Defuelling and decommissioning**
	Trawsfynydd	**Defuelling and decommissioning**
	Berkeley	**Defuelling and decommissioning**
	Chapelcross	**Operational**

2.1 The Nuclear fuel cycle

2.1.1 The fuel cycle

The nuclear fuel cycle is a series of process which underpin electricity generation from uranium and potentially other radioactive elements. It includes many stages, from uranium mining and milling to used fuel storage, reprocessing and disposal (**Figure 2.1**). Uranium is one of the heaviest natural elements. It is more abundant than silver, mercury and gold, similar as tin less than cobalt, molybdenum or lead.

The fuel cycle starts with uranium mining. Excavation is one of the commonly used techniques in uranium mining. It is a process which extracts rock from ground, breaks them down and removes the minerals. It can be conducted either underground or via surface (open pit) mining. The choice is governed by the consideration of nature of the orebody, safety and economics. Generally, for the deposits which lie close to surface, open pit mining is employed, and it requires holes larger than the deposit itself and remove large amount of overburden and waste rock. Underground mining is usually used to underpin mining of deposits of greater depth. It has smaller surface damage and generates a lower quantity of waste minerals, which has less impact to the environment (WNA, 2021). In situ leach (ISL) mining, which is also known as solution mining, is suitable for mining in sandstone or permeable sand deposits. It causes little surface disturbance and little waste rock or tailing generated, and an increasing portion of uranium are currently from this technique. ISL circulates acidified (alkaline) ground water with large amount of oxygen through the orebody to dissolve the uranium. Uranium oxide is dissolved and pumped to the surface with the solution and recovered (WNA, 2021). Acid or alkaline solutions may be applied in this process depending on the geology (Wilson, 1996). Acid leaching is commonly applied as it provides relatively higher uranium recovery and lower costs. Alkaline leach must be employed where significant levels of calcium exist in the orebody. Acid leaching provides relatively lower cost and higher uranium recovery and more commonly used (WNA, 2021).

The mined original ore may contain only 0.1% uranium. Uranium should be concentrated to a higher concentration via uranium milling (U.S.NRC, 2021). In a mill, ores are crushed and dissolved to separate from waste minerals. Dissolved uranium is recovered and precipitated to uranium oxide (U_3O_8). U_3O_8 is yellow colour and often referred as “yellow cake”, with a concentration of uranium higher than 80% (WNA, 2021, Wilson, 1996). The remained waste

ore and rocks are called “tailings”. It contains toxic heavy metal and radioactive materials, which its disposal is isolated from the wider environment (WNA, 2021).

Uranium occurs in several isotopes, which includes Uranium-238 (^{238}U), uranium-236 (^{236}U), uranium-235 (^{235}U), uranium-234 (^{234}U), uranium-233 (^{233}U), uranium-232 (^{232}U). Only ^{235}U is fissile and can be used to generate electricity. ^{235}U only accounts for 0.7% of natural in the Earth’s crust. Most nuclear reactors are light water reactors which require fissile ^{235}U at a concentration of 3% - 5%. Some special power reactors use high-assay uranium (HALEU) with uranium concentrations at 7% - 20%. Thus, a process to enrich for the ^{235}U is required. The most commonly used technique to enrich ^{235}U is based on the mass difference between ^{235}U and ^{238}U. U_3O_8 is first converted to uranium hexafluoride (UF_6) gas. UF_6 is then centrifuged, and ^{235}U and ^{238}U are separated by their 1% mass difference. The enriched $^{235}UF_6$ is recovered to UO_2 following the process described in **Figure 2.2**. UO_2 is pressed and baked (over 1400 ^{o}C) to ceramic UO_2 pellets. Fuel pallets are then fabricated to fuel rods (WNA, 2021).

The basis of the nuclear power reaction is a chain reaction of uranium fission. ^{235}U nucleus contains 143 neutrons and 92 protons. It will split in two (fission) after capturing a moving neutron. Energy is released in the form of heat and 2 or 3 neutrons are expelled during the fission. The released neutrons may further be captured by other ^{235}U nucleus and caused a chain-reaction. Millions of reactions occur and large amount of heat is released. The heat can be used to make steam to produce electricity (WNA, 2021). ^{238}U in the fuel rods may capture a neutron and become plutonium-239 (^{239}Pu). Further fission events will happen and yield energy when Pu-239 is hit by a neutron. Energy yielded from this process accounts for one

third of the total fission energy. ^{239}Pu atoms may simply capture a neutron and become Pu-240. The concentration of Pu-240 increases with time that fuels stay in the reactor. Similarly, the concentration of other fission fragments and heavy elements increase as well. Typically every 18-36 months, the concentration of fission fragments and heavy elements will reach a point where the fuels are unable to be used. The used fuels typically contain 1.0% Pu (0.6% fissile), 1.0% ^{235}U, 3% minor actinides and fission products, 95% ^{238}U (WNA, 2021).

The used fuels removed from reactors emit heat and radiation due to the fission fragments. Thus, these used fuels are immediately emplaced to a spent nuclear fuel storage pond for temporarily storage before the final disposal. The water in ponds absorbs the heat and shield the wider environment from radiation. After the spent fuels are stored in the pond for months or sometimes several years, they will be either stored for final disposal or reprocessed to recycle the usable portion. (WNA, 2021).

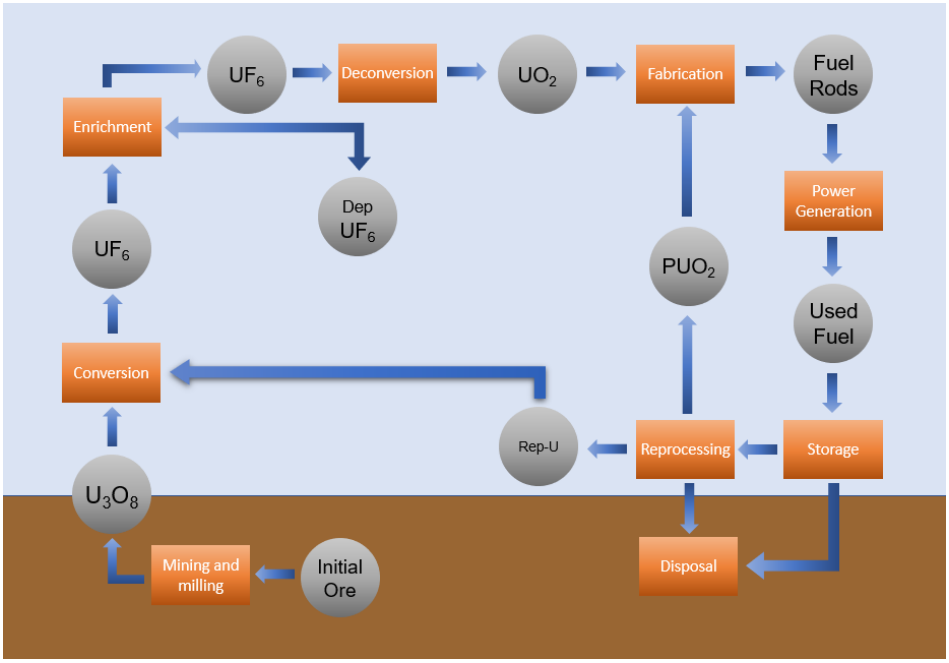

Figure 2. 1 Nuclear fuel cycle from uranium mining to disposal (WNA, 2021)

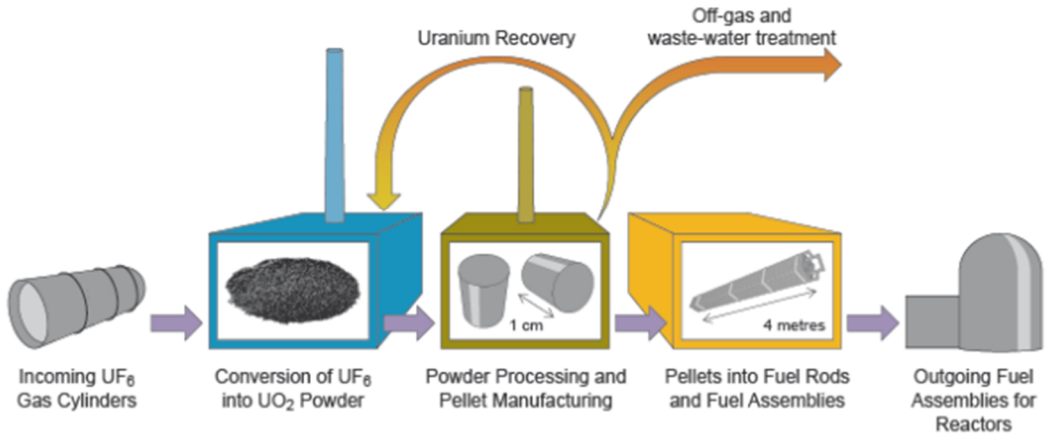

Figure 2.2 Process of fuel fabrication (WNA, 2021)

2. 1.2 First Generation Magnox Storage Pond (FGMSP) at Sellafield

Spent fuels from nuclear reactors generate heat and radioactive. They are temporally stored in Nuclear Fuel Storage Ponds (SNFPs) before the final decision of their disposal. SNFPs are filled with deionized water which can help cool down the spent fuels and shield the radioactivity (Chicote *et al*., 2005). Pond pH is tropically adjusted to alkaline to minimise the rate of corrosion of the spent fuels (Foster *et al*., 2020). Even though the extreme conditions, microorganisms are presented. SNFPs are initially designed to store spent fuels at most 20 years, which is assumed long enough for determining their final disposal (Sarro *et al*., 2005). However, many nuclear power plants (NPPs) in Europe doubled the capacity of the ponds to extend the lifetime to 40 years. The short-term or long-term impact of microbes to the spent fuels in pond and facilities remains a topic of debate requiring further investigation.

The Magnox reactors were a key part of the UK's nuclear fleet. The fuels for the reactors comprised non-enriched uranium covered by an alloy of Al and Mg in small quantities (Wilson, 1996). The First Generation Magnox Storage Pond (FGMSP) at Sellafield site is an open-air pond built to receive spent MAGNOX fuels. It is 6 m in depth, 20 m in width and 150 m in

length and contains deionised water. NaOH was used to kept an alkaline level of 11.4 to minimise the corrosion of material in the pond (Jackson *et al.*, 2014; Sellafield Ltd, 2016). It started to accept spent nuclear fuels from Magnox reactors for mid-term storage and reprocessing from 1950s. The site stopped reprocessing spent fuels by the 1970s, but kept accepting Magnox spent fuels for housing until 1992. Over long-term operation, significant amounts of wastes have been generated. For example, around 14,000 m^3 of water, 1500 m^3 of radioactive sludge and 500 tonnes of solid nuclear fuels are located at the bottom of ponds (Sellafield Ltd, 2016). The sludge contains fragments of metal and fuel rods, concrete degradation products, corroded fuel particles and animal remains (Gregson *et al.*, 2011). Although poised at high pH, the long-term operation and prolonged corrosion of the fuel and cladding has resulted in a significant level of radionuclides accumulating in the pond waters and sludges, including fission products, such as Sr and Cs (Jacckson *et al.*, 2014). In addition, FMGSP has proved susceptible to seasonal blooms. The blooms increase water turbidity and cause water visibility issues, which impact the waste retrieval operations and downstream process, and can results in increasing costs and schedule of the decommissioning programme. They can also generate radionuclide impregnated organic rich sludge, which complicates disposal plans for the spent fuels. Therefore, controlling the seasonal bloom in the FGMSP was now a priority. The FGMSP was a complex system, with high pH and fission products of uranium, such as Sr and Cs. Therefore, it was essential to uncover the interactions between the bloom dominated microorganisms and the radionuclides in the FGMSP before designing the bloom control strategies.

2.2. Microorganisms in nuclear storage facilities

2.2.1 Microbes in spent nuclear fuel ponds

Microorganisms and their bio products are common problems in a wide range of industrial contexts, such as food processing, paper mills, oil and nuclear power industries. Many problems such as microbial induced corrosion, lower heat conductivity and filter blocking, may be associated with the presence of microorganisms (Wolfram and Dirk, 1997; Melo and Bott 1977; Masurat *et al*, 2005). In addition, the presence of microorganisms in an industrial system is a warning of other subsequent fouling problems (Masurat *et al*, 2005). Solutions to biofouling are typically system specific due to the variable limiting factors in industrial systems (Costerton *et al.*, 1995). Industries tend to make the environment more extreme to prevent the growth of microorganisms. For example, using biocides or ultra-pure water in their system. However, microorganisms still can still persist in such extreme conditions. In recent years, various phylogenetic groups of microorganisms were reported and isolated from SNFPs. 21 bacteria belong to *α, β, γ-proteobacteria, actinobacteridae,* and *Firmicutes* were identified and isolated from SNFP at the Cofrentes NPP by Chicote *et al* (2004). Masurat *et al* (2005) isolated *Meiothermus sp.* which was the dominated organism of biofilms in Sweden's interim SNF storage facility. Tisakova *et al* (2012) isolated *Pseudomonas aeruginosa, Kocuria palustris, Ochrobactrum spp.* and *Micrococcus luteus* from the interim spent fuel storage pond in Slovak Republic and assessed the ability of accumulating Co and Cs. Microorganisms often develop biofilms as a survival strategy, consisting of surface attached microorganisms covered by extracellular polymers. The extracellular polymers contain 50-90% of the organic carbon in the biofilm. They contain channels that connect the microbes inside and surrounding environment (Christensen and Claracklis, 1989; Meesters et al. 2003). The conditions inside the biofilm are not constant. The change of outside environment such as water temperature and water chemistry may change the condition inside biofilm, which helps to minimise the pressure

on the microorganisms, particularly in extreme environments (Masurat et al., 2005). Biofilms are able to adherence to surfaces, potentially enhancing corrosion processes, which can increase the radioactivity and turbidity of the pond water.

Biofilms are also able to selectively accumulate metals and radionuclides via biosorption or bioaccumulation processes, especially when the concentration of radionuclides are at a very low level (Tisakova *et al.,* 2012). Chicote et al (2004) reported that some microorganisms formed biofilms on the surface of stainless steel in the SNFP and accumulated heavy metals and radionuclides equivalent to 5500 BQ cm^{-2} radioactivity. Some of these microorganisms have been identified and radionuclide-microbe interactions studied. For example, *Microbacterium sp.* can take up uranium and plutonium via siderophores-mediated processes (John *et al.,* 2001). *Pseudomonas* can interact with Cd, Co and U, and degrade many toxic compounds (Brooks et al., 1998; Pattanapipitpaisal et al., 2002; Lloyd and Renshaw, 2005). *Nocardia sp* showed ability of accumulating cadmium, nickel and copper (Kim et al., 2002). In addition, it is found that some radioactivity-tolerated microorganisms formed carbonate and hydroxide complexes with radionuclides through chemisorption or bio mineralization mechanisms (Chicote et al., 2005). Therefore, identifying the microbes presented in the system and investigating their interactions with radionuclides may help to develop the potential of using specific micro-species in bioremediation.

2.2.2 Microbial diversity in FGMSP

Despite the high pH and radioactive nature of the FGMSP at Sellafield site, seasonal blooms have been reported. Foster *et al* (2019) investigated the pond ecology by amplifying and sequencing the 16S rRNA of the pond water samples (**Figure 2.3**). 7 samples from August

2014 to September 2017, covering both bloom periods and no bloom periods of the pond. 28 genera were identified from the pond sample. The prokaryotic community was dominated by *proteobacterial phyla*. The microbial community changed from 2014 to 2016 and 2017. The most abundant genera were S*phingomonas* and *Sediminicoccus* in 2014, and these declined in 2016 and 2017. The microbial community between 2016 and 2017 was relatively stable, with 6% - 12% *Porphyrobacter*, 8 - 17% *Roseococcus*, 8 - 18% *Rhodobacter*, 9% - 22% *Mongoliitalea* and 12% - 28%, *Hydrogenpphaga* detected in all samples. Cyanobacteria were detected in all samples collected from the FGMSP. During the no bloom periods, cyanobacteria accounted for less than 2.5%. During the bloom period in 2014, cyanobacteria readings increased, include *Geitlerinema* (<0.1%), *Cyanoium* (<0.1%), *Synechocystis* (<0.4%), *Nodosilinea* (<0.8%), *Pseudanabaena* (0.3% to 7%). The abundances of cyanobacteria increased to 30.1% in 2016 bloom event, wherein the *Pseudanabaena* abundances raised to 28.9%. In addition, species of the *Pseudanabaena* genus presented in all samples except September 2017, which suggested that *Pseudanabaena* species were the main contributor to the bloom event (Foster *et al,* 2020). Therefore, investigating the physiology of *Pseudanabaena* and its interactions with radionuclides present in the pond is important for understanding the fate of radionuclides in the pond, and for developing control methods of the bloom in FGMSP.

2.3 Interactions of microorganisms and radionuclides

Nuclear power industry generates chemically toxic and radioactive compounds at all stages. Weapons testing and nuclear disasters, such as Fukushima in 2011 and Chernobyl in 1986, released massive amounts of radionuclides into the environment (Rivasseau *et al.*, 2012). Microorganisms play an important role in environmental fate of radionuclides in terrestrial and aquatic ecosystems. They are able to change the mobility and speciation of radionuclides through physico-chemical and biological process (Gadd, 1996). Microorganisms exist at both

start point as primary producers and end point as decomposers in food chains and are crucial in all biogeochemical cycles (Lovley, 1995). Microorganisms accumulate radionuclides by biosorption or transport them into the cell and can bound, precipitate and localize with cell organelles or cell structures (Gadd, 1996). Thus, radionuclides can be transported through the food chain. In addition, the movement of microorganisms will transport radionuclides in aquatic environments. In addition, radionuclides can be reduced and the mobility can be changed by some microorganism-catalysed reactions.

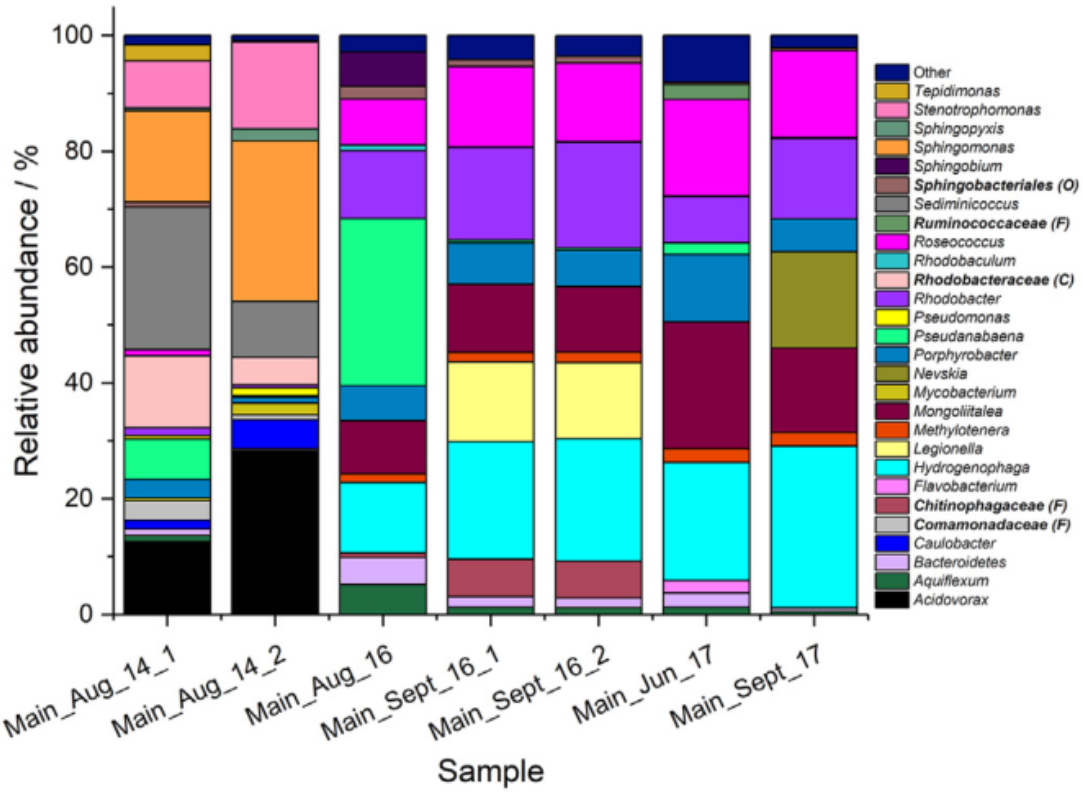

Figure 2.3 Microbial community comparison of FGMSP samples based on 16S rRNA gene sequences, samples were collected between August 2014 and September 2017 (Foster *et al,* 2020)

Cells can accumulate radionuclides through non-specific physico-chemical interactions or specific mechanisms of transport or sequestration. Microbial uptake of insoluble or soluble

radionuclides by physico-chemical mechanisms is called biosorption. This process may be affected by metabolic activities (Schultzelam and Beveridge, 1994). The constituents of microbial cell wall importantly affect the affinity of radionuclides and almost all biological macromolecules have some affinity for radionuclides. Microbial exopolymers contain glycoproteins and proteins associated with lipopolysaccharide and polysaccharide. Many of exopolymers act as negatively charged polyanions which can catch cationic radionuclides (Ehrlich and Brierley, 1990). Ligands such as amine, sulfhydryl, carboxyl, hydroxyl and phosphate groups of microbial exopolymers are the main binding sites of radionuclides (Simonoff *et al.,* 2007). Such polymers and humic materials in soil are important sorbents of radionuclides in the terrestrial environment (Gadd, 1996).

Cationic radionuclide species can penetrate the cell through specific or non-specific transport systems. For heavier radionuclides like uranium, the toxicity increases the permeability of membrane and allowed intercellular accumulation of uranium (Simonoff *et al.,* 2007). Once in the cell, metals often prefer to locate in vacuoles. Some metals may precipitate in cell structures or organelles as oxides, sulphides or phosphates. Function of metal-binding peptides and proteins may be induced by their presence. For example, metallothioneins contains polypeptides rich in cysteine, which can bind to Zn, Cu and Cd (Turner and Robinson, 1995).

Another main mechanism of radionuclides immobilization is forming mineral or sulphide formation by chemical reduction or precipitation. Dissimilatory reduction or bioreduction is an important microbial transformation that can affect the solubility of metal elements. It is coupled with the metabolism of obligate anaerobes in anaerobic conditions. Metallic elements can act as electron acceptors for respiration in this process (Lovley, 1993). For example, *Shewanella*

putrefaciens and *Geobacter metallireducens* are able to reduce U^{+6} to less soluble U^{+4}, and hence form black precipitate of uranium oxide (Fortin *et al.,* 1995). By contrast, bioreduction may indirectly increase the solubility of some radionuclides. For example, it is reported that some iron- and sulphate-reducing bacteria increased the solubility of radium from uranium mine tailings (Landa and Gray, 1991). Iron-reducing *Bacillus strains* solubilized 90% soil PuO_2 with presence of nitrilotriacetic acid in anaerobic conditions (Rusin et al., 1994). Sulphate-reducing bacteria such as *Desulfotomaculum sp.* and *Desulfovibrio* can produce hydrogen sulphide, which forms low soluble sulphides with metal cations. Sulphate-reducing activities are commonly observed during the anaerobic decay of biomass. Sulphidic immobilization of toxic metals and radionuclides cam be observed in sediments and wastes (White and Gadd, 1996). By contrast, some autotrophic bacteria, such as *Thiobacillus ferrooxidans*, can lead to oxidation of minerals under aerobic conditions. Heterotrophic bacteria may produce chelating agents, organic and proton acids, which can change the solubility of radionuclides. For example, salicylic acids, gluconic acids and dicarboxylic acids are efficient chelators of metallic species and can increase metal mobility in soil. Some soil organisms, such as *Aspergillus niger* are able to both increase the metal immobilization by oxalate formation and metal solubilization by critic acid (Francis *et al.*, 1992; Gadd, 1996; Morley *et al.,* 1996).

2.3.1 Interaction between microbes from SNFPs and radionuclides

As mentioned above, microorganisms have been identified in many SNFPs. And the interactions between microbes and radionuclides have been studied. Microorganisms living in SNFPs show strong resistance to radionuclides and capacity of accumulating radionuclides. For examples, bacteria isolated from an external storage pond at Sellafield site showed resistance to Co and Cs, wherein, bacteria closely related to *Tardiphaga* and *Curvibacter* genera can grew in the presence of 3 mM CoCl and bacteria related to *Yersinia* and *Serratia*

genera are able to survive in presence of 500 mM CsCl (Dekker et al, 2014). In addition, microbes in SNFPs show the ability of absorbing and accumulating radionuclides. The autotrophic algae *Coccomyxa actinabiotis* nov. sp. isolated from the storage pool of a nuclear site has the ability of accumulating radionuclides, including ^{14}C, ^{54}Mn, ^{60}Co, ^{65}Zn, ^{110m}Ag, ^{137}Cs, ^{238}U, via the mucilage shell surrounding the cell (Rivasseau *et al*, 2013). Microorganisms form biofilms as a survival strategy in extreme conditions, and in this context corrosion problems related to biofilm formation were reported in the wet interim storage of spent fuel at the Atomic Energy Research Institute in Budapest. Bacteria isolated from the water sample formed biofilm and showed ability of accumulating Cd, Co and Sr during the growth. The formation of biofilm changed the cathodic and anodic microenvironments and accelerated the corrosion rates on metal surface (Diosi *et al.,* 2003; Littile and Wagner, 1996; Costerton *et al.,* 1987).

Pseudanabaena catenate, a close relative of the bloom-forming cyanobacterium in the FGMSP at Sellafield Nuclear Facility are able to remove Sr^{2+} ions from laboratory cultures. Most of the Sr^{2+} was precipitated as minerals containing Ca and carbonate, with a small proportion entering the cell and forming polyphosphates. (Foster *et al.,* 2020). The growth of cells was not affected by presence of Sr. Similar studies have been documented by Anderson and Appanna (1994), with the growth of *Pseudomonas fluorescens* not hindered by Sr, as the cells involved in formation of strontium carbonate minerals. Cyanobacteria form extracellular carbonate minerals driven by increases in external pH by photosynthetic activity (Cam et al., 2015). The mechanism of forming intracellular strontium polyphosphates is not known in detail, but many research has shown metals such as Pb, Cd and Ca can bind to polyphosphates and then export out of cells via Pit transport system to reduce the toxic effect (Baxter and Jensen, 1980; Jensen *et al.,* 1982; van Veen *et al.,* 1994 Albi and Serrano, 2016).

2.3.2 Interaction between microbes and Cs

Cs is the rarest alkali metal, has no essential biological role and little economic value. The main geographic sources of stable Cs are in form of caesium oxide in Africa and USA. The concentration of natural Cs varies in different environments. In marine systems, concentrations of Cs range from 0.5 to 2.0 ng ml^{-1}; in fresh water systems, the concentration range from 0.01 to 1.2 ng ml^{-1}, while its concentration is soils ranges between 0.3 and 25 μg g^{-1} (Avery, 1996). Cs can exist in 20 isotopic forms, including ^{123}Cs to ^{144}Cs, wherein ^{133}Cs is the only stable isotope. ^{134}Cs and ^{137}C are fission products of uranium and other actinides (Poinssot and Geckeis, 2012). The nuclear industry has released significant quantities of Cs radioisotopes, particularly ^{134}Cs and ^{137}Cs, into environment. Interactions between Cs (and other radionuclides) and microorganisms are components of terrestrial and aquatic food chain and play important roles in biogeochemical cycling. The activities of microorganism's impact on the retention and accumulation of Cs in upper soil layers, the leaching of Cs from plant in terrestrial ecosystems and mobilisation of Cs in aquatic sediments. (Angel, 1983; Clint *et al.,* 1992; Johnson *et al.,* 1991; Witkamp and Frank, 1970). In addition, Cs as a fission product, largely exists in effluents from nuclear industry. Understanding its interactions with microbes are important to tracking the fate of Cs and develop Cs removal strategies.

Cs is alkali metal. It is the most electropositive metal, easily oxidized and forming strong bases. It exists as the monovalent cation Cs^+ form in solution (Gadd, 1992). Cs^+ is a very weak Lewis acid when compared to other environmental metals, such as Cu^{2+} and Cd^{2+}. The charge/ radius ratio of Cs ion is very low. Therefore, it has low polarizing power and charge density (Hughes and Poole, 1991). Consequently, it is difficult for Cs to interact with ligands (Avery, 1996).

The toxicity of metals is related to their coordinating ability. Generally, soft metals are toxic to microorganism, while hard metals are often essential nutrients for microbial growth (Avery and Tobin, 1993). Cs is a hard metal and trace amounts have been detected in many organisms, but no essential biological role is documented (Ghosh *et al.*, 1993). Cs^+ is chemically similar to other alkali monovalent cations, especially K^+. The ionic radius of Cs^+ is 165, which is close to K^+ (133) and Rb^+ (149). Thus, many K^+ transport system located in the plasma membranes of microorganisms cannot discriminate them and transport Cs^+ into cells as an analogue for K^+ (Avery *et al.*, 1992; Bossemeyer et al., 1989).

Internal K^+ concentrations are usually hundreds fold higher than external K^+ concentration. The monovalent cation fluxes through the cell membranes against concentration gradients. Thus, energy is required in the process. Monovalent cation uptake via primary active transport, such as K^+ - ATPase, is common observed in bacteria. Energy for driving the process comes from ATP (Walderhaug *et al.,* 1987). The transport of monovalent cations can also be driven by the electrochemical proton gradient produced by the process that membrane-bound H^+-ATPase expels protons. The transport of monovalent cations is not directly driven by the hydrolysis of ATP, but sustained transport requires consumption of ATP and maintain H^+ efflux (Jones and Gadd, 1990)

2.4 Bloom control methods

There are numerous commonly used methods for cyanobacteria and algal removal or growth prevention. However, the condition in the FGMSP was unique. The pond was open to air and high pH. In addition, the pond was suspended with radionuclides and fuel rods were stayed at the bottom of the ponds. These features limited the effectiveness of most commonly used bloom control methods. Here several commonly used bloom control methods were assessed.

2.4.1 Nutrients Removal

Limiting or removing the nutrients, such as nitrogen and phosphate, is an approach to limit the growth of microorganism chronically, and could be considered in priority (Sigee, 2005). Many chemicals can be used for this purpose. For instance, polyaluminium chloride, ferric or aluminium sulphate can efficiently remove ortho-phosphate (Aguilar *et al.,* 2005). Calcium carbonate-based regent can be used to remove inorganic nitrogen and activated carbon shows distinct ability in absorbing organic nitrogen (Wending *et al.,* 2013). Copper sulphate can also be used to remove nitrogen. In addition to nutrients removal, copper sulphate could induce lysis of cyanobacteria (Peterson et al., 1995; Fan et al., 2013a). Besides using chemical additions, biological methods can be used in nutrients removal. Schmack *et al* (2012) used a mixture of 6 bacterial cultures in controlling algal bloom in a river system. The bacteria did not directly attack or lyse the algal cells but reduced the algal growth by competing for the nutrients. However, the inhibitory effects were not long-term. For instance, the effect of $CuSO_4$ only lasted for 3 days (Fan et al., 2013a). In addition, the FGMSP is open to air, and is in a flow through system which limiting the nutrient ingress control options.

2.4.2 Oxidation and Photocatalysts

Oxidants could be used for microbial bloom removal. Hydrogen peroxide, potassium permanganate and ozone are widely used in bloom control. The effectiveness of oxidants is dose dependent. Potassium permanganate and hydrogen peroxide could damage cell membranes and effectively result in cell lysis (Fan *et al.,* 2014). Fan *et al.* (2013b) reported that 3 mg/L of potassium permanganate show damage effect on cyanobacteria cell, 10 mg/L caused obvious of reduction of cell density. The experiment used a toxin producing strain of *Microcystis aeruginosa*. The dose of potassium permanganate damaged the cell and led to toxin

release. The toxins were totally oxidised by potassium permanganate after 7 h contact time. Ozone is more reactive than potassium permanganate and hydrogen peroxide in relatively alkaline environment (Li *et al.,* 2011). Ozone could prevent the formation of biofilm even in low concentration. In addition, ozone could damage cell wall and lyse the cell (Fan *et al., 2014*). The removal of algae by ozone increases with temperature however, the solubility of ozone was negatively corresponded to temperature (Farooq *et al.,* 1977; Roth and Sullivan, 1981). However, oxidation was not suggested due to the high pH of pond and the possibility of chemical reactions with the pond inventory

Photocatalysts could be a possible way in controlling the growth of algae (Peller et al., 2007). Photocatalysts provides long-term suppression on algal growth, as the losses of catalyst in process are low. Titanium dioxide has been studied for decades in destruction of environmental contaminants. The mechanism that titanium dioxide removing algae is oxidation (Peller et al., 2007). It could disrupt the cell structure and break up any microbial colonies (Kim and Lee, 2005; Metzler et al., 2011) Oxidation takes place at the surface of photocatalyst. Therefore, maximising the surface area of photocatalyst is important. The inhibition of photocatalysts to algal cells is affected by oxygen availability, dose of photocatalysts and length of the treatment (Kim and Lee, 2005; Hong and Otaki, 2006; Song *et al*., 2008; Metzler *et al.*, 2011). Due to the condition of FGMSP, powdered form photocatalysts might be flushed out or act as catalysts to unwanted chemical reactions in pond. And immobilised photocatalysts would require large contact area, therefore would suspended in the water and hinder the pond routine maintenance work.

2.4.3 Sonication, UV and Flushing

Apart from using chemicals, there are physical methods for bloom control. Many reports demonstrated sonication could be an effective approach (Mason and Phillip, 2002; Wu et al., 2012). Sonication is an approach that generates cavitation bubbles by ultrasonic radiation with frequency higher than 20 kHz (Rajasekhar et al., 2012). The pressure can increase up to 100 MPa and the temperature can increase up to 5000 °C during the collapse of the bubbles (Suslick, 1990). In addition, free radicals which could disrupt the cell wall and results in the leaching of intracellular matter are generated in this process (Tang et al., 2004). Sonication suppresses the growth of microorganisms by disturbing the metabolic activity, cell multiplication and collapsing gas vacuoles (Zhang et al., 2006; Xu et al., 2006; Rajasekhar et al., 2012; Wu et al., 2012; Ahn *et al.,* 2003). The efficiency of sonication treatments depends on exposure time, the chemical composition of culture, frequency and power supplied per volume (Rajasekhar *et al.,* 2012; Suslick 1990; Zhang et al., 2006; Zhang et al., 2009). For cyanobacteria, sonication has maximal effects on those with gas vacuoles (Tang *et al.,* 2004). Sonication is a short live approach and cells can recover after the treatment. Therefore, it is better to combine sonication with other kinds of treatment (Nakano et al., 2001; Gavand et al., 2007). For instance, sonication combined with polyaluminium chloride could improve treatment efficiency (Zhang *et al.*, 2006; Zhang *et al.*, 2009). Sonication has little impact on pond inventory and water chemistry. However, sonication would lysis the cells and nutrients would release back to the system and recycled by the microbial community. UV light could also be used to control cyanobacterial blooms. The mechanism is that UV light are able to change the cell shape, damage cell membranes and degrading chlorophyll (Tao *et al.*, 2010). The effect of UV treatment depends on the length of treatment and irradiation intensity. UV is not a long-term approach, it should be applied periodically as cell number starts to recover after the irradiations has been stopped (Ou et al., 2011). UV irradiation coupled with other treatments, for examples

photocatalysts, could enhance the effect of suppressing the bloom (Ou *et al.,* 2011; Metzler *et al.*, 2011). Flushing is also an effective method for algal bloom control in high nutrient concentration waters (Cooke e*t al.,* 2005). Flushing directly decreases the concentration of nutrients and cells (Pfafflin and Ziegler). The nutrient concentrations in flushing water should be lower than the water with algal culture. It is suggested that the water exchange should be at least 10% - 15% to have an obvious effect (Welch and Patmont, 1980). Flushing was reported more effective on cyanobacteria relative to algae (Hudnell *et al.,* 2010). However, during the flushing, the water might be disturbed and particles at the bottom of the water body may release, which may affect the effectiveness of the treatment (Cooke et al., 2005).

2.5. Potassium in Microorganisms

2.5.1 Roles of potassium in bacteria

Potassium is the activator of a number of cell enzymes. Ions of similar size, such as Rb^+ and NH_4^+ can replace K^+ in some situations. Monovalent cations such as Na^+ and Li^+, with smaller size but larger hydration shells present antagonization effect to K^+ activation (Suelter, 1970). Ennis and Lubin reported (1961) that protein synthesis was inhibited while DNA and RNA synthesis continued when the cell K^+ decreased and Na^+ increased in a mutant of *Escherichia coli.* The K^+ concentrations in microorganisms ranged from 18 mM in a freshwater thermophile to 4 M in a *Halobacterium halobium* (Kushner, 1978; Christian and Waltho, 1962). K^+ required for activation of enzymes is around 10 mM ((Suelter, 1970). High concentrations of K^+ generally inhibit enzymes (Kushner, 1978). K^+ has a function in controlling cell osmotic potentials. The osmotic activity of intracellular K^+ depends on the type of anion associated with K^+. K^+ associated with low molecular weight anionic compounds has higher osmotic activity than K^+ associated with large molecular weight compounds such as proteins and nucleic acids (Alexandrowicz, 1962). In bacteria, cell osmolarity is kept at a higher level than the medium.

The difference of osmotic pressure is essential for growth of bacteria and other cells with walls (Knaysi, 1951). As potassium is an important element for bacteria. Changing the environmental concentration of potassium might affect the growth of cells. Parker *et al.* (1997) reported that potassium ions strongly inhibited the growth of *Microcystis.* In terms of the FGMSP at Sellafield site, the pond was continuously flushed by NaOH buffered deionised water. Thus, in this thesis, I assessed the inhibitory effect of KOH to *P.catenata* dominated culture to justify the possibility of using KOH instead of NaOH as a pH buffer in the pond system to achieve the goals of keeping alkaline environment and bloom control simultaneously.

2.5.2 Potassium transport system

Potassium transport systems are species specific. Two potassium transport system were identified in *Streptococcus faecalis*. KtrI transports K^+ with a maximum speed around 80 μm g^{-1} min^{-1} and could transport Rb^+ in similar kinetics. ATP and Photon-motive force (PMF) were required for transport. The KtrII system is expressed in the environment with high concentration of Na^+, low concentration of K^+. It is not dependent on the PMF. The maximum velocity is around 30 μm g^{-1} min^{-1}. The KtrII system did not transport Rb^+ well (Kakinuma and Harold, 1985; Kobayashi, 1982). Another two K^+ transport system was identified in *Escherichia coli*. The Trk system is a constitutively expressed K^+ transport system. It has the lowest affinity for K^+. The Trk system can transport K^+ at 500 μm g^{-1} min^{-1}. The Kdp system has a high affinity for K^+ and is only expressed when K^+ is low. The Kpd system consists of KdpA, KdpB and KdpC proteins, wherein the KpdA subunit is important in binding K^+ for transport. Kdp is ATP dependent system, the maximum velocity is around 150 μm g^{-1} min^{-1} (Walderhaug *et al.,* 1987). Previous studies reported that Cs as an analogue of K might transported via K transport system (Avery *et al.,* 1992). Identifying the expressed K transport system and monitoring its regulation in Cs dosed conditions provided information for

understanding Cs transport and the adaption mechanism of *P.catenata* to Cs abundant environment.

2.6 Aims and objectives

As mentioned above, the decommissioning work of FGMSP was a priority at Sellafield Site. *Pseudanabaena sp.* dominated seasonal blooms were presented in the pond, which increased water turbidity and caused water visibility issues. In addition, the microbes presented in the pond increased the risk of increasing the radiation of pond water, as the mobility of radionuclides might be affected. Hence, the bloom impacted the downstream process and hindered the decommissioning work. Uncovering the adaption mechanism of the *Pseudanabaena sp.* to the radionuclides are the basis for designing the bloom control methods. And identifying the fate of radionuclides in the microbe active system might provide remediation options for radionuclides. Therefore, understanding the interactions between the most abundant radionuclides Sr and Cs in the system was crucial for making pond management strategies. Previous work had identified that the Sr could be biomineralized by *P.catenata* and form carbonate minerals. However, there was a gap in the knowledge of Cs - *P.catenata* interactions. In addition, controlling the microbial bloom in the FGMSP was another purpose of the project. As the pond was opened to air and flushed by NaOH dosed deionised water, many commonly used bloom control methods were not effective. And the nature that pond stored spent nuclear fuel rods and suspended with radionuclides also makes the designing of control methods for the bloom more challenging. Therefore, this work aims to fill the gaps that the knowledge of Cs – *P.catenata* interactions and designing the bloom control method for the *Pseudanabaena* dominated microbial bloom in the FGMSP.

2.6.1 Aims

The overall aim of this project was to understand the interactions between *Pseudanbaena* and Cs. This was achieved in chapter 4 by determining the adaptive mechanisms of *P. catenata* to Cs abundant environment and the fate of Cs in the *P.catenata* active system Further to this, the project aims to develop a bloom control method for the *Pseudanabaena* dominated FGMSP pond. This was achieved in chapter 5 by comparing the inhibitory effect between KOH and NaOH on *P.catenata* growth and identifying the impact of Na and K on cell protein expression.

Four main objectives were formulated and investigated using a wide range of techniques, including optical density, microscopy, ICP-MS, STXM, 16S rRNA gene sequencing and proteomics techniques.

2.6.2 Objectives

1. **To determine the adaptive mechanisms of *P. catenata* to a Cs abundant environment.**
   The FGMSP has an inventory of radionuclides, wherein Sr and Cs were the most abundant fission products of uranium in the FGMSP. By understanding the physiological adaptations that microorganisms use to colonize the FGMSP, a better understanding of their impact on pond management could be achieved. Here a laboratory culture of *P.catenata* was dosed with Cs and K. The effect of Cs on cell growth kinetics, cell morphology and protein expression were determined by using optical density measurement, light microscopy and proteomic tools.
2. **To identify the fate of Cs in the *P. catenata* active culture.**
   Cs is mobile in aquatic system. Identifying the fate of Cs in *P.catnata* active system provides remediation options to Cs. Inductively coupled plasma mass spectrometry (ICP-MS) and scanning transmission X-ray microscope were used to determine the mobile and

accumulated Cs respectively.

3. **To compare the inhibitory effect between NaOH and KOH on *P. catenata* growth.**

   Based on the outcome from understanding the adaption mechanism of *P. catenata* to Cs abundant environment. It is found that *P.catenata* was sensitive to K, which provides a bloom control option for *P. catenata* dominated algal bloom. Here a batch culture experiment and a chemostat experiment which simulated the pond system were used to compare the inhibitory effect between NaOH and KOH on *P. catenata* growth, which could justify the possibility of using KOH instead of NaOH as a pH buffer to keep the alkaline environment of the pond system and control the *Pseudanabaena sp.* dominated microbial bloom simultaneously. The inhibitory effect was evaluated by measuring the growth using optical density, the microbial community by using 16s rRNA gene sequencing.

4. **To identify the impact of K and Na on *P. catenata* protein expression**

   Identifying the impact of K and Na on *P.catenata* gave an insight into the mechanism of inhibitory effect of K. It was achieved by analyzing the protein expression profile of K and Na dosed culture.

2.7 Reference

Aguilar, M. I., Sáez, J., Lloréns, M., Soler, A., Ortuño, J. F., Meseguer, V., & Fuentes, A. (2005). Improvement of coagulation–flocculation process using anionic polyacrylamide as coagulant aid. Chemosphere, 58(1), 47-56.

Albi, T., & Serrano, A. (2016). Inorganic polyphosphate in the microbial world. Emerging roles for a multifaceted biopolymer. World Journal of Microbiology and Biotechnology, 32(2), 27.

Alexandrowicz, Z. (1962). Osmotic and Donnan equilibria in polyacrylic acid–sodium bromide solutions. Journal of Polymer Science, 56(163), 115-132.

Anderson, S., & Appanna, V. D. (1994). Microbial formation of crystalline strontium carbonate. FEMS Microbiology Letters, 116(1), 43-48.

Angel, M. V. (1983). Are there any potentially important routes whereby radionuclides can be transferred by biological processes from the sea-bed towards the surface. In Ecological aspects of radionuclide release.

Ahn, C. Y., Park, M. H., Joung, S. H., Kim, H. S., Jang, K. Y., & Oh, H. M. (2003). Growth inhibition of cyanobacteria by ultrasonic radiation: laboratory and enclosure studies. Environmental science & technology, 37(13), 3031-3037.

Avery, S. V. (1996). Fate of caesium in the environment: distribution between the abiotic and biotic components of aquatic and terrestrial ecosystems. Journal of Environmental Radioactivity, 30(2), 139-171.

Avery, S. V., Codd, G. A., & Gadd, G. M. (1992). Interactions of cyanobacteria and microalgae with caesium. Impact of Heavy Metals on the Environment, 133-182.

Avery, S. V., & Tobin, J. M. (1993). Mechanism of adsorption of hard and soft metal ions to *Saccharomyces cerevisiae* and influence of hard and soft anions. Applied and

Environmental Microbiology, 59(9), 2851-2856.

Baxter, M., & Jensen, T. (1980). Uptake of magnesium, strontium, barium, and manganese by *Plectonema boryanum* (Cyanophyceae) with special reference to polyphosphate bodies. Protoplasma, 104(1-2), 81-89.

Bossemeyer, D. I. R. K., Schlösser, A., & Bakker, E. P. (1989). Specific cesium transport via the *Escherichia coli* Kup (TrkD) K+ uptake system. Journal of bacteriology, 171(4), 2219-2221.

Brooks, S. C., Herman, J. S., Hornberger, G. M., & Mills, A. L. (1998). Biodegradation of cobalt–citrate complexes: Implications for cobalt mobility in groundwater. Journal of contaminant hydrology, 32(1), 99-115.

Cam, N., Georgelin, T., Jaber, M., Lambert, J. F., & Benzerara, K. (2015). In vitro synthesis of amorphous Mg-, Ca-, Sr-and Ba-carbonates: what do we learn about intracellular calcification by cyanobacteria? Geochimica et Cosmochimica Acta, 161, 36-49.

Chicote, E., Moreno, D. A., Garcia, A. M., Sarro, M. I., Lorenzo, P. I., & Montero, F. (2004). Biofouling on the walls of a spent nuclear fuel pool with radioactive ultrapure water. Biofouling, 20(1), 35-42.

Christensen, B. E., & Characklis, W. G. (1990). Physical and chemical properties of biofilms. Biofilms, 93, 130.

Christian, J. H. B., & Waltho, J. A. (1962). Solute concentrations within cells of halophilic bacteria.

Clint, G. M., Harrison, A. F., & Howard, D. M. (1992). Rates of leaching of ^{137}Cs and potassium from different plant litters. Journal of environmental radioactivity, 16(1), 65-76.

Cooke, G. D., Welch, E. B., Peterson, S., & Nichols, S. A. (2016). Restoration and management

of lakes and reservoirs. CRC press.

Costerton, J. W., Cheng, K. J., Geesey, G. G., Ladd, T. I., Nickel, J. C., Dasgupta, M., & Marrie, T. J. (1987). Bacterial biofilms in nature and disease. Annual Reviews in Microbiology, 41(1), 435-464.

Costerton, J. W., Lewandowski, Z., Caldwell, D. E., Korber, D. R., & Lappin-Scott, H. M. (1995). Microbial biofilms. Annual review of microbiology, 49(1), 711-745.

Dekker, L., Osborne, T. H., & Santini, J. M. (2014). Isolation and identification of cobalt-and caesium-resistant bacteria from a nuclear fuel storage pond. FEMS microbiology letters, 359(1), 81-84.

Ewing, R. C. (2015). Long-term storage of spent nuclear fuel. Nature Materials, 14(3), 252-257.

Ehrlich, H. L., & Brierley, C. L. (1990). Microbial mineral recovery. McGraw-Hill, Inc.

Fortin, D., Davis, B., Southam, G., & Beveridge, T. J. (1995). Biogeochemical phenomena induced by bacteria within sulfidic mine tailings. Journal of Industrial Microbiology, 14(2), 178-185.

Ennis, H. L., & Lubin, M. (1961). Dissociation of ribonucleic acid and protein synthesis in bacteria deprived of potassium. Biochimica et biophysica acta, 50(2), 399-402.

Fan, J., Ho, L., Hobson, P., & Brookes, J. (2013a). Evaluating the effectiveness of copper sulphate, chlorine, potassium permanganate, hydrogen peroxide and ozone on cyanobacterial cell integrity. Water research, 47(14), 5153-5164.

Fan, J., Daly, R., Hobson, P., Ho, L., & Brookes, J. (2013b). Impact of potassium permanganate on cyanobacterial cell integrity and toxin release and degradation. Chemosphere, 92(5), 529-534.

Fan, J., Hobson, P., Ho, L., Daly, R., & Brookes, J. (2014). The effects of various control and water treatment processes on the membrane integrity and toxin fate of cyanobacteria. Journal of hazardous materials, 264, 313-322.

Farooq, S., Engelbrecht, R. S., & Chian, E. S. (1977). Influence of temperature and UV light on disinfection with ozone. Water Research, 11(8), 737-741.

Foster, L., Boothman, C., Ruiz-Lopez, S., Boshoff, G., Jenkinson, P., Sigee, D., ... & Lloyd, J. R. (2020). Microbial bloom formation in a high pH spent nuclear fuel pond. Science of The Total Environment, 720, 137515.

Francis, A. J., Dodge, C. J., & Gillow, J. B. (1992). Biodegradation of metal citrate complexes and implications for toxic-metal mobility. Nature, 356(6365), 140-142.

Gadd, G. M. (1992). Metals and microorganisms: a problem of definition. FEMS Microbiology Letters, 100(1-3), 197-203.

Gadd, G. M. (1996). Influence of microorganisms on the environmental fate of radionuclides. Endeavour, 20(4), 150-156.

Gavand, M. R., McClintock, J. B., Amsler, C. D., Peters, R. W., & Angus, R. A. (2007). Effects of sonication and advanced chemical oxidants on the unicellular green alga *Dunaliella tertiolecta* and cysts, larvae and adults of the brine shrimp *Artemia salina*: a prospective treatment to eradicate invasive organisms from ballast water. Marine pollution bulletin, 54(11), 1777-1788.

Ghosh, A., Sharma, A., & Talukder, G. (1993). Effects of cesium on cellular systems. Biological trace element research, 38(2), 165-203.

Gregson, C. R., Goddard, D. T., Sarsfield, M. J., & Taylor, R. J. (2011). Combined electron microscopy and vibrational spectroscopy study of corroded Magnox sludge from a legacy spent nuclear fuel storage pond. Journal of Nuclear Materials, 412(1), 145-156.

Hong, J., & Otaki, M. (2006). Association of photosynthesis and photocatalytic inhibition of algal growth by TiO2. Journal of bioscience and bioengineering, 101(2), 185-189.

Hudnell, H. K., Jones, C., Labisi, B., Lucero, V., Hill, D. R., & Eilers, J. (2010). Freshwater harmful algal bloom (FHAB) suppression with solar powered circulation (SPC). Harmful Algae, 9(2), 208-217.

Hughes, M. N., & Poole, R. K. (1991). Metal speciation and microbial growth—the hard (and soft) facts. Microbiology, 137(4), 725-734.

Jackson, S. F., Monk, S. D., & Riaz, Z. (2014). An investigation towards real time dose rate monitoring, and fuel rod detection in a First Generation Magnox Storage Pond (FGMSP). Applied Radiation and Isotopes, 94, 254-259.

John, S. G., Ruggiero, C. E., Hersman, L. E., Tung, C. S., & Neu, M. P. (2001). Siderophore mediated plutonium accumulation by *Microbacterium flavescens (JG-9)*. Environmental science & technology, 35(14), 2942-2948.

Johnson, E. E., O'Donnell, A. G., & Ineson, P. (1991). An autoradiographic technique for selecting Cs-137-sorbing microorganisms from soil. Journal of microbiological methods, 13(4), 293-298.

Jones, R. P., & Gadd, G. M. (1990). Ionic nutrition of yeast—physiological mechanisms involved and implications for biotechnology. Enzyme and Microbial Technology, 12(6), 402-418.

Kakinuma, Y., & Harold, F. M. (1985). ATP-driven exchange of Na+ and K+ ions by Streptococcus faecalis. Journal of Biological Chemistry, 260(4), 2086-2091.

Kim, D. W., Cha, D. K., Wang, J., & Huang, C. P. (2002). Heavy metal removal by activated sludge: influence of *Nocardia amarae*. Chemosphere, 46(1), 137-142.

Knaysi, G. (1945). Elements of bacterial cytology. AJN The American Journal of Nursing, 45(2), 166.

Kobayashi, H. I. R. O. S. H. I. (1982). Second system for potassium transport in *Streptococcus faecalis*. Journal of bacteriology, 150(2), 506-511.

Kushner, D. J. (1978). Life in high salt and solute concentrations: halophilic bacteria. Microbial life in extreme environments.

Landa, E. R., & Gray, J. R. (1995). US Geological Survey research on the environmental fate of uranium mining and milling wastes. Environmental Geology, 26(1), 19-31.

Kim, S. C., & Lee, D. K. (2005). Preparation of TiO2-coated hollow glass beads and their application to the control of algal growth in eutrophic water. Microchemical Journal, 80(2), 227-232.

Li, H., Yao, C., Dong, X., Dong, W. and Fan, Z. (2011) 'Effect of pH on inactivation of *Microcystis aeruginosa* by ozonation air in sequencing batch reactor', Journal of Chemical Technology & Biotechnology, 86(3), pp. 468-471.

Little, B., & Wagner, P. (1996). An overview of microbiologically influenced corrosion of metals and alloys used in the storage of nuclear wastes. Canadian journal of microbiology, 42(4), 367-374.

Lloyd, J.R. & Renshaw, J.C. (2005) Bioremediation of radioactive waste: radionuclide-microbe interactions in laboratory and field-scale studies. Current Opinions in Biotechnology. 16: 254-260.

Lovley, D. R. (1993). Dissimilatory metal reduction. Annual review of microbiology, 47(1), 263-290.

Lovley, D. R. (1995). Bioremediation of organic and metal contaminants with dissimilatory

metal reduction. Journal of industrial microbiology, 14(2), 85-93.

Foster, L., Cleary, A., Bagshaw, H., Sigee, D., Pittman, J. K., Morris, K., ... & Vettese, G. (2020). Biomineralization of Sr by the cyanobacterium *Pseudanabaena catenata* under alkaline conditions. Frontiers in Earth Science, 8.

Mason, T. J., & Lorimer, J. P. (2002). Applied sonochemistry: the uses of power ultrasound in chemistry and processing (Vol. 10). Weinheim: Wiley-Vch.

Masurat, P., Fru, E. C., & Pedersen, K. (2005). Identification of *Meiothermus* as the dominant genus in a storage system for spent nuclear fuel. Journal of applied microbiology, 98(3), 727-740.

Meesters, K. P. H., Van Groenestijn, J. W., & Gerritse, J. (2003). Biofouling reduction in recirculating cooling systems through biofiltration of process water. *Water Research*, *37*(3), 525-532.

Metzler, D. M., Li, M., Erdem, A., & Huang, C. P. (2011). Responses of algae to photocatalytic nano-TiO2 particles with an emphasis on the effect of particle size. Chemical Engineering Journal, 170(2-3), 538-546.

Morley, G. F., Sayer, J. A., Wilkinson, S. C., Gharieb, M. M., & Gadd, G. M. (1996). Fungal sequestration, mobilization and transformation of metals and metalloids. In Fungi and environmental change: symposium of the British Mycological Society, held at Cranfield University, March 1994. Cambridge [England]; New York: Published for the British Mycological Society [by] Cambridge University Press, 1996.

Nakano, K., Lee, T. J., & Matsumura, M. (2001). In situ algal bloom control by the integration of ultrasonic radiation and jet circulation to flushing. Environmental science & technology, 35(24), 4941-4946.

NDA (2002), Managing the nuclear legacy—a strategy for action, Whitepaper of the UK

Nuclear Decommissioning Authority. Available at: http://webarchive.nationalarchives.gov.uk/+/http:/www.dti.gov.uk/nuclearcleanup/ach/whitepaper.pdf. Last accessed: 12/05/2021.

NDA, (2015) Nuclear Decommissioning Authority. Available at: http://www.nda.gov.uk/. Last accessed: 12/05/2021.

Pattanapipitpaisal, P., Mabbett, A. N., Finlay, J. A., Beswick, A. J., Paterson-Beedle, M., Essa, A., Wright, J., Tolley, M. R., Badar, U., Ahmed, N., Hobman, J. L., Brown, N. L. & Macaskie, L. E. (2002). Reduction of Cr (VI) and bioaccumulation of chromium by Gram positive and Gram-negative microorganisms not previously exposed to Cr-stress. Environmental technology, 23(7), 731-745.

Ou, H., Gao, N., Deng, Y., Qiao, J., Zhang, K., Li, T., & Dong, L. (2011). Mechanistic studies of *Microcystic aeruginosa* inactivation and degradation by UV-C irradiation and chlorination with poly-synchronous analyses. Desalination, 272(1-3), 107-119.

Peller, J. R., Whitman, R. L., Griffith, S., Harris, P., Peller, C., & Scalzitti, J. (2007). TiO2 as a photocatalyst for control of the aquatic invasive alga, *Cladophora*, under natural and artificial light. Journal of Photochemistry and Photobiology A: Chemistry, 186(2-3), 212-217.

Peterson, H. G., Hrudey, S. E., Cantin, I. A., Perley, T. R., & Kenefick, S. L. (1995). Pfafflin, J. R., & Ziegler, E. N. (Eds.). (1992). Encyclopedia of environmental science and engineering (Vol. 1). Taylor & Francis.

Physiological toxicity, cell membrane damage and the release of dissolved organic carbon and geosmin by *Aphanizomenon flos-aquae* after exposure to water treatment chemicals. Water Research, 29(6), 1515-1523.

Poinssot, C., & Geckeis, H. (Eds.). (2012). Radionuclide behaviour in the natural environment:

science, implications and lessons for the nuclear industry. Elsevier.

Rivasseau, C., Farhi, E., Atteia, A., Couté, A., Gromova, M., Saint Cyr, D. D. G., ... & Bligny, R. (2013). An extremely radioresistant green eukaryote for radionuclide bio-decontamination in the nuclear industry. Energy & Environmental Science, 6(4), 1230-1239.

Rajasekhar, P., Fan, L., Nguyen, T., & Roddick, F. A. (2012). A review of the use of sonication to control cyanobacterial blooms. Water research, 46(14), 4319-4329.

Roth, J. A., & Sullivan, D. E. (1981). Solubility of ozone in water. Industrial & Engineering Chemistry Fundamentals, 20(2), 137-140.

Rusin, P. A., Quintana, L., Brainard, J. R., Strietelmeier, B. A., Tait, C. D., Ekberg, S. A., ... & Clark, D. L. (1994). Solubilization of plutonium hydrous oxide by iron-reducing bacteria. Environmental science & technology, 28(9), 1686-1690.

Sarró, M. I., Moreno, D. A., Chicote, E., Lorenzo, P. I., García, A. M., & Montero, F. (2003). Biofouling on austenitic stainless steels in spent nuclear fuel pools. Materials and Corrosion, 54(7), 535-540.

Sarró, M. I., García, A. M., & Moreno, D. A. (2005). Biofilm formation in spent nuclear fuel pools and bioremediation of radioactive water. International microbiology, 8(3), 223-230.

Schmack, M., Chambers, J., & Dallas, S. (2012). Evaluation of a bacterial algal control agent in tank-based experiments. Water research, 46(7), 2435-2444.

Schultze-Lam, S., & Beveridge, T. J. (1994). Nucleation of celestite and strontianite on a cyanobacterial S-layer. Applied and Environmental Microbiology, 60(2), 447-453.

Sellafield Ltd. (2016) Sellafield Ltd. Available at: https://www.gov.uk/government/publications/sellafield-magazine-issue-4. Last accessed

12/05/2021.

Simonoff, M., Sergeant, C., Poulain, S., & Pravikoff, M. S. (2007). Microorganisms and migration of radionuclides in environment. Comptes Rendus Chimie, 10(10-11), 1092-1107.

Sigee, D. (2005). Freshwater microbiology: biodiversity and dynamic interactions of microorganisms in the aquatic environment. John Wiley & Sons.

Song, J. J., Cho, S. H., Lee, S. W., Kim, T. H., & Hayashi, Y. (2007). Removing algae with Pt-doped TiO2 coatings on foamed glass. In Materials science forum (Vol. 544, pp. 135-138). Trans Tech Publications Ltd.

Suelter, C. H. (1970). Enzymes activated by monovalent cations. Science, 168(3933), 789-795.

Suslick, K. S. (1990). Sonochemistry. science, 247(4949), 1439-1445.

Tang, J. W., Wu, Q. Y., Hao, H. W., Chen, Y., & Wu, M. (2004). Effect of 1.7 MHz ultrasound on a gas-vacuolate cyanobacterium and a gas-vacuole negative cyanobacterium. Colloids and Surfaces B: Biointerfaces, 36(2), 115-121.

Tao, Y., Zhang, X., Au, D. W., Mao, X., & Yuan, K. (2010). The effects of sub-lethal UV-C irradiation on growth and cell integrity of cyanobacteria and green algae. Chemosphere, 78(5), 541-547.

Tišáková, L. E. N. K. A., Pipíška, M. A. R. T. I. N., Godány, A. N. D. R. E. J., Horník, M. I. R. O. S. L. A. V., Vidová, B., & Augustín, J. (2013). Bioaccumulation of 137 Cs and 60 Co by bacteria isolated from spent nuclear fuel pools. Journal of Radioanalytical and Nuclear Chemistry, 295(1), 737-748.

Turner, J. S., & Robinson, N. J. (1995). Cyanobacterial metallothioneins: biochemistry and molecular genetics. Journal of industrial microbiology, 14(2), 119-125.

UN DESA (2017), World population projected to reach 9.8 billion in 2050, and 11.2 billion in 2100. Available at: https://www.un.org/development/desa/en/news/population/world-population-prospects-2017.html. Last Accessed: 12/05/2021.

U.S.NRC (2021) Stages of the nuclear fuel cycle. United States Nuclear Regulatory Commission. Available at: https://www.nrc.gov/materials/fuel-cycle-fac/stages-fuel-cycle.html. Last Accessed: 12/05/2021.

Van Veen, H. W., Abee, T., Kortstee, G. J., Konings, W. N., & Zehnder, A. J. (1994). Translocation of metal phosphate via the phosphate inorganic transport system of Escherichia coli. Biochemistry, 33(7), 1766-1770.

Walderhaug, M. O., Dosch, D. C., & Epstein, W. (1987). Potassium transport in bacteria. In Ion transport in prokaryotes (pp. 85-130). Academic Press.

Welch, E. B., & Patmont, C. R. (1980). Lake restoration by dilution: Moses lake, Washington. Water Research, 14(9), 1317-1325.

Wendling, L. A., Douglas, G. B., Coleman, S., & Yuan, Z. (2013). Nutrient and dissolved organic carbon removal from natural waters using industrial by-products. Science of the total environment, 442, 63-72.

White, C., & Gadd, G. M. (1996). A comparison of carbon/energy and complex nitrogen sources for bacterial sulphate-reduction: potential applications to bioprecipitation of toxic metals as sulphides. Journal of industrial microbiology, 17(2), 116-123.

Wilson, P. D. (1996). The nuclear fuel cycle from ore to wastes.

Witkamp, M., & Frank, M. L. (1970). Effects of Temperature, Rainfall, and Fauna on Transfer of (137) CS, K, MG, and Mass in Consumer-Decomposer Microcosms. Ecology, 51(3), 465-474.

WNA (2012) The Nuclear Fuel Cycle. World Nuclear Association. Available at: https://www.world-nuclear.org/information-library/nuclear-fuel-cycle/introduction/energy-for-the-world-why-uranium.aspx. Last Accessed: 12/05/2021

Wu, X., Joyce, E. M., & Mason, T. J. (2012). Evaluation of the mechanisms of the effect of ultrasound on *Microcystis aeruginosa* at different ultrasonic frequencies. Water research, 46(9), 2851-2858.

Xu, Y., Yang, J. I., Wang, Y., Liu, F., & Jia, J. (2006). The effects of jet cavitation on the growth of *Microcystis aeruginosa*. Journal of Environmental Science and Health, Part A, 41(10), 2345-2358.

Zhang, G., Wang, B., Zhang, P., Wang, L., & Wang, H. (2006). Removal of algae by sonication-coagulation. Journal of Environmental Science and Health, Part A, 41(7), 1379-1390.

Zhang, G., Zhang, P., & Fan, M. (2009). Ultrasound-enhanced coagulation for *Microcystis aeruginosa* removal. Ultrasonics sonochemistry, 16(3), 334-338.

Chapter 3 Methodology

3.1 Measurement of *Pseudanabaena catenata* growth

Because the radiological safety limitations prevented obtaining organisms directly from water from the Spent Nuclear Fuel Pond (SNFP), the closest related strain to the *Pseudanabaena* sp. Identified from the pond was obtained from a stock centre: *Pseudanabaena catenata* was obtained from the NIVA Culture Collection of Algae (NIVA-CYA 152 *Pseudanabaena catenata* Helbig's Pond, Warburg, Alberta, Edmonton, Canada, 1980-07) and was used as a representative culture for the pond system. An axenic culture of *P. catenata* was not available, and the culture used in this thesis was a mixed community and also contained other bacteria taxa (Foster et al., 2020). The *P. catenata* genome has been sequenced by Dr Lynn Foster (University of Manchester Geomicrobiology Group), and the amino acid sequence was used as a database for the proteomics analysis. The mixed community contained several bacterial genera that were also present in the FGMSP, therefore the culture is highly representative of the microbial community in the pond (Foster et al., 2020).

Cultures were grown in BG-11 medium (Appendix 1). All batch cultures were incubated in a light cabinet with light intensity of 30 μmol m^{-2} s^{-1} on a 16:8 h light-dark cycle, and were shaken at 140 rpm. The temperature was set to 20 ± 1 °C. Lights used in the batch culture experiment are LED lights. For the chemostat experiment, cells were grown in a PG-120 growth tent (Progrow, UK) with light intensity of 30 μmol m^{-2} s^{-1} with 16:8 h light-dark regime on a magnetic stirrer (Fisher Scientific Isotemp, China) operating at 50 rpm. The lights used in the chemostat are fluorescent lights. The growth of the *P. catenata* was monitored by measuring the optical density at 600 nm (OD_{600}).

3.2 Cell morphology

Cell morphology was observed by using a Zeiss Imager A1 microscope (Carl Zeiss International) fitted with an Axiocam 506 mono camera using Zen2 imaging software. The length and width of *P. catenata* cells were measured using ImageJ software. By comparing the cell morphology in control, K and Cs dosed culture justified the impact of Cs on cell morphology, the results were shown in chapter 4.

3.3 Scanning transmission X-ray microscope

3.3.1 Description of STXM

A simplified view of STXM is shown in **Figure 3.1**. The X-ray from the synchrotron source is focused by the Fresnel zone plate. The focal point is 50 nm in diameter over a 3 – 10 μm waist. The X-ray raster-scans through a thin section of a sample. The transmitted signal is measured by single photon counting using counting periods of 0.2-0.5 ms per pixel for imaging. The detailed chemical analysis can be achieved by taking a series of images at energies around the absorption edge of interest (Koprinarov and Hitchcock, 2000).

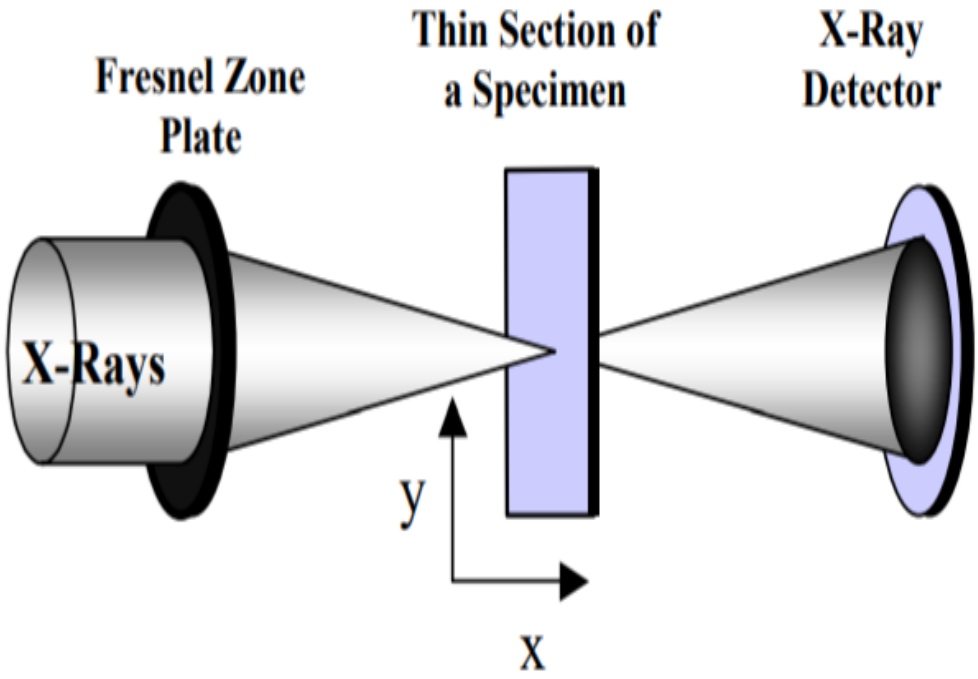

Figure 3.1 Schematic scanning x-ray transmission microscope (STXM) (Koprinarov and Hitchcock, 2000)

3.3.2 Near Edge X-ray Absorption Fine Structure (NEXAFS)

When the X-ray passes through substance, it is absorbed to some extent. The absorbed photons induced excitation of the inner shell electrons of the atoms in the substance.

A short-lived excited state or ionized state are formed, as the excited inner shell electrons are promoted to unoccupied energy levels. X-ray absorption spectroscopy is described in terms of absorption edges (**Figure 3.2**), all elements have an X-ray absorption edge in the energy range of 100 – 1200 eV. NEXAFS spectra are different even for similar structures (**Figure 3.3**). Therefore, NEXAFS spectrum can be used to identify organic polymers. Finally, comparisons with NEXAFS spectra of pure standards provides a method to quantitative composition maps of a complex material from a series of X-ray microscopy images (Koprinarov and Hitchcock, 2000).

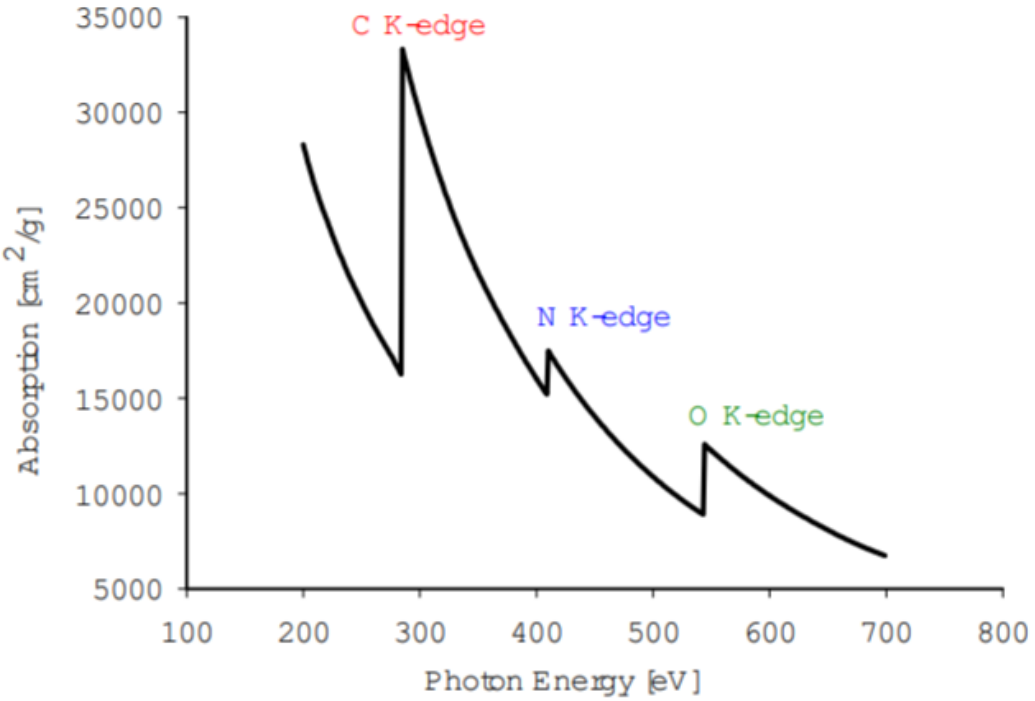

Figure 3.2 X-ray absorption edges of carbon, nitrogen and oxygen (Koprinarov and Hitchcock, 2000)

For our experiment, STXM were used to identify the distribution of cell accumulated Cs. Cells from the control, 1 ml Cs and 1 mM Cs + 2.5 mM K cultures were analysed by STXM. 1 ml of culture sample was taken after 10 days incubation. Samples were centrifuged at 14000 x *g* for 10 minutes. Supernatant was removed and pellets were washed with deionised water. 0.2 µl of washed samples were placed on a Formvar/Carbon Film 200 mesh Cu grid and stored in a desiccator. STXM images were measured at Dimond Light Source Ltd using the I08 beamline. Carbon K-edge (280-320 eV) stack images were collected using the following settings: 280-283 eV, 0.5 eV energy step; 283 - 290 eV, 0.1 eV energy step; 290 - 293 eV, 0.2 eV energy step; 293 - 295 eV, 0.5 eV energy step; 295 - 303eV, 0.2 eV energy step; 303 - 320 eV, 0.5 eV

energy step. Sequenced images were then collected at the Cs M-edge (720 - 745 eV) by using the following settings: 720 – 728 eV, 1 eV energy step; 728.5 – 740 eV, 0.5 eV energy step; 740 – 745 eV, 1 eV energy step. Data processing was performed by using the aXis 2000 software package. Results were shown in chapter 4

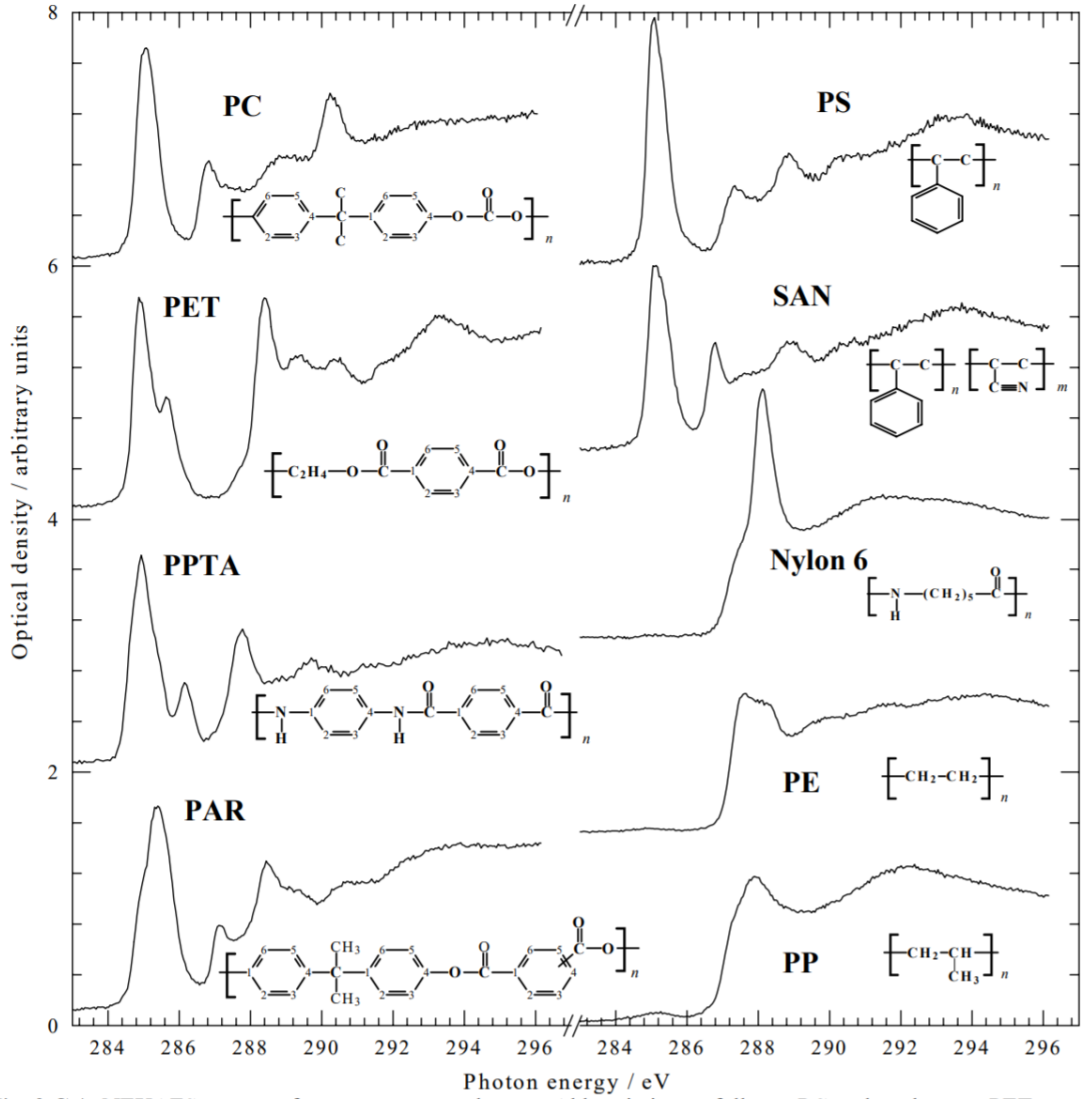

Figure 3.3 NEXAFS spectra of common polymers. PC, polycarbonate; PET, poly (ethylene terephthalate); PPTA, poly (**p-phenylene terephthalamide); PAR, polyacrylate; PS, polystyrene; SAN, styrene-acrylonitrile; Nylon-6, poly(ε-caprolactam); PP, polypropylene; PE, polyethylene (Koprinarov and Hitchcock, 2000)**

3.4 Inductively coupled plasma mass spectrometry (ICP-MS)

Total Cs, K and Na concentrations were measured by Inductively coupled plasma mass spectrometry (ICP-MS). 1 mM of samples were centrifuged for 10 minutes to separate cells and supernatants. 100 μL of supernatant was then added to 9.9 ml of 2% nitric acid for ICP-MS analysis. In the ICP-MS, the inductively coupled plasma atomizes the sample and creates atomic ions. The ions from inductively coupled plasma are extracted and then separated on the basis of their mass to charge ratio. The ion signal is proportional to the concentration. The concentration of a sample is determined by calibration with reference materials. In chapter 4, ICP-MS were used to identify the mobile Cs, coupled with the accumulated Cs identified by STXM, the objective that identify the fate of Cs in *P.catenata* active system was achieved. In chapter 5, ICP-MS used to trace the concentration of K and Na.

3.5 16S rRNA Gene Sequencing

16S rRNA gene sequencing is a commonly used tool for identification, classification and quantitation of prokaryotic microorganisms in biological samples (Schmidt *et al.,* 1991). The 16S rRNA gene is highly conserved in all prokaryotes (Cox *el al.*, 2013). The 16S rRNA gene contains variable and conserved regions (**Figure 3.4**). The conserved regions of 16S rRNA gene can be targeted by Universal PCR primers and the gene can be amplified. The variable regions are used for discrimination of different microorganisms. In this thesis, 16S rRNA gene sequencing was applied in chapter 5 to identify the change of microbial community before and after the system were continuously flushed by KOH and NaOH dosed medium. In addition, the differences between KOH and NaOH flushed system were used to estimate the inhibitory effect of KOH and NaOH to the *P.catenata* dominated culture.

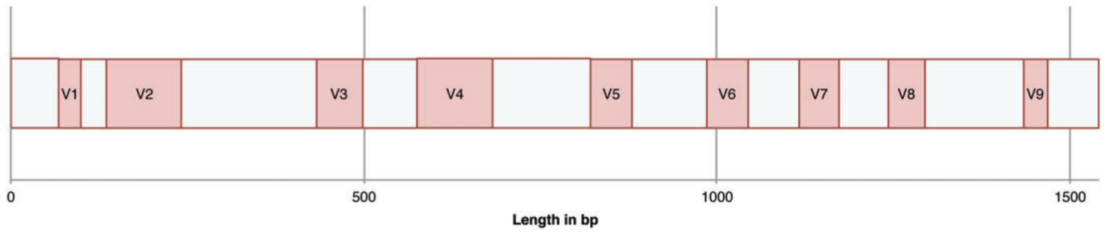

Figure 3.4 16S RNA gene of *Escherichia coli* showing nine variable regions

DNA was extracted from 200 µl of sample using a DNAeasy PowerSoil Pro Kit (Qiagen, Manchester, U.K). Sequencing of PCR amplicons of 16S rRNA genes were conducted with the Illumina MiSeq platform (Illumina, San Diego, CA, USA) targeting the V4 hyper variable region (forward primer, 515F, 5′-GTGYCAGCMGCCGCGGTAA-3′; reverse primer, 806R, 5′-GGACTACHVGGGTWTCTAAT-3′) for 2 × 250-bp paired-end sequencing (Illumina). PCR amplification was performed using Roche FastStart High Fidelity PCR System (Roche Diagnostics Ltd, Burgess Hill, UK) in 50 µl reactions under the following conditions: initial denaturation at 95°C for 2 min, followed by 36 cycles of 95°C for 30 s, 55°C for 30 s, 72°C for 1 min, and a final extension step of 5 min at 72°C (Caporaso et al., 2011; Caporaso et al., 2012). The PCR products were purified and normalised to ~20 ng each using the SequalPrep Normalization Kit (Fisher Scientific, Loughborough, UK). The PCR amplicons from all samples were pooled in equimolar ratios. The run was performed using a 4.5 pM sample library spiked with 4.5 pM PhiX to a final concentration of 12% following the method of Kozich et al (2013).

Raw sequences were divided into samples by barcodes (up to one mismatch was permitted) using a sequencing pipeline. Quality control and trimming was performed using Cutadapt,

FastQC and Sickle (Martin, 2011; Joshi and Fass, 2011). MiSeq error correction was performed using SPADes (Nurk et al., 2013). Forward and reverse reads were incorporated into full-length sequences with Pandaseq, and chimeras were removed using ChimeraSlayer (Hass et al., 2011).

For the 16S rRNA gene sequences, Operational Taxonomic Units (OTUs) were generated with UPARSE (Masella et al., 2012; Edgar, 2013). OTUs were classified by Usearch at the 97% similarity level, and singletons were removed (Edgar, 2010). Rarefaction analysis was conducted using the original detected OTUs in Qiime (Caporaso et al., 2010). The taxonomic assignment was performed by the RDP naïve Bayesian classifier version 2.2, used in combination with the Silva SSU 132 ribosomal RNA gene database (Wang et al., 2007; Quast et al., 2013). The OTU tables were rarefied to the sample containing the lowest number of sequences, all samples having less than 5,000 sequences were removed from analyses prior to the rarefaction step. The step size used was 2000 and 10 iterations were performed at each step.

3.6 Molecular biology- Cell lysis, Protein Extraction, Identification and Quantification

3.6.1 Cell lysis

Samples were centrifuged at 14000 x *g* for 10 minutes. Supernatant was removed and cell pellets were refined with 130 µl lysis buffer (5% SDS with 50 mM TEAB pH 7.5). Samples were then lysed using a LE220-plus Focused-ultrasonicator with the following parameters, peak power: 500 W, duty factor: 40%, cycle/burst: 200, average power 200 W. Each sample was lysed for 600 seconds.

3.6.2 Protein Extraction

S-Trap sample processing technology is a method that use SDS in S - Trap columns or 96-well plates for proteomics sample preparation. SDS is a universal protein solvent that can support the dissolve of poorly soluble membrane proteins. S -Trap protein extraction starts with the lysed cell samples in 5% SDS. Samples were further denatured by acidification to pH<1 and exposure to high concentration of methanol. These 3 steps damaged any enzymatic activity. Then, sample is alkylated and reduced in 5% SDS. Denatured proteins bond to the silica S-Trap with maximum surface area by centrifugation. Contaminants can be easily washed out later. Then protease was added to the S-Trap column for digestion. Peptides were the final product in protein extraction (**Figure 3.5**) (Protifi, 2021).

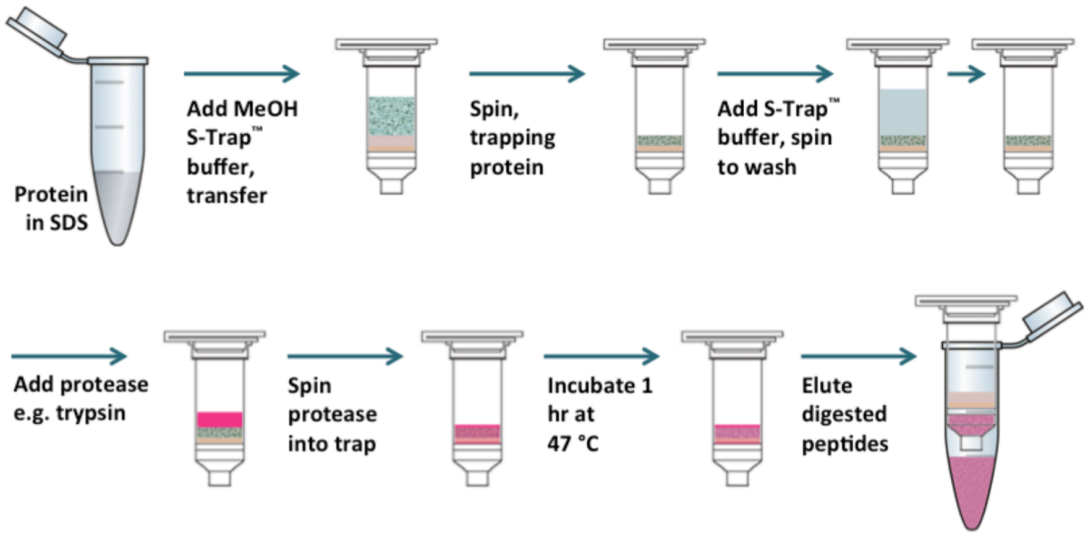

Figure 3.5 Schematic of the protocol for protein extraction using S-trap coloumn (Protifi, 2021)

3.6.3 Protein Identification and Quantitation

Liquid Chromatography- mass spectrometry (LC-MS) is an analytical chemistry technique that combines liquid chromatography and mass spectrometry (**Figure 3.6**). Liquid chromatography

is a physical separation method which distributed the liquid mixture into a mobile and stationary phase. When analytes were injected, it is distributed on the stationary, and solvent passes through the column to separate the compounds one by one based on their relative affinity to the packing materials and the solvent, the component with the most affinity to the stationary phase is the last to separate. The separated sample species are then sprayed into an atmospheric pressure ion source (API) where the compounds are converted to ions in the gas phase. The ions were sent to the mass spectrometry and be determined by mass to charge ratio (Chemyx, 2021). Proteins were identified and quantified by search the spectra from the LC-MS against referenced amino acid database. The proteomic tools gave a landscape of all expressed proteins and their regulations under specific conditions (Stalmach *et al.*, 2015). Differences between physiological states at cellular level are reflected by the state and expression level of all proteins. Therefore, the mechanism that *P.catenata* adapted to Cs abundant environment was identified by using proteomic tools in chapter 4. And the impact of K and Na on *P.catenata* protein expression level was justified by applying proteomic tools in chapter 5.

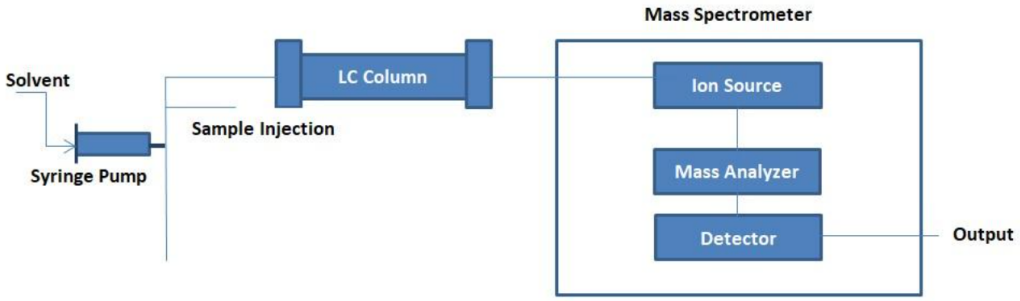

Figure 3.6 Schematic of LC-MS system (Chemyx, 2021)

3.6.4 Workflow of proteomics study in this project

The workflow of the proteomics study in this project is shown in **Figure 3.7** Samples of 1 ml volume were taken at day 10 of the incubation. Samples were centrifuged at 14000 x *g* for 10

minutes. Supernatant was removed and cell pellets were refined with 130 µl lysis buffer (5% SDS with 50 mM TEAB pH 7.5). Samples were then lysed using a LE220-plus Focused-ultrasonicator with the following parameters, peak power: 500 W, duty factor: 40%, cycle/burst: 200, average power 200 W. Each sample was lysed for 600 seconds.

Figure 3.7 Workflow for proteomics study

Lysed samples were reduced and alkylated with dithiothreitol and iodoacetamide. Protein concentrations were quantified by using the Millipore Direct Detect system. Protein concentrations were then normalized to 1 mg/l for subsequent protein extraction. 5 µl of 12% aqueous phosphoric acid was added to 50 ml (50 µg) protein lysate. 330 µl of S-Trap binding buffer (90% aqueous methanol containing a final concentration of 100 mM TEAB, pH 7.1) was added to acidified protein lysate and mixed. Protein solutions were loaded onto a S-Trap column (PROTIFI) and centrifuged at 4000 RCF for 2 mins, and then the S-Trap column were washed with 150 µl S-Trap binding buffer 4 times. 20 µl of digestion buffer (50 mM triethylammonium bicarbonate) and 20 µl of 0.25 µg/µl trypsin were added to the S-Trap column and incubated at 47 °C for 1 hour. 3 washes with 65 µl digestion buffer, 65 µl of 0.1% aqueous formic acid and 30 µl of 30% aqueous acetonitrile containing 0.1% formic acid were

applied in order to elute peptides. For sample desalination, the digested sample solutions were moved to a Corning FiltrEX desalt filter plates and mixed them with pre-washed beads for 5 mins at 800 RPM. Liquids were removed by centrifuging at 200 x *g* for 1 minute. The wells with beads in were then washed by using 0.1% formic acid twice. Then the peptides were extracted to by 2 washes with 50 µl 0.1% formic acid in 30% acetonitrile. 100 µl peptides solutions were transferred to sample vials and dried in Heto vacuum centrifuge. Dried samples were kept in a freezer at -20 °C for subsequent analysis.

Digested samples were analysed by Liquid chromatography–mass spectrometry (LC-MS/MS) using an UltiMate® 3000 Rapid Separation LC (RSLC, Dionex Corporation, Sunnyvale, CA) coupled to a QE-HF (Thermo Fisher Scientific, Waltham, MA) mass spectrometer. Mobile phase A was 0.1% formic acid in water and mobile phase B was 0.1% formic acid in acetonitrile and the column used was a 75 mm x 250 µm i.d. 1.7 µm CSH C18, analytical column (Waters). A 1 µl aliquot of the sample was transferred to a 5 µl loop and loaded on to the column at a flow of 300 nl/min for 5 minutes at 5% mobile phase B. The loop was then taken out of line and the flow was reduced from 300 nl/min to 200 nl/min in 0.5 min. Peptides were separated using a gradient that went from 5% to 18% mobile phase B in 34.5 min, then from 18% to 27% mobile phase B in 8 min and finally from 27% mobile phase B to 60% mobile phase B in 1 min. The column is washed at 60% mobile phase B for 3 min before re-equilibration to 5% mobile phase B in 1 min. At 55 min the flow is increased to 300 nl/min until the end of the run at 60 min. Mass spectrometry data were acquired in a data directed manner for 60 min in positive mode. Peptides were selected for fragmentation automatically by data dependent analysis on a basis of the top 12 peptides with m/z between 300 to 1750 Th and a charge state of 2, 3 or 4 with a dynamic exclusion set at 15 sec. The MS Resolution was set at 120,000 with an AGC target of 3e6 and a maximum fill time set at 20 ms. The MS2 Resolution was set to

30,000, with an AGC target of 2e5, a maximum fill time of 45 ms, isolation window of 1.3 Th and a collision energy of 28.

Proteome Discoverer software (Version 2.5.0.400) (Thermo Scientific) were applied for protein identification and quantification. MS1 spectra with precursor mass between 350 Da and 5000 Da was selected. Raw data was searched against the amino acid sequence of the same culture (**By Lynn Foster**) by using Sequest HT search engine. A fragment with peptide length between 6 and 144 was selected. Trypsin was used as digestion enzyme. Maximum 2 missed cleavage sites with a fixed amino acid modification through carbamidomethyl and a dynamic amino acid modification by N-terminal acetyl oxidation was accepted. Fragment mass tolerance was set to 0.02 Da and precursor mass tolerance 10 ppm. Highly confident peptide hits, peptide-spectrum matches (PSMs) and proteins were selected with False discovery rate (FDR) at 0.01. Precursor Ions Quantifier was used for protein quantification, intensities were used to calculate the peptide abundances. The summed abundances of connected peptide groups were used to calculate protein abundance. Protein abundances ratio was calculated as the median of all possible pairwise peptide ratios calculated between replicates of all connected peptides. The protein file was loaded to Perseus software for further comparative analysis. Differently expressed proteins between treatment group (LC, HC, CK) and control group were screened by using multi-sample-test, proteins with an p-value < 0.05 and log2 folder change >1.5 or < -1.5 were considered to be differently expressed. KEGG pathway enrichment analysis was conducted by using an R package clusterprofiler (and pathview (Wu *et al.,* 2021; Luo *et al.,* 2017).

3.7 References

Caporaso, J. G., et al. (2011). "Global patterns of 16S rRNA diversity at a depth of millions of sequences per sample." Proceedings of the National Academy of Sciences 108(Supplement 1): 4516-4522.

Caporaso, J. G., et al. (2012). "Ultra-high-throughput microbial community analysis on the Illumina HiSeq and MiSeq platforms." ISME J 6(8): 1621-1624.

Chemyx (2021). Basic Principles of LC, HPLC, MS, & MS. Available at https://www.chemyx.com/support/knowledge-base/applications/basic-principles-hplc-ms-lc-ms/ .Last accessed: 29/08/2021.

Cox, M. J., Cookson, W. O., & Moffatt, M. F. (2013). Sequencing the human microbiome in health and disease. Human molecular genetics, 22(R1), R88-R94.

Foster, L., Boothman, C., Ruiz-Lopez, S., Boshoff, G., Jenkinson, P., Sigee, D., ... & Lloyd, J. R. (2020). Microbial bloom formation in a high pH spent nuclear fuel pond. Science of The Total Environment, 720, 137515.

Koprinarov, I., & Hitchcock, A. P. (2000). X-ray Spectromicroscopy of Polymers: An introduction for the non-specialist. Unicorn Mcmaster (BIMR).

Kozich, J. J., et al. (2013). "Development of a Dual-Index Sequencing Strategy and Curation Pipeline for Analyzing Amplicon Sequence Data on the MiSeq Illumina Sequencing Platform." Applied and Environmental Microbiology 79(17): 5112-5120. Supplemental Material.

Martin, M. (2011). "Cutadapt removes adapter sequences from high-throughput sequencing reads." 2011 17(1). https://www.bioinformatics.babraham.ac.uk/projects/fastqc/

Joshi NA, Fass JN. (2011). Sickle: A sliding-window, adaptive, quality-based trimming tool for FastQ files (Version 1.33) [Software]. Available at https://github.com/najoshi/sickle.

Nurk, S., et al. (2013). Assembling Genomes and Mini-metagenomes from Highly Chimeric Reads. Research in Computational Molecular Biology: 17th Annual International Conference, RECOMB 2013, Beijing, China, April 7-10, 2013. Proceedings. M. Deng, R. Jiang, F. Sun and X. Zhang. Berlin, Heidelberg, Springer Berlin Heidelberg: 158-170.

Masella, A. P., et al. (2012). "PANDAseq: paired-end assembler for illumina sequences." BMC Bioinformatics 13(1): 1-7.

Haas, B. J., et al. (2011). "Chimeric 16S rRNA sequence formation and detection in Sanger and 454-pyrosequenced PCR amplicons." Genome Research 21(3): 494-504.

Edgar, R. C. (2013). "UPARSE: highly accurate OTU sequences from microbial amplicon reads." Nat Meth 10(10): 996-998.

Edgar, R. C. (2010). "Search and clustering orders of magnitude faster than BLAST." Bioinformatics 26(19): 2460-2461.

Caporaso, J. G., et al. (2010). "QIIME allows analysis of high-throughput community sequencing data." Nat Meth 7(5): 335-336.

Protifi (2021) S-Trap™ Micro spin column digestion protocol. Available at http://mass-spec.wp.st-andrews.ac.uk/files/2019/10/S-Trap-method.pdf. Last accessed: 30/08/21

Wang, Q., et al. (2007). "Naïve Bayesian Classifier for Rapid Assignment of rRNA Sequences into the New Bacterial Taxonomy." Applied and Environmental Microbiology 73(16): 5261-5267.

Quast C, Pruesse E, Yilmaz P, Gerken J, Schweer T, Yarza P, Peplies J, Glöckner FO (2013) The SILVA ribosomal RNA gene database project: improved data processing and web-based tools. Nucl. Acids Res. 41 (D1): D590-D596.

Schmidt, T. M., DeLong, E. F., & Pace, N. R. (1991). Analysis of a marine picoplankton community by 16S rRNA gene cloning and sequencing. Journal of bacteriology, 173(14), 4371-4378.

Chapter 4 The interplay between Cs, K and the cyanobacterium *Pseudanabaena catenata*, the fate of Cs and its impact on cell growth and protein expression

Kejing Zhang, Lynn Foster, Naji Bassil, Jon K Pittman and Jonathan R Lloyd

Abstract

The cyanobacterium *Pseudanabaena was* reported to dominate microbial blooms in the First-Generation Magnox Storage Pond (FGMSP) at the Sellafield site. The fission produce Cs is a radiologically significant radionuclide in the pond, and understanding the interactions between Cs and *Pseudanabaena spp.* is therefore important for determining facility management strategies. This study used culturing methods coupled with bioimaging and proteomic techniques to evaluate the fate of Cs following interactions with *P. catenate,* a model laboratory culture most closely related to the organism dominating FGMSP blooms. A growth kinetics experiment showed that Cs did not affect the growth of *P. catenate,* while a high concentration of K caused a reduction in cell yield. Light microscopy and scanning transmission X-ray microscopy elemental mapping identified that some Cs can be accumulated by *P.catenata* cells, localised to discrete cytoplasmic locations. Light microscopy also showed the uptake of Cs can result in distinct changes in cell morphology. The protein expression patterns of *P. catenata* were dramatically changed when exposed to 1 mM of Cs. Several stress response proteins and proteins related to nutrient limitation were stimulated by Cs treatment. The expression of KdpD, which is involved in the regulation of the Kdp-ATPase higher-affinity K^+ pump, was identified to be affected by K concentration, with Cs acting as an inhibitor of expression of the KdpA protein. The expression of high velocity, moderate K affinity Trk transport system proteins TrkA and TrkB were also up regulated by Cs.

4.1 Introduction

^{137}Cs is a fission product of uranium that has no known biological role and limited economic value (Avery, 1995). However, with the development of the nuclear industry, large scale dispersal of ^{137}Cs has been observed worldwide, for example, in contaminated land and spent fuel ponds used by the nuclear energy industry (Czirjak *et al.,* 2010; Hoyos-Hernandez *et al.,* 2019; Koarashi *et al.,* 2012; Chicote *et al.,* 2005; Sarro *et al.,* 2005; Tisakova *et al.*, 2006). ^{137}Cs has a long half-life (28 years) and it exists in a high water-soluble (Cs^+ form. Nuclear industries have continuously discharged radionuclides including ^{137}Cs into environment and the associated pollution attracted great concerns in the 1980s and 1990s, particularly following the Chernobyl nuclear disaster (Avery, 1995; Singh *et al.,* 1997). More recently, after the accident at the Fukushima Dai-ichi nuclear power plant in Japan, radionuclides like ^{137}Cs, ^{90}Sr, and ^{131}I were released into the atmosphere, soil and aquatic system (MeGraw *et al.,* 2018; Povinec *et al,* 2013). Since these radionuclides can be concentrated via food chains, the biological fate of Cs has attracted great attention (Fukuda *et al.,* 2014).

Many reports indicate that most organisms including plants, algae, bacteria and fungi are able to accumulate Cs, often via K transport systems due to the similar chemical and physical properties of Cs and the essential nutrient K (Avery et al., 1992; Haselwandter et al., 1988; Bakken and Olsen, 1990; Perkins and Gadd, 1995; Saski et al., 2016). Most of the research have focussed on understanding the mechanism of Cs accumulation, while the consequences of Cs exposure to cell physiology are less well understood, particularly in cyanobacteria. Previous studies demonstrated that in most cases Cs^+ uptake is energy dependent and regulated by a K^+ transport system (Avery et al., 1992). Extracellular Na^+ affect Cs^+ uptake to similar extent as K^+ (Avery et al., 1991) while nitrogen species, such as NH_4^+may act as another competitor for Cs^+ uptake. For example, a mutant strain of *Anabaena variabilis* with deficient

NH_4^+ transport accumulates less Cs^+ than the nitrogen-fixing cells (Avery et al., 1993). Cs is considered the most toxic Group 1 metal and the presence of Cs leads to inhibition of cell growth (Pekins and Gadd, 1995).

Many microorganisms including cyanobacteria have a wide range of metabolic and adaptive capabilities, which allows them to adapt to a wide range of stressful environments including those with extremes of temperature, pH, pressure, salinity, radiation and availability of water (Pikuta et al., 2007; Nazina et al., 2007; Billi and potts, 2002; Katz et al., 2007; Blanco-Rivero et al., 2005; Foster et al., 2020). The Cyanobacterium *Pseudanabaena* sp. was reported to be the dominant microbe of the seasonal algal bloom in the First-Generation Magnox Storage Pond (FGMSP) at the Sellafield nuclear processing site in Cumbria, UK (Foster et al., 2020). This pond started to accept spent MAGNOX nuclear fuels from the 1950s. The long-term operation and prolonged corrosion of the fuel and cladding has resulted in a significant level of radionuclides accumulating in the pond waters and sludges, including fission products, such as Sr and Cs (Jackson et al, 2014; NDA, 2017). The presence of microorganisms has led to several problems for facility maintenance, which include reducing visibility of pond waters, biofouling of surfaces, the potential for microbial-induced corrosion, and interactions with fission products and redox sensitive radionuclides (Avery *et al.,* 1992; Foster *et al.,* 2020; MeGraw *et al.,* 2018). *Pseudanabaena spp.* are filamentous cyanobacteria that are able to act as a primary producer in pond systems, frequently identified in algal bloom events (Singh et al., 1993), They can also be toxic to aquatic organisms and humans due to the production of hepatotoxic microcystin (Zhu et al., 2015). However, studies of *Pseudanabaena spp.* and knowledge about their physiology and metabolism are limited. Understanding their interactions with Cs might be helpful in developing bloom control strategies and also of a remediation method for Cs in pondwaters. Modern imaging and omics techniques provide a chance to

investigate the fate of Cs and its impacts on cell protein expression in more detail. This study utilized scanning transmission X-ray microscopy (STXM) and Liquid chromatography–mass spectrometry (LC-MS) based proteomic approaches to demonstrate Cs^+ transport and to understand the biological impacts of Cs exposure at the protein expression level in *Pseudanabaena catenata*.

4.2 Materials and Methods

4.2.1 Culturing of *P.catenata*

Radiological safety limitations prevented obtaining organisms directly from water in the Spent Nuclear Fuel Pond (SNFP). Therefore, a closely related strain to the organism identified in SNFP called *Pseudanabaena catenata* was obtained from the NIVA Culture Collection of Algae (NIVA-CYA 152 *Pseudanabaena catenata*, Helbig's Pond, Warburg, Alberta, Edmonton, Canada, 1980-07) and was used as a representative culture for the pond system. Cultures were set up by inoculating *P. catenata* into BG-11 medium (**Appendix 4.1**) to a final volume of 30 ml. The starting optical density (measured at 600 nm) was set to 0.2. Cultures with no Cs or K addition were set as a control. Two sets of cultures were prepared with the addition of 0.5 mM or 1 mM Cs to explore the impact of Cs exposure on *P. catenata.* To explore the impact of high concentrations of K, two sets of cultures were prepared with the addition of 2.5 mM or 5 mM K. A set of cultures were prepared with 1 mM Cs and 2.5 mM K to explore the combined effect of Cs and K exposure on *P. catenata.* Biological triplicates were prepared for all 6 treatments, which were incubated for 2 weeks on a shaker at 140 rpm, under a white light intensity of 30 μmol m^{-2} s^{-1} with a 16:8 h light-dark cycle. The temperature of the incubator was controlled at 20 ± 1°C. Samples were taken at day 0, 3, 7, 10 and 14 for growth measurement, cell morphology recording and water chemistry analysis.

4.2.2 Growth measurement, cell morphology and water chemistry

Absorbance values at 600 nm (OD_{600nm}) of 1 mL aliquots of *P. catenata* cultures were recorded by using a Jenway 6700 UV/Vis spectrophotometer (Bibby Scientific Limited, Staffordshire) to quantify the total biomass in the cultures by turbidity.

A Zeiss Axio Imager A1 light microscope (Carl Zeiss Microimaging 234 GmbH, Germany) fitted with an Axiocam 506 mono camera was utilized for recording cell morphology. Images were processed by Zen 2 imaging software. Cell length and width were measured by using ImageJ. The removal of Cs and K were evaluated by measuring the concentration of dissolved K and Cs in supernatants of growth media samples by inductively coupled plasma mass spectrometry (ICP-MS) using an Agilent 7700 Series. Samples of 1 ml volume taken at day 0, 3, 7, 10 and 14 were centrifuged at 14000 *g* for 10 mins to remove cells, and 100 μL of supernatant was then added to 9.9 ml of 2% nitric acid for ICP-MS analysis.

4.2.3 Scanning transmission X-ray microscopy (STXM)

Cells from the control culture, and those containing 1 ml Cs and 1 mM Cs + 2.5 mM K cultures were analysed by STXM. 1 ml of samples were taken after 10 days incubation. Samples were centrifuged at 14000 x *g* for 10 minutes. Supernatant was removed and pellets were washed by deionised water. 0.2 μl of washed samples was placed on a Formvar/Carbon Film 200 mesh Cu grid and stored in a desiccator. STXM images were measured at Dimond Light Source Ltd using the I08 beamline. Carbon K-edge (280-320 eV) stack images were collected using the following settings: 280-283 eV, 0.5 eV energy step; 283 - 290 eV, 0.1 eV energy step; 290 - 293 eV, 0.2 eV energy step; 293 - 295 eV, 0.5 eV energy step; 295 - 303eV, 0.2 eV energy step; 303 - 320 eV, 0.5 eV energy step. Sequenced images were then collected at the Cs M-edge (720 - 745 eV) by using the following settings: 720 – 728 eV, 1 eV energy step; 728.5 –

740 eV, 0.5 eV energy step; 740 – 745 eV, 1 eV energy step. Data processing was performed by using the aXis 2000 software package.

4.2.4 LC-MS sample preparation, protein identification and quantification

Samples of 1 ml volume were taken at day 10 of the incubation. Samples were centrifuged at 14000 x *g* for 10 minutes. Supernatant was removed and cell pellets were resuspended in 130 µl lysis buffer (5% SDS with 50 mM TEAB pH 7.5). Samples were then lysed by LE220-plus Focused-ultrasonicator with the following parameters; peak power: 500 W, duty factor: 40%, cycle/burst: 200, average power 200 W. Each sample was lysed for 600 seconds. Lysed samples were then reduced and alkylated with dithiothreitol and iodoacetamide. Protein concentrations were quantified by using the Millipore Direct Detect. Protein concentrations were then normalized to 1 mg/l for subsequent protein extraction. 5 µl of 12% aqueous phosphoric acid was added to 50 ml (50 µg) protein lysate. 330 µl of S-Trap binding buffer (90% aqueous methanol containing a final concentration of 100 mM TEAB, pH 7.1) was added to acidified protein lysate and mixed. Protein solutions were loaded onto a S-Trap column (PROTIFI) and centrifuged at 4000 x *g* for 2 mins, and then the S-Trap column were washed with 150 µl S-Trap binding buffer 4 times. 20 µl of digestion buffer (50 mM triethylammonium bicarbonate) and 20 µl of 0.25 ug/ul trypsin were added to the S-Trap column and incubated at 47 °C for 1 hour. 3 washes with 65 µl digestion buffer, 65 µl of 0.1% aqueous formic acid and 30 µl of 30% aqueous acetonitrile containing 0.1% formic acid were applied, in order to elute peptides. For sample desalination, the digested sample solutions were moved to a Corning FiltrEX desalt filter plates and mixed them with pre-washed beads for 5 mins at 800 RPM. Liquids were removed by centrifuging at 200 x *g* for 1 minute. The wells with beads in were then washed by using 0.1% formic acid twice. Then the peptides were extracted to by 2 washes with 50 µl 0.1% formic acid in 30% acetonitrile. 100 µl peptides solutions were transferred to sample vials and

dried in Heto vacuum centrifuge. Died samples were kept in a freezer at -20 °C for subsequent analysis.

Digested samples were analysed by Liquid chromatography–mass spectrometry (LC-MS/MS) using an UltiMate® 3000 Rapid Separation LC (RSLC, Dionex Corporation, Sunnyvale, CA) coupled to a QE-HF (Thermo Fisher Scientific, Waltham, MA) mass spectrometer. Mobile phase A was 0.1% formic acid in water and mobile phase B was 0.1% formic acid in acetonitrile and the column used was a 75 mm x 250 µm i.d. 1.7 µm CSH C18, analytical column (Waters). A 1 µl aliquot of the sample was transferred to a 5 µl loop and loaded on to the column at a flow of 300 nl/min for 5 minutes at 5% mobile phase B. The loop was then taken out of line and the flow was reduced from 300 nl/min to 200 nl/min in 0.5 min. Peptides were separated using a gradient that went from 5% to 18% mobile phase B in 34.5 min, then from 18% to 27% mobile phase B in 8 min and finally from 27% mobile phase B to 60% mobile phase B in 1 min. The column was washed with 60% mobile phase B for 3 min before re-equilibration to 5% mobile phase B for 1 min. At 55 min the flow was increased to 300 nl/min until the end of the run at 60 min. Mass spectrometry data were acquired in a data directed manner for 60 min in positive mode. Peptides were selected for fragmentation automatically by data dependent analysis on a basis of the top 12 peptides with m/z between 300 to 1750 Th, and a charge state of 2, 3 or 4 with a dynamic exclusion set at 15 sec. The MS Resolution was set at 120,000 with an AGC target of 3e6 and a maximum fill time set at 20 ms. The MS2 Resolution was set to 30,000, with an AGC target of 2e5, a maximum fill time of 45 ms, isolation window of 1.3 Th and a collision energy of 28.

Proteome Discoverer software (Version 2.5.0.400) (Thermo Scientific) was used for protein identification and quantification. MS1 spectra with precursor masses between 350 Da and 5000

Da were selected. Raw data were searched against the amino acid sequence of the same culture (provided by Dr Lynn Foster, University of Manchester) by using Sequest HT search engine. Fragments with peptide lengths between 6 and 144 was selected. Trypsin was used as digestion enzyme. A maximum of 2 missed cleavage sites with a fixed amino acid modification through carbamidomethyl and a dynamic amino acid modification by N-terminal acetyl oxidation was accepted. Fragment mass tolerance was set to 0.02 Da and precursor mass tolerance 10 ppm. Highly confident peptide hits, peptide-spectrum matches (PSMs) and proteins were selected with a False discovery rate (FDR) at 0.01. The Precursor Ions Quantifier was used for protein quantification, and intensities were used to calculate the peptide abundances. The summed abundances of connected peptide groups were used to calculate protein abundance. The protein abundances ratio was calculated as the median of all possible pairwise peptide ratios calculated between replicates of all connected peptides. The protein file was loaded to Perseus software for further comparative analysis. Differently expressed proteins between treatment group (LC, HC, CK) and the control group were screened by using multi-sample-t-test; proteins with an p-value < 0.05 and log2 folder change >1.5 or < -1.5 were considered to be differently expressed. KEGG pathway enrichment analysis was conducted by using an R package clusterprofiler and pathview (Wu *et al.,* 2021; Luo *et al.,* 2017). The definition and procedure of Enrichment analysis were described by Reimand *et al.* (2019).

4.3 Results and Discussion

4.3.1 Impact of Cs and K on cell growth and morphology

In order to evaluate the impact of Cs on growth kinetics and cell morphology of *P. catenata* cultures, optical density values at 600 nm (OD_{600nm}) were recorded routinely for 2 weeks (**Figure 4.1**). The addition of 0.5 mM Cs, 1 mM Cs and 2.5 mM K showed little impact on the growth of cultures compared to the control, whereas 5 mM K inhibited the growth. The 1

mM Cs + 2.5 mM K treatment showed an inhibition of cell growth after day 10. OD_{600nm} values of all cultures increased steadily in the first 10 days. The growth rates were almost the same, except for the 5 mM K treatment which was much lower. After day 10, cells from the Control, 0.5 mM Cs, 1 mM Cs and 2.5 mM K groups grew at a slightly higher rate than before and reached OD_{600nm} 2.8 ± 0.189, 3.03 ± 0.044, 2.82 ± 0.217 and 2.6 ± 0.040, respectively at day 14. Cells from the 1 mM Cs + 2.5 mM K group kept growing but the growth rate decreased and reached OD_{600nm} 1.77 ± 0.122 at day 14. The highest OD_{600nm} of the 5 mM K group was reached at day 10 with a value of 1.04 ± 0.039, then decreased to 0.45 ± 0.002 at day 14.

Cell morphology was monitored by light microscopy. Cells in standard BG-11 samples were rectangular in shape, typically 3 µm to 6 µm in length, and around 2 µm in width. With the addition of 1 mM Cs, round and elliptical shaped cells appeared frequently in the culture (more images in **Appendix 4.2**). This type of morphological change was not observed in the 1 mM Cs + 2.5 mM K group, or in the 0.5 mM Cs culture either, where cells typically became thinner and longer, approximately 5 µm to 11 µm in length, and 1 µm to 1.5 µm in width. Cells from the 2.5 mM K and 5 mM K cultures were slightly thicker than the control, at around 2.8 µm in width for the 2.5 mM K cells and around 2.5 µm in width for the 5 mM K cells. The observation that morphological change of *P. catenata* cells presented in the 1 mM Cs group but not in the 0.5 mM Cs group indicated that the concentration of Cs needs to be over a threshold concentration in order to cause this change. The observation that K protected *P. catenata* cells from morphological change caused by Cs (as seen in the 1 mM Cs + 2.5 mM K group cultures) indicated that K might act as a competitor of Cs uptake, as also suggested in other previous studies (Avery *et al.,* 1992). The concentration of K and Cs was monitored in the growth medium supernatant following cell removal, to evaluate the uptake of Cs and K. Another treatment was prepared in which cells were incubated in a version of BG 11 medium lacking

K (BG11M), but with addition of 1 mM Cs (the background K were removed by replacing the K_2HPO_4 with Na_2HPO_4). The results showed that the presence of Cs did not significantly reduce the uptake of K and the concentration of Cs in the supernatant did not change significantly over time (**Appendix 4.3 A and B**), indicating that Cs may not be uptake by cells or that the amount of removal Cs is very small compared to the concentration in the growth medium.

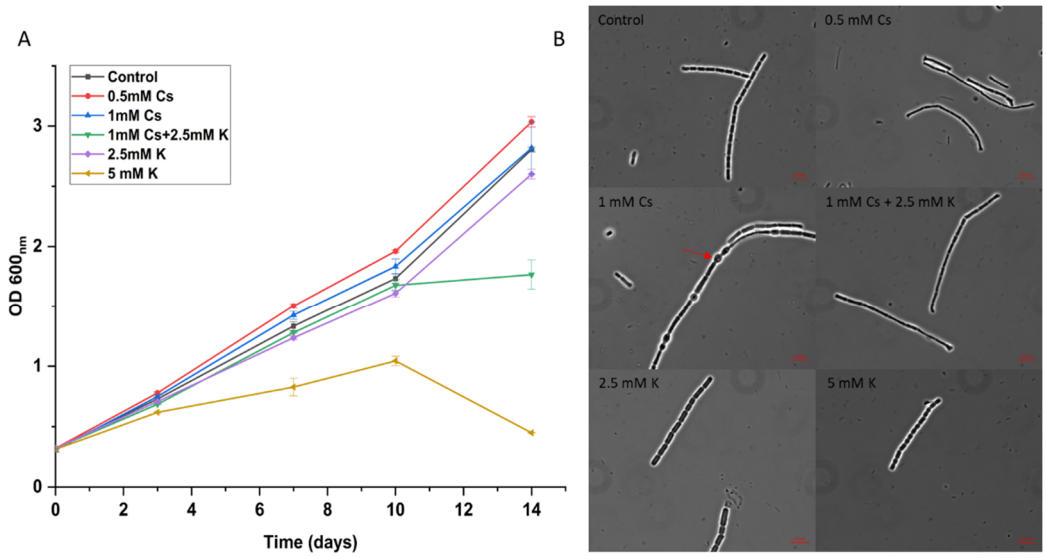

Figure 4.1 (A) Growth curves of *P. catenata* cultures obtained by plotting the mean values of the optical density at 600 nm. Cultures were spiked with 0.5 mM CsCl, 1 mM CsCl, 2.5 mM KCl, 5 mM KCl and 1 mM Cs + 2.5 mM K, or were untreated (Control). Error bars show the standard deviation. (B) Representative cells observed under light microscopy, x1000 amplification. Samples were taken after 10 days incubation.

4.3.2 Fate of Cs in *P. catenata* culture

Measuring the concentration of dissolved Cs and K in the growth medium over time suggested low levels of Cs uptake. STXM-based elemental imaging was used to further investigate whether Cs taken up into the cells was localised or distributed evenly in the biomass, and to further investigate the impact of K on this process. Cells from the control treatment, an elliptical

cell from the 1 mM Cs sample, a normal shaped cell from the 1 mM Cs sample and a cell from the 1 mM Cs + 2.5 mM K sample (**Figure 2 A**) were all imaged. Image sequences at the carbon K-edge (280 eV– 320 eV) were collected to identify the *P. catenata* cell, and image sequences at the Cs M-edge (720 eV – 745 eV) were collected to determine the distribution of Cs. Carbon signals were detected in all 4 samples (**Figure 4.2 B a**) and the near edge X-ray absorption fine structure (NEXAFS) spectra at 288.2 eV (Mitsunobu *et al.,* 2015) which correspond to amide C were used to map the cell structure, with the spectra at 735 eV (Suzuki *et al.,* 2019) used to map the distribution of Cs. Cs signals were found in both the "normal" shaped cell and the elliptical shaped cell from the 1mM Cs sample, but not in the sample with additional K (**Figure 4.2 B b**). Cs was uniformly distributed in the normal shaped cells (**Figure 4.2 A c**). In the elliptical shaped cell, Cs was accumulated in several areas (such as the spot labelled as R3), while relatively weaker signal was detected in other areas of the cell (such as the area labelled as R2) (**Figure 2 A b**). The results confirmed that in the 1 mM sample, Cs was accumulated by the *P. catenata* cell, and the cell morphological change was coincident to the accumulation of Cs.

Cell morphological changes were only present in the 1 mM Cs culture. Neither 0.5 mM Cs nor 1 mM Cs + 2.5 mM K was able to induce the change of cell morphology. This indicates that the cell morphological change can only be induced when *P.catenata* cells are exposed to relatively high Cs levels, but that K is able to protect the cells from morphological change induced by Cs. Here we hypothesised that Cs could be accumulated by *P. catanata* cells, and that Cs and K shared the same transport system （Avery *et al.,* 1992）. The STXM data showing that Cs was only associated with the cell from the 1 mM Cs sample while no Cs signal was detected in the 1 mM Cs + 2.5 mM K sample supported this hypothesis. While Cs signal was detected in both the normal shaped cell and the elliptical shaped cell, several spots with very

strong Cs signal were observed only in the elliptical shaped cell, which suggested that the morphological change might be induced by the concentration of Cs.

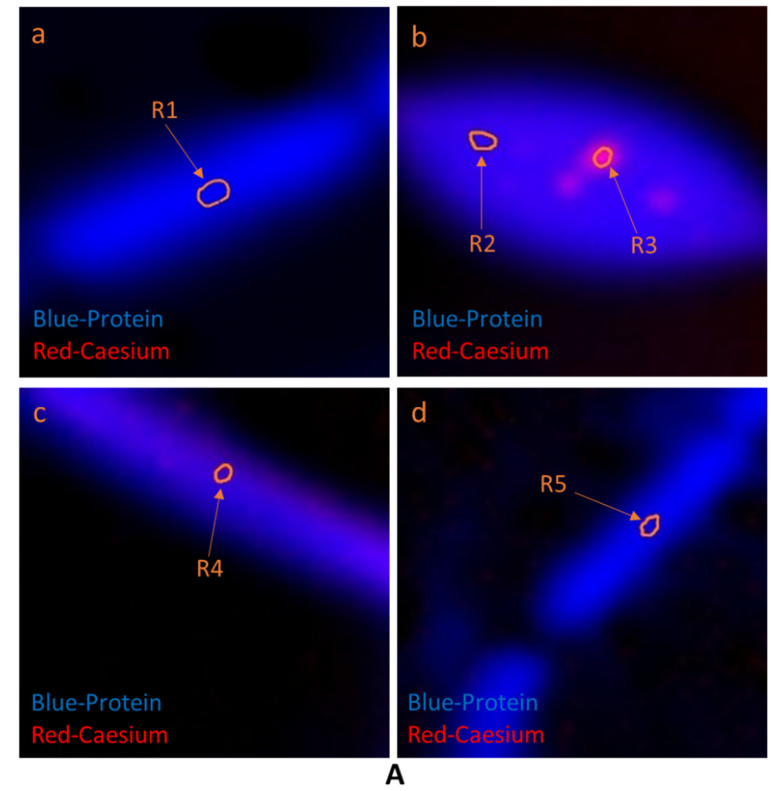

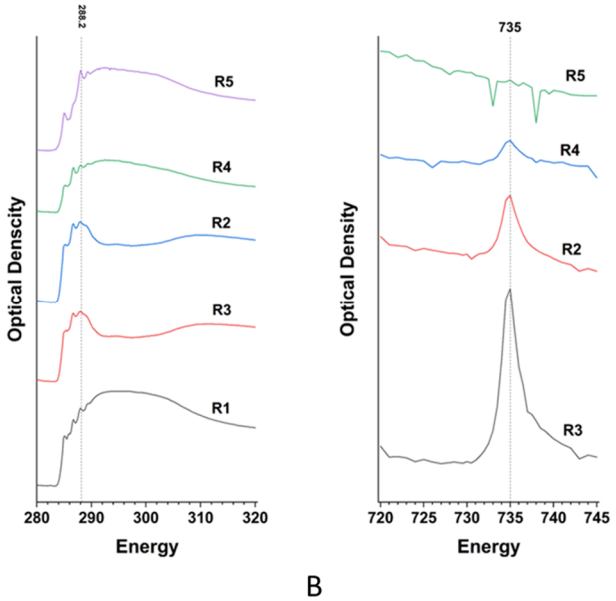

Figure 4.2 (A) STXM elemental maps of *P. catenata* cells. Proteins (Blue): 288.2 eV; Cs (Red): 735.0 eV (a) *P. catanata* cell from the control sample (b) Heteromorphic *P. catanata*

cell from the 1 mM Cs sample. (c) Normal shape *P. catanata* cell from the 1 mM Cs sample. (d) *P. catanata* cell from the 1 mM Cs + 2.5 mM K sample (B) STXM-based NEXAFS spectra corresponding to R1 - R5 showing in the elemental map. (a) NEXAFS carbon spectra. (b) NEXAFS caesium spectra

4.3.3 Impact of Cs and K on *P. catenata* protein expression

4.3.3.1 Overview of quantitative proteomics analysis

1776 proteins from a total 3816 proteins in the *P. catenata* database were identified in the cultures generated in this study (**Figure 4.3 A**). Normalized protein abundance values of the identified proteins were evaluated by multiple-sample test using Perseus software. 1604 proteins with p-value < 0.05 were accepted as significantly differentially expressed proteins. The 1604 proteins include hypothetical proteins and putative proteins for which the function is unknown. 886 of the 1604 proteins were annotated to KEGG with predicted function and were used for differential expression analysis. The proteins in each sample were subjected to hierarchical clustering to generate a heatmap showing changes in expression in the cultures (**Figure 4.3 B**). The control group were distinct out of the 6 treatments, with a relatively lower expression of proteins. The expression profile of the 0.5 mM Cs group and the 1 mM Cs + 2.5 mM K group were more similar. Proteins in these two groups were slightly up regulated in cluster 3, and mostly up regulated in cluster 6. The expression pattern of proteins in the 1 mM Cs and 2.5 mM K groups were similar, and the proteins were mostly up-regulated.

The significantly differentially expressed proteins were annotated to KEGG and plotted in **Figure 4.3 C and D**. All treatments induced more up-regulation of proteins than down-regulation of proteins. The 1 mM Cs group and 2.5 mM K group induced more up-regulated proteins, but less down-regulated proteins than the 0.5 mM Cs and 1 mM Cs + 2.5 mM K

groups. The expression of proteins related to metabolism, including peptidases and inhibitors, amino acid related enzymes, and photosynthesis proteins were affected dramatically. Down regulation of amino acid related enzymes and peptidases and inhibitors were only detected in the 0.5 mM Cs and 1 mM Cs + 2.5 mM K groups. By contrast, 1 mM Cs and 2.5 mM K stimulated more amino acid related enzymes, photosynthesis proteins and peptidases and inhibitors. Dramatically up regulated proteins were related to genetic information processing including DNA repair and recombination proteins, chromosome and associated proteins, ribosome proteins, proteins related to mitochondrial biogenesis, proteins related to transfer RNA biogenesis and proteins related to chaperones and folding catalysts. Down regulation of proteins related to transfer RNA biogenesis were mainly identified in the 0.5 mM Cs and 1 mM Cs + 2.5 mM K groups. The down regulation of proteins related to chaperones and folding catalysts and proteins related to mitochondrial biogenesis were mainly detected in the 5 mM K group. 1 mM Cs and 2.5 mM K induced relatively stronger up regulation of proteins related to transfer RNA biogenesis, membrane trafficking, mitochondrial biogenesis, ribosome proteins and DNA repair and recombination proteins. In terms of proteins related to signalling and cellular processes, the expression of transporters was dramatically influenced. In addition, proteins of the secretion system, two-component system and prokaryotic defense system and exosome proteins were stimulated. Exosome proteins and proteins related to prokaryotic defence system were up regulated more dramatically in the 1 mM Cs and 2.5 mM K group. The exosome proteins and proteins related to prokaryotic defence system were down regulated more in the 0.5 mM Cs group. 5 mM K also induced relatively stronger down regulation of prokaryotic defence system proteins.

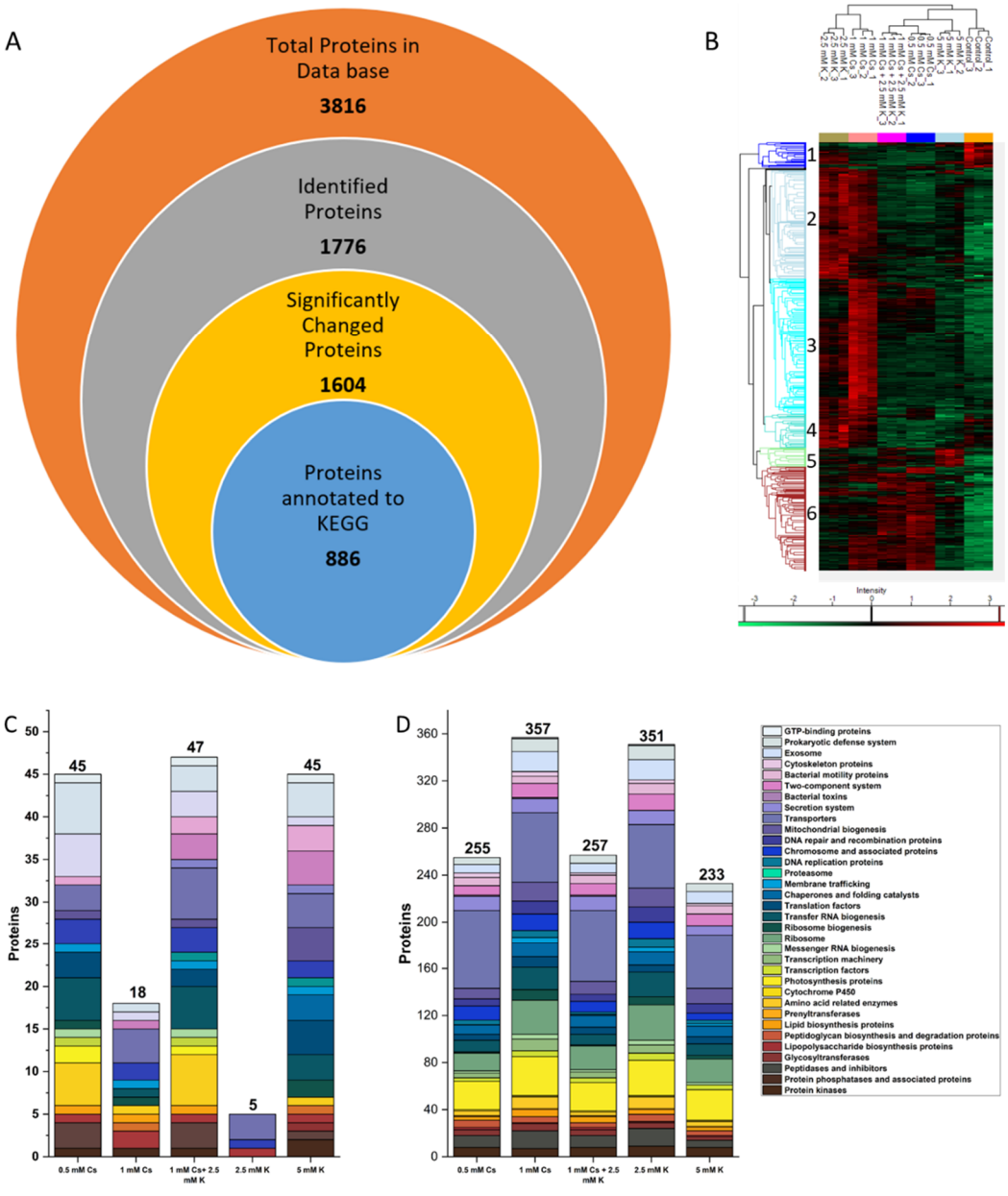
A
Total Proteins in Data base
3816
Identified Proteins
1776
Significantly Changed Proteins
1604
Proteins annotated to KEGG
886
B
Intensity
C
Proteins
45
18
47
5
45
0.5 mM Cs
1 mM Cs
1 mM Cs+ 2.5 mM K
2.5 mM K
5 mM K
D
Proteins
255
357
257
351
233
0.5 mM Cs
1 mM Cs
1 mM Cs + 2.5 mM K
2.5 mM K
5 mM K
GTP-binding proteins
Prokaryotic defense system
Exosome
Cytoskeleton proteins
Bacterial motility proteins
Two-component system
Bacterial toxins
Secretion system
Transporters
Mitochondrial biogenesis
DNA repair and recombination proteins
Chromosome and associated proteins
DNA replication proteins
Proteasome
Membrane trafficking
Chaperones and folding catalysts
Translation factors
Transfer RNA biogenesis
Ribosome biogenesis
Ribosome
Messenger RNA biogenesis
Transcription machinery
Transcription factors
Photosynthesis proteins
Cytochrome P450
Amino acid related enzymes
Prenyltransferases
Lipid biosynthesis proteins
Peptidoglycan biosynthesis and degradation proteins
Lipopolysaccharide biosynthesis proteins
Glycosyltransferases
Peptidases and inhibitors
Protein phosphatases and associated proteins
Protein kinases

Figure 4.3 Comparative proteomic analysis between treatment groups. (A) Venn diagram summary the number of labelled proteins in the total proteins data base. (B) Hierarchical clustering showing the changes in abundances of the identified proteins. Missing values were imputed from normal distribution. The protein abundances were normalized by z-score (the mean of each protein was subtracted; the results were then divided by the standard deviation). Z-scores were used for hierarchical clustering into heat map. The nearness of two items was defined by Euclidean distance. The distance between 2 clusters was defined by average distances between 2 single items. (C)Histogram of down-regulated proteins. (D) Histogram of up-regulated proteins. Differentially expressed proteins were evaluated by using multiple-sample test. Proteins with p< 0.05 and log2 folder change >1.5 or < - 1.5 were considered as significantly differentially expressed proteins. Significantly differentially expressed proteins were then categorized to KEGG for the histogram of up- / down- regulated proteins.

4.3.3.2 Differentially expressed pathways

To evaluate the specific biological reactions that were affected by Cs and K, the identified proteins were related the KEGG pathways. The enrichment analysis was carried out by using an R package Clusterprofiler. The Pathways with p-value <0.05 were accepted as differentially expressed pathways. The results are shown in **Appendix 4.4.** Proteins from the two-component system were differentially expressed in all treatments except for the 5 mM K group. The differentially expressed pathways, such as the carbon fixation pathways and lysine biosynthesis presented in the 2.5 mM K groups were also differentially expressed in the 1 mM Cs group. In addition, photosynthesis and cysteine and methionine metabolism pathways were differentially expressed in the 1 mM Cs group. ABC transporters and oxidative phosphorylation pathways were differentially expressed in the 0.5 mM Cs and 1 mM Cs + 2.5 mM K groups. Protein

export pathway and pyrimidine metabolism pathway were differentially expressed in the 0.5 mM Cs and 5 mM K groups, respectively. The regulation of photosynthesis pathway and two-component system are shown in Figure 4 and 5. Other differentially expressed pathways are shown in **Appendix 4.8**.

4.3.3.2.1 Impact on Photosynthesis

Cyanobacteria store light energy by synthesizing organic compounds from carbon dioxide and water via photosynthesis. Photosynthesis consists of a light reaction and carbon fixation. The light reaction occurs in the thylakoid in cyanobacteria. Light energy is used by photosystems I and II to generate NAD(P)H and proton motive force (PMF), which provides the driving force for generating ATP. ATP and NADPH are then used to fix carbon dioxide (Golbeck and Bryant, 1991; Mccvoy and Brudvig, 2006). It was found that in all treatments, the proteins related to photosynthesis were up regulated to some extent (**Figure 4.4**). Wherein, 1 mM Cs caused relatively stronger regulation than other treatments. Up regulated proteins in photosystem II including photosystem II P680 reaction centre proteins (psbA, psbD), photosystem II CP43 chlorophyll apoprotein (psbC), photosystem II cytochrome b559 subunit (psbE), photosystem II oxygen-evolving enhancer protein (psbO and psbP) and photosystem II 13kDa protein (psb28). psbO protein and Psb28 protein were only up regulated with the 1 mM Cs suspended culture. Wherein, Psb28 protein protects and assists the assembly intermediate RC47 convert to functional Photosystem II. It is an important protein when cells are in a stress condition and the Photosystem II is damaged frequently (Weisz *et al.*, 2017. Sakata *et al.,* 2013). Up regulation of photosystem I proteins including photosystem I subunits (psaC, psaD, psaE and psaL) were detected. The cytochrome b_6f complex connects the electron flow between photosystem I and II to transport electron from water to $NADP^+$ (Anderson, 1992; Baniulis *et al.,* 2008). cytochrome b6 (petB, petC, petD) and apocytochrome f (petA) were up-regulated.

Wherein, more up-regulation of petA and petC were presented in the 1mM Cs group. Ferredoxin (petF) is an electron carrier protein, it transports electrons from Photosystem I to Fd-dependent enzymes such as Fd-$NADP^+$ oxidoreductase (petH, FNR) and Fd-thioredoxin reductase (FTR) for $NADP^+$ reduction (Kurisu *et al.,* 2001). In addition, petF acts as electron donor to a series of enzymes involved in sulfur metabolism, nitrogen metabolism and carbon metabolism (Knaff, 1996). Down regulation of petF was detected in the 0.5 mM Cs and 1 mM Cs + 2.5 mM K cultures. petH was up regulated with the addition of Cs and K. F – type H^+ -transporting ATPase subunits (atpA, atpB, atpH, atpE and atpF) were stimulated. Wherein, atpA, atpF and atpH were stronger up-regulated in 1 mM Cs group, atpB and atpE were up-regulated more in the 0.5 mM Cs and 1 mM Cs + 2.5 mM K group.

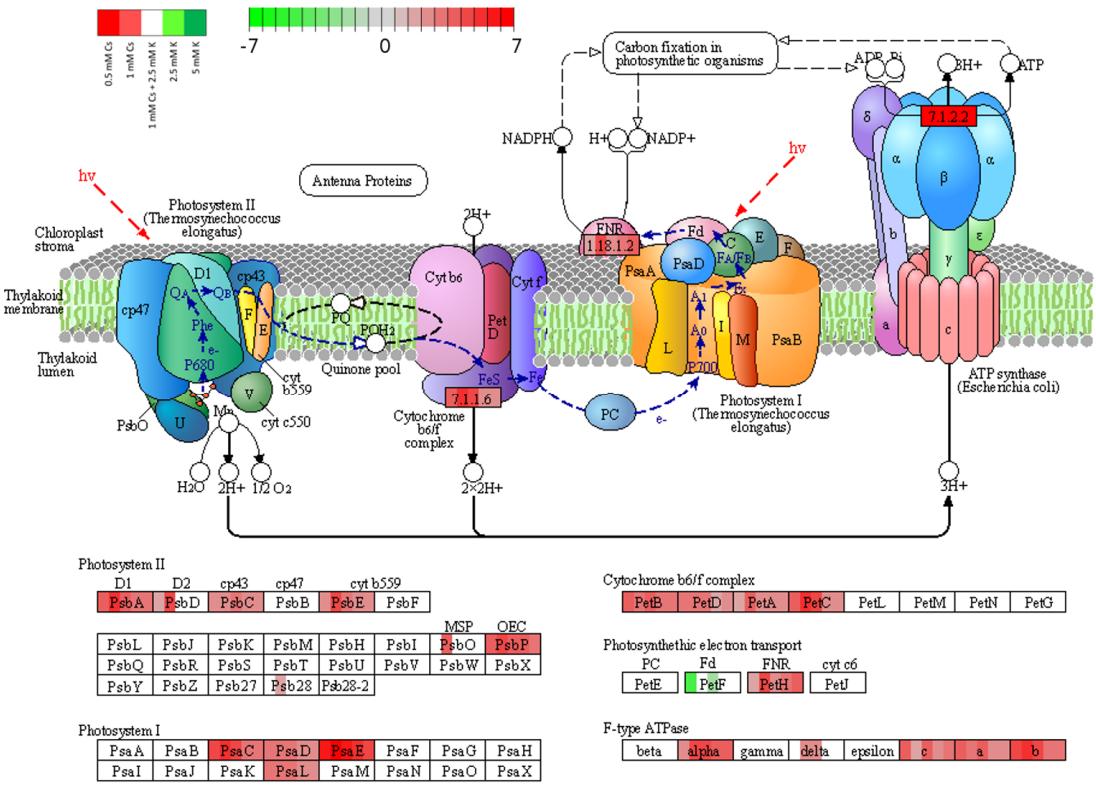

Figure 4.4 Schematic of photosynthesis pathway regulated by Cs and K treatment. The results were obtained by plotting the log2 fold change of the quantified proteins identified in the KEGG database. Up-regulated proteins are shown in red colour and down-regulated proteins are shown in green colour in the boxes representing each protein. Each box is divided into 5 segments, the 5 segments from left to right correspond to the expression of proteins in the 0.5 mM Cs, 1 mM Cs, 1 mM Cs + 2.5 mM K, 2.5 mM K and 5 mM K treatments respectively.

4.3.3.2.2 Impact on the two-component system

The two-component system consists of a sensor protein-histidine kinase to sense the signals in the environment, and a regulator response to the signals by regulating the cellular physiology and gene expression. Kdp-ATPase is a higher-affinity K^+ pump. Kdp-ATPase comprising of kdpFABC complex is regulated by sensor protein KdpD/E (Ballal et al., 2007). KdpD can be triggered by turgor pressure, osmolarity, K^+ concentration, ATP concentration and coupled with the response regulator KdpE to control the expression of kdpFABC (Freeman *el al.,* 2013). In our experiment, kdpD proteins were up-regulated in the 0.5 mM Cs, 1 mM Cs, 1 mM Cs + 2.5 mM K and 2.5 mM K groups, but down regulated in the 5 mM K group (**Figure 4.5**). The lowest abundances of kdpD proteins were detected in the 5 mM K group and the highest concentration of kdpD were detected in the K depleted group (**Appendix 4.5 A**) suggesting that the expression of kdpD might be regulated by the concentration of external K^+. Down regulation of KdpA was detected in 1 mM K group. The abundance values of KdpA were lower in all Cs presented samples (**Appendix 4.5 B**), which indicated that Cs might act as an inhibitor of kdpA expression.

The up regulation of phoB which responds to phosphate limitation, phoP proteins which respond to Mg^{2+} limitation, mntA response to Mn^{2+} limitation and nitrogen regulatory protein glnA and glnB were also detected in the 1mM Cs group and 2.5 mM K group (Makino *et al.,* 1989; Groisman, 2001; Yamaguchi *et al.,* 2002; Newsholme et al., 2003; Ven *el al.,* 1991). nblS is involved in controlling photosynthesis related gene expression in high light intensity and nutrient stress conditions, and the cicadian timing mediator protein sasA were all overexpressed in our experiment (Van *et al.,* 2002; Takai *et al.,* 2006). It should be pointed out that the over expression shown here was because of no related proteins were detected in the control. The abundances of nblS and sasA were shown to be higher in the 1 mM Cs group (**Appendix 4.6 A and B).** Other stress response proteins including HtrA proteins which are involved in stress response by removal of misfolded or damaged proteins to prevent the accumulation of unfolded proteins, polJ, pilG, pilH and pixH which are related to cell motility, and the light sensory system proteins cph1 and rcp1, were also up-regulated in the 1 mM Cs and 2.5 mM K groups (Yeh et al., 1997; Psakis *et al.,* 2011; Hansen and Hilgenfeld, 2013; Yoshihara and Ikeuchi, 2004; Chung *et al.,* 2001; Whitchurch *et al.,* 2004). crp which is related to biofilm formation was down-regulated in the 0.5 mM Cs and 1 mM Cs + 2.5 mM K groups (Tao et al., 2010).

Pseudanabaena dominated microbial blooms present in the SNFPs inhibited the maintenance work of the facility and increased the risk of enhancing the radioactivity. Understanding the interactions between *P. catenata* and the abundant radionuclides including Cs in the pond is important for determining pond management strategies. Previous studies investigating Cs-microorganism interactions suggested that Cs as an analogue of K might be accumulated via K transport systems (Avery et al., 1992). Therefore, this study evaluated the interactions between Cs, K and P. catenata. The growth kinetics experiment indicated that Cs did not inhibit biomass

yields. By contrast, lower concentration of Cs slightly stimulated the growth of culture. In addition, it has been previously shown that radiation does not significantly affect the growth of P. catenata cells (Foster et al., 2020). This probably is the reason why Pseudanabaena spp. dominated blooms could occur in the nuclear fuel pond.

Two K transport system were expressed in *P.cateata*. A high K^+ affinity, low transport velocity KdpD-ATPase transport system which is normally expressed in low K environments, and a modest K^+ affinity, high transport velocity trK system, which is normally expressed in high K environments (Polarek *et al.,* 1987; Walderhaug *et al.,* 1987). The Kdp-ATPase transport system was switched off due to the high concentration of Cs. However, the high velocity Trk K transport system was strongly stimulated by Cs (**Appendix 4.7 A and B**), which potnetially increased the uptake of Cs/K. The up regulation of the Trk system suggests that the Trk transport system can not discriminate between K and Cs. Previous studies also reported that Cs could be transported via K transport systems (Avery *et al.,* 1992). The similar protein expression patten of 1 mM Cs and 2.5 mM K group indicated that K uptake was increased in the 1mM Cs group. This could explain the up regulation of metabolisms such as photosynthesis presented in the 1 mM Cs group, as K acted as an activator for many enzymes in metabolism (Suelter, 1970). In summary, even though Cs switched off the Kdp-ATPase transport system, a higher velocity Trk system was stimulated. This mechanism may give *P.catenata* the ability to live in a Cs-abundant K-limited environment. The mechanism of Cs inhibition of kdpA expression is unknown. A previous study reported that the N-terminal cytoplasmic region of kdpD is specifically bound to cyclic di-AMP produced by *Staphylococcus aureus,* and resulted in the down regulation of kdp potassium transporters during osmotic stress conditions (Moscoso *et al.,* 2016). It is possible that the uptake of Cs induced the production of this type

of response. Another possible mechanism could be that the KdpD sensor can not discriminate between K and Cs. Further studies are required to uncover the mechanisms at play.

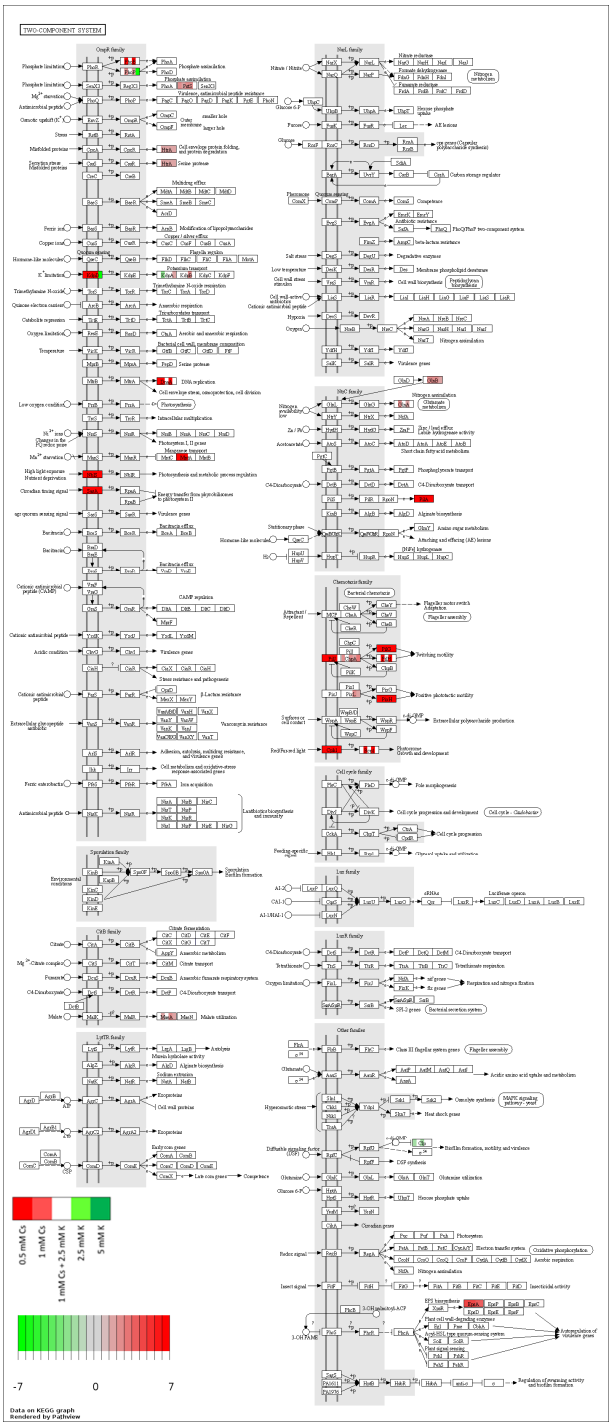

Figure 4.5 Schematic of the two-component system regulated by Cs and K treatment. The results were obtained by plotting the log2 fold change of the quantified proteins identified in the KEGG database. Up-regulated proteins are shown in red colour and down-regulated proteins are shown in green colour in the boxes representing each protein. Each box was divided into 5 segments, the 5 segments from left to right correspond to the expression of proteins in the 0.5 mM Cs, 1 mM Cs, 1 mM Cs + 2.5 mM K, 2.5 mM K and 5 mM K treatments respectively.

4.4 Conclusion

Cs did not affect the growth of *P. catenata* but high concentrations of K significantly inhibited growth. The *P. catenata* cells were able to uptake Cs probably via a K transport system when the concentration of Cs is high enough, and accumulated in discrete locations within the cell, which remain to identified. Understanding the mechanisms by which the Cs is concentrated in discrete zones may help uncover detoxification processes for this metal, and also has implications for Cs retention in biomass within FGMSP and other radioactive environments. Cell morphology also changed with the cellular concentration of Cs, and the impact of Cs on *P. catenata* protein expression was, perhaps not surprisingly dramatic. Exposing cells to 1 mM Cs up regulated many of the photosystem I and II proteins. In addition, a series of stress response proteins and nutrient regulation proteins were stimulated. The proteomic study showed that the expression of the sensor protein kdpD can be induced by the concentration of K and expression of kdpA can be inhibited by Cs. However, the expression of the Trk K transport system proteins TrkA and TrkB could be stimulated by Cs. In summary, these experiments have uncovered mechanisms that *P.catenata* adapt to Cs abundant environment and provide evidence that Cs can be accumulated in discrete zones by *P. catenata.* However, the sub-cellular region where Cs is stored is unknown. Further experiments can identify the

structures or proteins that Cs is associated with, which may allow further understanding of the cellular Cs response mechanisms.

4.5 References

Anderson, J. M. (1992). Cytochrome b 6 f complex: dynamic molecular organization, function and acclimation. Photosynthesis Research, 34(3), 341-357.

Avery, S. V., Codd, G. A., & Gadd, G. M. (1991). Caesium accumulation and interactions with other monovalent cations in the cyanobacterium *Synechocystis PCC 6803*. Microbiology, 137(2), 405-413.

Avery, S. V., Codd, G. A., & Gadd, G. M. (1992). Caesium transport in the cyanobacterium *Anabaena variabilis*: kinetics and evidence for uptake via ammonium transport system (s). FEMS microbiology letters, 95(2-3), 253-258.

Avery, S. V., Codd, G. A., & Gadd, G. M. (1992). Replacement of cellular potassium by caesium in *Chlorella emersonii*: differential sensitivity of photoautotrophic and chemoheterotrophic growth. Microbiology, 138(1), 69-76.

Avery, S. V. (1995). Microbial interactions with caesium—implications for biotechnology. Journal of Chemical Technology & Biotechnology: International Research in Process, Environmental AND Clean Technology, 62(1), 3-16.

Bakken, L. R., & Olsen, R. A. (1990). Accumulation of radio caesium in fungi. Canadian journal of microbiology, 36(10), 704-710.

Baniulis, D., Yamashita, E., Zhang, H., Hasan, S. S., & Cramer, W. A. (2008). Structure–function of the cytochrome b6f complex. Photochemistry and photobiology, 84(6), 1349-1358.

Billi, D., & Potts, M. (2002). Life and death of dried prokaryotes. *Research in microbiology*, *153*(1), 7-12.

Blanco-Rivero, A., Leganes, F., Fernandez-Valiente, E., Calle, P., & Fernandez-Pinas, F. (2005). mrpA, a gene with roles in resistance to Na+ and adaptation to alkaline pH in the cyanobacterium *Anabaena sp. PCC7120*. *Microbiology*, *151*(5), 1671-1682.

Chicote, E., García, A. M., Moreno, D. A., Sarró, M. I., Lorenzo, P. I., & Montero, F. (2005). Isolation and identification of bacteria from spent nuclear fuel pools. *Journal of Industrial Microbiology and Biotechnology*, *32*(4), 155-162.

Chung, Y. H., Cho, M. S., Moon, Y. J., Choi, J. S., Yoo, Y. C., Park, Y. I., ... & Park, Y. M. (2001). ctr1, a gene involved in a signal transduction pathway of the gliding motility in the cyanobacterium *Synechocystis sp. PCC 6803*. FEBS letters, 492(1-2), 33-38.

Czirják, G. Á., Møller, A. P., Mousseau, T. A., & Heeb, P. (2010). Microorganisms associated with feathers of barn swallows in radioactively contaminated areas around Chernobyl. *Microbial ecology*, *60*(2), 373-380.

Foster, L., Muhamadali, H., Boothman, C., Sigee, D., Pittman, J. K., Goodacre, R., ... & Lloyd, J. R. (2020). Radiation tolerance of *Pseudanabaena catenata*, a cyanobacterium relevant to the first generation magnox storage pond. *Frontiers in microbiology*, *11*, 515.

Freeman, Z. N., Dorus, S., & Waterfield, N. R. (2013). The KdpD/KdpE two-component system: integrating K+ homeostasis and virulence. PLoS pathogens, 9(3), e1003201.

Fukuda, S. Y., Iwamoto, K., Atsumi, M., Yokoyama, A., Nakayama, T., Ishida, K. I., ... & Shiraiwa, Y. (2014). Global searches for microalgae and aquatic plants that can eliminate radioactive cesium, iodine and strontium from the radio-polluted aquatic environment: a bioremediation strategy. Journal of plant research, 127(1), 79-89.

Golbeck, J. H., & Bryant, D. A. (1991). Photosystem I. Current topics in bioenergetics, 16, 83-177.

Groisman, E. A. (2001). The pleiotropic two-component regulatory system PhoP-PhoQ. Journal of bacteriology, 183(6), 1835-1842.

Hansen, G., & Hilgenfeld, R. (2013). Architecture and regulation of HtrA-family proteins involved in protein quality control and stress response. Cellular and Molecular Life Sciences, 70(5), 761-775.

Haselwandter, K., Berreck, M., & Brunner, P. (1988). Fungi as bioindicators of radio caesium contamination: pre-and post-Chernobyl activities. Transactions of the British Mycological Society, 90(2), 171-174.

Hoyos-Hernandez, C., Courbert, C., Simonucci, C., David, S., Vogel, T. M., & Larose, C. (2019). Community structure and functional genes in radionuclide contaminated soils in Chernobyl and Fukushima. *FEMS microbiology letters*, *366*(21), fnz180.

Jackson, S. F., Monk, S. D., & Riaz, Z. (2014). An investigation towards real time dose rate monitoring, and fuel rod detection in a First Generation Magnox Storage Pond (FGMSP). Applied Radiation and Isotopes, 94, 254-259.

Katz, A., Waridel, P., Shevchenko, A., & Pick, U. (2007). Salt-induced changes in the plasma membrane proteome of the halotolerant alga Dunaliella salina as revealed by blue native gel electrophoresis and nano-LC-MS/MS analysis. *Molecular & Cellular Proteomics*, *6*(9), 1459-1472.

Knaff, D. B. (1996). Ferredoxin and ferredoxin-dependent enzymes. In Oxygenic photosynthesis: the light reactions (pp. 333-361). Springer, Dordrecht.

Koarashi, J., Moriya, K., Atarashi-Andoh, M., Matsunaga, T., Fujita, H., & Nagaoka, M. (2012). Retention of potentially mobile radio cesium in forest surface soils affected by the Fukushima nuclear accident. Scientific reports, 2(1), 1-5.

Kurisu, G., Kusunoki, M., Katoh, E., Yamazaki, T., Teshima, K., Onda, Y., ... & Hase, T. (2001). Structure of the electron transfer complex between ferredoxin and ferredoxin-NADP+ reductase. Nature structural biology, 8(2), 117-121.

Luo, W., Pant, G., Bhavnasi, Y. K., Blanchard Jr, S. G., & Brouwer, C. (2017). Pathview Web: user friendly pathway visualization and data integration. Nucleic acids research, 45(W1), W501-W508.

Makino, K., Amemura, M., Kawamoto, T., Kimura, S., Shinagawa, H., Nakata, A., & Suzuki, M. (1996). DNA binding of PhoB and its interaction with RNA polymerase. Journal of molecular biology, 259(1), 15-26.

McEvoy, J. P., & Brudvig, G. W. (2006). Water-splitting chemistry of photosystem II. Chemical reviews, 106(11), 4455-4483.

MeGraw, V. E., Brown, A. R., Boothman, C., Goodacre, R., Morris, K., Sigee, D., ... & Lloyd, J. R. (2018). A novel adaptation mechanism underpinning algal colonization of a nuclear fuel storage pond. *MBio*, *9*(3).

Mitsunobu, S., Zhu, M., Takeichi, Y., Ohigashi, T., Suga, H., Makita, H., ... & Takahashi, Y. (2015). Nanoscale identification of extracellular organic substances at the microbe–mineral interface by scanning transmission X-ray microscopy. Chemistry Letters, 44(1), 91-93.

Moscoso, J. A., Schramke, H., Zhang, Y., Tosi, T., Dehbi, A., Jung, K., & Gründling, A. (2016). Binding of cyclic di-AMP to the *Staphylococcus aureus* sensor kinase KdpD occurs via the universal stress protein domain and downregulates the expression of the Kdp potassium transporter. Journal of bacteriology, 198(1), 98-110.

Nazina, T. N., Shestakova, N. M., Grigor'yan, A. A., Mikhailova, E. M., Tourova, T. P., Poltaraus, A. B., ... & Belyaev, S. S. (2006). Phylogenetic diversity and activity of

anaerobic microorganisms of high-temperature horizons of the Dagang oil field (PR China). *Microbiology*, *75*(1), 55-65.

Newsholme, P., Lima, M. M. R., Procopio, J., Pithon-Curi, T. C., Bazotte, R. B., & Curi, R. (2003). Glutamine and glutamate as vital metabolites. Brazilian Journal of Medical and Biological Research, 36(2), 153-163.

NDA (2017). Nuclear Decommissioning Authority: Business plan 2017 to 2020. Gov.uk. Available at: https://www.gov.uk/government/consultations/nuclear-decommissioning-authority-business-plan-2017-to-2020 [Accessed June 14, 2020].

Psakis, G., Mailliet, J., Lang, C., Teufel, L., Essen, L. O., & Hughes, J. (2011). Signaling kinetics of cyanobacterial phytochrome Cph1, a light regulated histidine kinase. Biochemistry, 50(28), 6178-6188.

Pikuta, E. V., Hoover, R. B., & Tang, J. (2007). Microbial extremophiles at the limits of life. *Critical reviews in microbiology*, *33*(3), 183-209.

Perkins, J., & Gadd, G. M. (1995). The influence of pH and external H+ concentration on caesium toxicity and accumulation in *Escherichia coli* and *Bacillus subtilis*. Journal of industrial microbiology and biotechnology, 14(3-4), 218-225.

Polarek, J. W., Walderhaug, M. O., & Epstein, W. (1988). [51] Genetics of Kdp, the K+-transport ATPase of *Escherichia coli.* Methods in enzymology, 157, 655-667.

Povinec, P. P., Aoyama, M., Biddulph, D., Breier, R., Buesseler, K., Chang, C. C., ... & Zhang, L. Y. (2013). Cesium, iodine and tritium in NW Pacific waters–a comparison of the Fukushima impact with global fallout. Biogeosciences, 10(8), 5481-5496.

Reimand, J., Isserlin, R., Voisin, V., Kucera, M., Tannus-Lopes, C., Rostamianfar, A., ... & Bader, G. D. (2019). Pathway enrichment analysis and visualization of omics data using g: Profiler, GSEA, Cytoscape and EnrichmentMap. Nature protocols, 14(2), 482-517.

Sarró, M. I., García, A. M., & Moreno, D. A. (2005). Biofilm formation in spent nuclear fuel pools and bioremediation of radioactive water. *International microbiology*, *8*(3), 223-230.

Sasaki, H., Tamaoki, H., Nakata, Y., Sato, K., Yamaguchi, Y., & Takenaka, H. (2016). Localization of cesium and strontium in terrestrial cyanobacteria *Nostoc commune*. Algal Resources, 9(2), 87-92.

Suzuki, C., Yaita, T., Suzuki, S., Pacold, J., Altman, A. B., Minasian, S. G., ... & Osaka, M. (2019). Evaluation of electronic state of Cs-adsorbed clay minerals by NEXAFS analysis using DFT calculations. Journal of Physics and Chemistry of Solids, 127, 169-177.

Sakata, S., Mizusawa, N., Kubota-Kawai, H., Sakurai, I., & Wada, H. (2013). Psb28 is involved in recovery of photosystem II at high temperature in *Synechocystis sp. PCC 6803*. Biochimica et Biophysica Acta (BBA)-Bioenergetics, 1827(1), 50-59.

Singh, S., Singh, A. K., Chakravarthy, D., Singh, T. P. K., & Singh, H. N. (1997). Characteristics of a caesium-resistant (Cs+-R) mutant of the N2-fixing cyanobacterium Nostoc muscorum: dependence on Cs+ or Rb+ for normal diazotrophy and osmotolerance. New phytologist, 136(2), 223-229.

Suelter, C. H. (1970). Enzymes activated by monovalent cations. Science, 168(3933), 789-795.

Takai, N., Nakajima, M., Oyama, T., Kito, R., Sugita, C., Sugita, M., ... & Iwasaki, H. (2006). A KaiC-associating SasA–RpaA two-component regulatory system as a major circadian timing mediator in cyanobacteria. Proceedings of the National Academy of Sciences, 103(32), 12109-12114.

Tao, F., He, Y. W., Wu, D. H., Swarup, S., & Zhang, L. H. (2010). The cyclic nucleotide monophosphate domain of *Xanthomonas campestris* global regulator Clp defines a new class of cyclic di-GMP effectors. Journal of bacteriology, 192(4), 1020-1029.

Tišáková, L. E. N. K. A., Pipíška, M. A. R. T. I. N., Godány, A. N. D. R. E. J., Horník, M. I. R. O. S. L. A. V., Vidová, B., & Augustín, J. (2013). Bioaccumulation of 137 Cs and 60 Co by bacteria isolated from spent nuclear fuel pools. *Journal of Radioanalytical and Nuclear Chemistry*, *295*(1), 737-748.

Van den Hoff, M. J., Geerts, W. J., Das, A. T., Moorman, A. F., & Lamers, W. H. (1991). cDNA sequence of the long mRNA for human glutamine synthase. Biochimica et biophysica acta, 1090(2), 249-251.

Van Waasbergen, L. G., Dolganov, N., & Grossman, A. R. (2002). nblS, a gene involved in controlling photosynthesis-related gene expression during high light and nutrient stress in *Synechococcus elongatus PCC 7942*. Journal of bacteriology, 184(9), 2481-2490.

Walderhaug, M. O., Dosch, D. C., & Epstein, W. (1987). Potassium transport in bacteria. In Ion transport in prokaryotes (pp. 85-130). Academic Press.

Weisz, D. A., Liu, H., Zhang, H., Thangapandian, S., Tajkhorshid, E., Gross, M. L., & Pakrasi, H. B. (2017). Mass spectrometry-based cross-linking study shows that the Psb28 protein binds to cytochrome b559 in Photosystem II. Proceedings of the National Academy of Sciences, 114(9), 2224-2229.

Whitchurch, C. B., Leech, A. J., Young, M. D., Kennedy, D., Sargent, J. L., Bertrand, J. J., ... & Mattick, J. S. (2004). Characterization of a complex chemosensory signal transduction system which controls twitching motility in *Pseudomonas aeruginosa*. Molecular microbiology, 52(3), 873-893.

Wu, T., Hu, E., Xu, S., Chen, M., Guo, P., Dai, Z., ... & Yu, G. (2021). clusterProfiler 4.0: A universal enrichment tool for interpreting omics data. The Innovation, 100141.

Yamaguchi, K., Suzuki, I., Yamamoto, H., Lyukevich, A., Bodrova, I., Los, D. A., ... & Murata, N. (2002). A two-component Mn2+-sensing system negatively regulates expression of the mntCAB operon in *Synechocystis*. The Plant Cell, 14(11), 2901-2913.

Yeh, K. C., Wu, S. H., Murphy, J. T., & Lagarias, J. C. (1997). A cyanobacterial phytochrome two-component light sensory system. Science, 277(5331), 1505-1508.

Yoshihara, S., & Ikeuchi, M. (2004). Phototactic motility in the unicellular cyanobacterium *Synechocystis sp. PCC 6803*. Photochemical & Photobiological Sciences, 3(6), 512-518.

Zhu, M., Yu, G., Song, G., Chang, J., Wan, C., & Li, R. (2015). Molecular specificity and detection for *Pseudanabaena* (cyanobacteria) species based on rbcLX sequences. Biochemical Systematics and Ecology, 60, 110-115.

4.6 Appendix

Appendix 4.1 Chemical composition of BG-11 medium

Chemical	Concentration in BG11 (mM)
NaNO3	17.64913519
K2HPO4	0.229647491
MgSO4.7H2O	0.304296669
CaCl2.2H2O	0.244881301
CITRIC ACID (C6H8O7)	0.031230481
FeC6H11NO7	0.022641509
EDTANa2	0.002974332
Na2CO3	0.188697047
H3BO3	0.046255863
MnCl2.4H2O	0.009145571
ZnSO4.7H2O	0.000765058
Na2MoO4.2H2O	0.001611903
CuSO4.5H2O	0.000320397
Co(NO3)2.6H2O	0.000171804

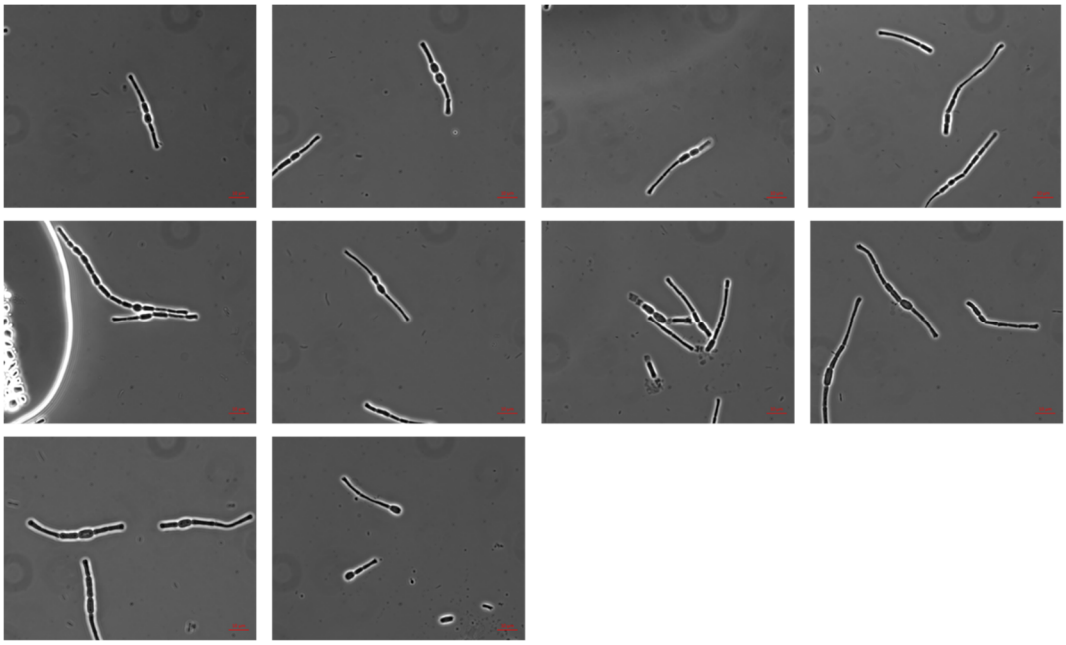

Appendix 4.2 Cells in 1 mM Cs group observed under light microscopy, x1000 amplification. Samples were taken after 10 days incubation

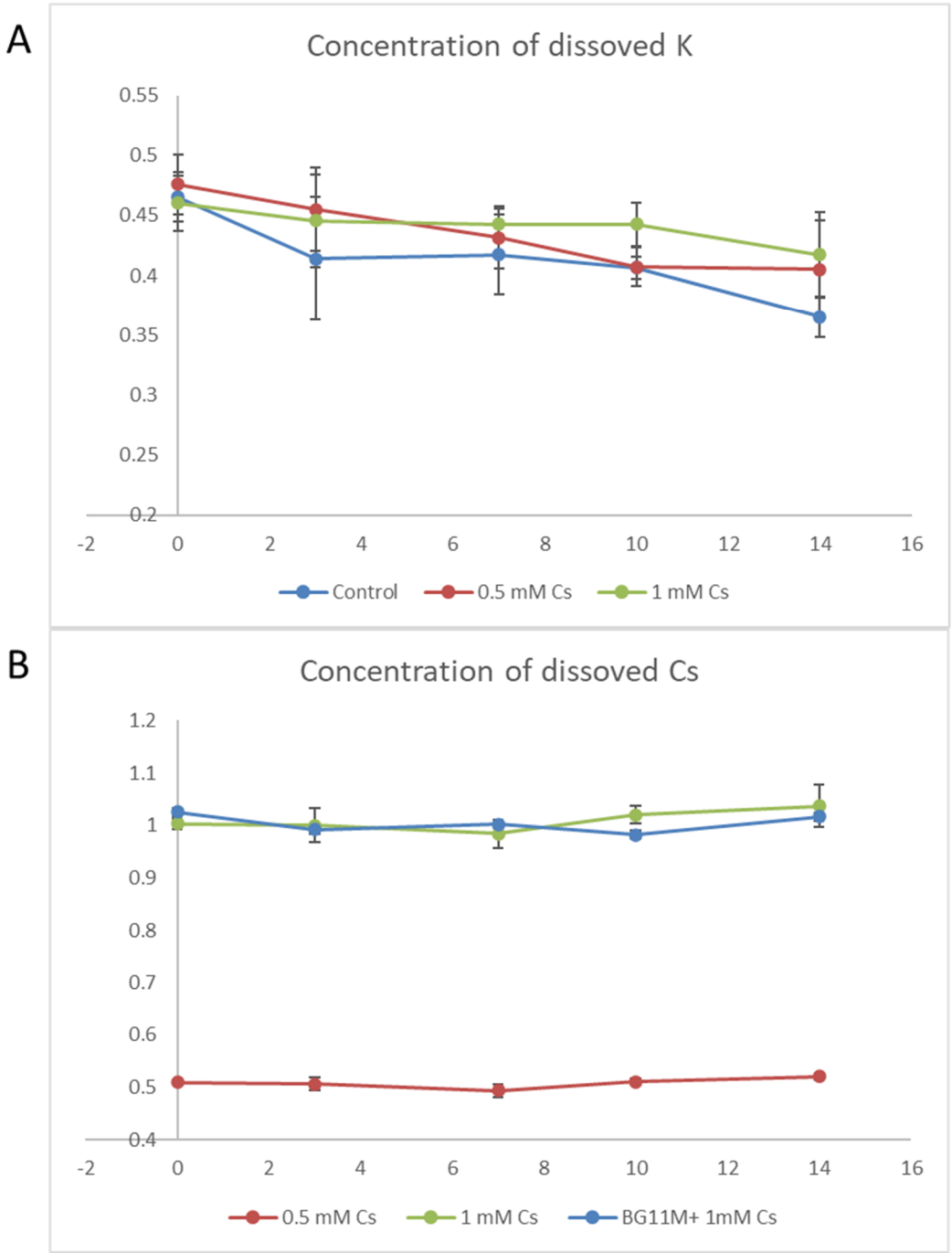

Appendix 4.3. (A) concentration of K in supernatant. (B) concentration of Cs in supernatant

Appendix 4.4. Enrichment results of the differentially expressed pathways.

5 mM K	Description	setSize	p-value
ko00270	Cysteine and methionine metabolism	15	0.009055627
ko00300	Lysine biosynthesis	10	0.009915014
ko00195	Photosynthesis	27	0.030732861
ko00240	Pyrimidine metabolism	12	0.048209366
2.5 mM K			
ko02020	Two-component system	32	0.01807229
ko00720	Carbon fixation pathways in prokaryotes	12	0.03181336
ko00300	Lysine biosynthesis	10	0.0369164
1 mM Cs + 2.5 mM K			
ko02020	Two-component system	29	0.005733945
ko00195	Photosynthesis	27	0.018306636
ko00400	Phenylalanine, tyrosine and tryptophan biosynthesis	12	0.019417476
ko00190	Oxidative phosphorylation	26	0.02173913
ko00240	Pyrimidine metabolism	65	0.033985582
ko02010	ABC transporters	48	0.038297872
1 mM Cs			
ko00300	Lysine biosynthesis	10	0.003232759
ko00270	Cysteine and methionine metabolism	15	0.00619195
ko02020	Two-component system	34	0.009045226
ko00720	Carbon fixation pathways in prokaryotes	12	0.019047619
ko00195	Photosynthesis	27	0.042253521
0.5 mM Cs			
ko02020	Two-component system	31	0.003401361
ko02010	ABC transporters	49	0.011904762
ko00190	Oxidative phosphorylation	26	0.03959276
ko03060	Protein export	10	0.044136192

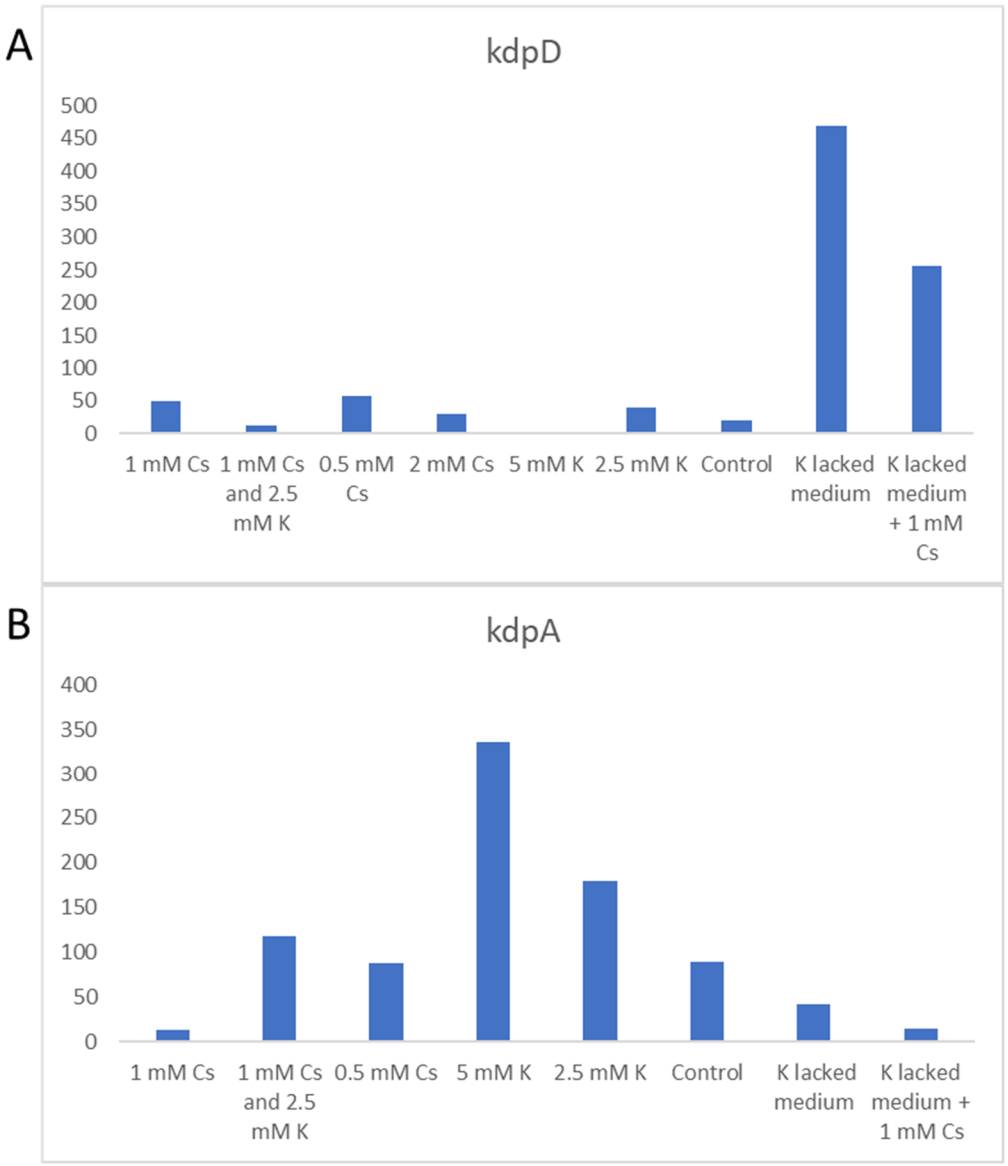

Appendix 4.5 (A) Grouped abundance values of kdpD proteins (B) Grouped abundance values of kdpA proteins

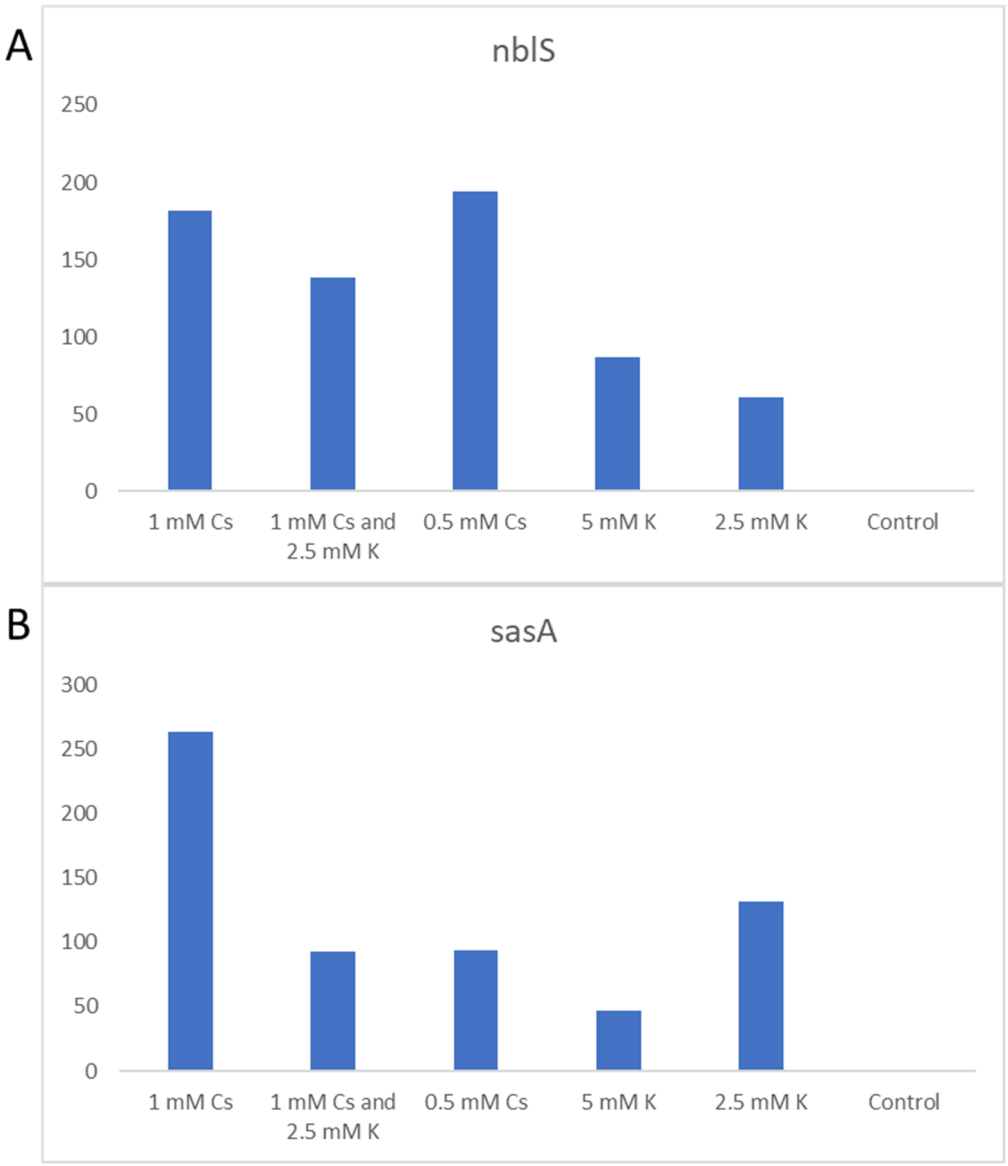

Appendix 4.6 (A) Grouped abundance values of nblS proteins (B) Grouped abundance values of sasA proteins

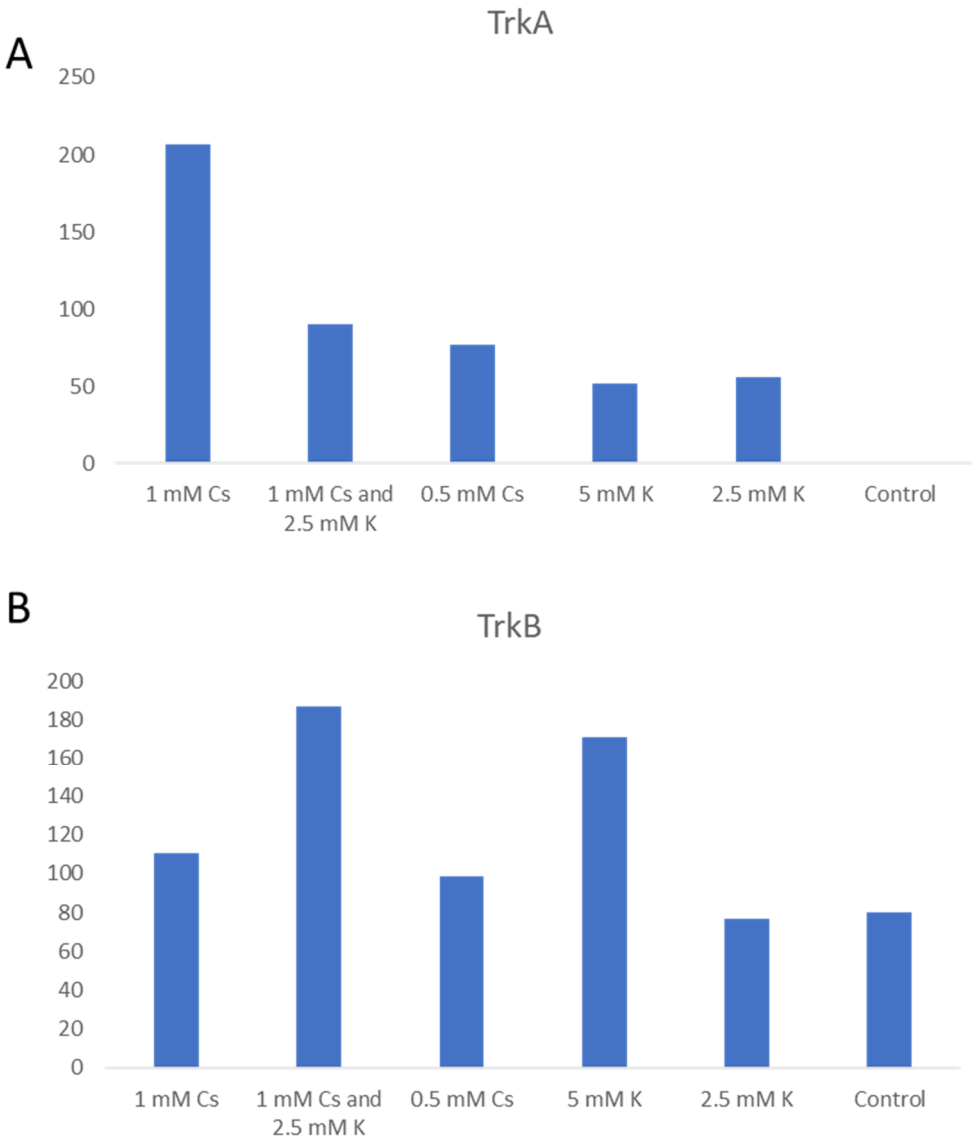

Appendix 4.7 (A) Grouped abundance values of TrkA proteins (B) Grouped abundance values of TrkB proteins

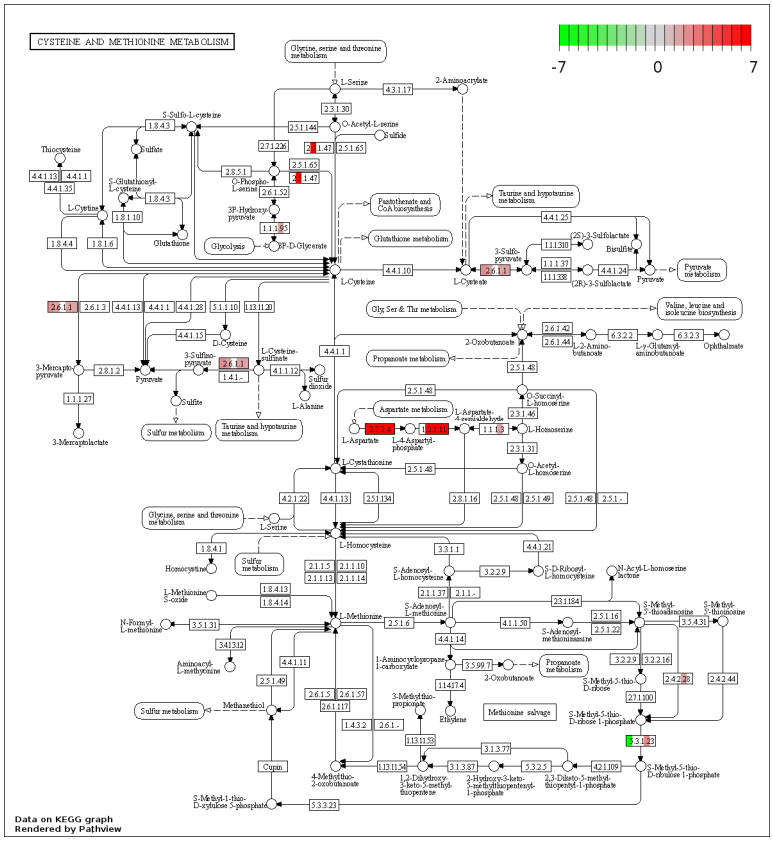
CYSTEINE AND METHIONINE METABOLISM
-7
0
7
Glycine, serine and threonine metabolism
L-Serine
2-Aminoacrylate
S-Sulfo-L-cysteine
O-Acetyl-L-serine
Sulfide
Thiocysteine
Sulfate
S-Glutathiocyl-L-cysteine
L-Cystine
Glutathione
O-Phospho-L-serine
3P-Hydroxy-pyruvate
Glycolysis
3P-D-Glycerate
Pantothenate and CoA biosynthesis
Glutathione metabolism
Taurine and hypotaurine metabolism
3-Sulfo-pyruvate
(2S)-3-Sulfolactate
Bisulfite
(2R)-3-Sulfolactate
Pyruvate
Pyruvate metabolism
L-Cysteine
Gly, Ser & Thr metabolism
Valine, leucine and isoleucine biosynthesis
2-Oxobutanoate
L-2-Amino-butanoate
L-γ-Glutamyl-aminobutanoate
Ophthalmate
Propanoate metabolism
D-Cysteine
L-Cysteine-sulfinate
3-Sulfino-pyruvate
3-Mercapto-pyruvate
Sulfur dioxide
L-Alanine
Sulfite
3-Mercaptolactate
Sulfur metabolism
Taurine and hypotaurine metabolism
Aspartate metabolism
L-Aspartate
L-4-Aspartyl-phosphate
L-Aspartate-4-semialdehyde
L-Homoserine
O-Succinyl-L-homoserine
O-Acetyl-L-homoserine
L-Cystathionine
Glycine, serine and threonine metabolism
L-Serine
L-Homocysteine
Sulfur metabolism
Homocysteine
L-Methionine S-oxide
N-Formyl-L-methionine
L-Methionine
S-Adenosyl-L-homocysteine
S-D-Ribosyl-L-homocysteine
N-Acyl-L-homoserine lactone
S-Adenosyl-L-methionine
S-Adenosyl-methioninamine
S-Methyl-5'-thioadenosine
S-Methyl-5'-thioinosine
Aminoacyl-L-methionine
1-Aminocyclopropane-1-carboxylate
Propanoate metabolism
2-Oxobutanoate
S-Methyl-5-thio-D-ribose
S-Methyl-5-thio-D-ribose 1-phosphate
Sulfur metabolism
Methanethiol
3-Methylthio-propanoate
Ethylene
Methionine salvage
Cupin
4-Methylthio-2-oxobutanoate
1,2-Dihydroxy-3-keto-5-methyl-thiopentene
3-Hydroxy-3-keto-5-methylthiopentenyl-1-phosphate
2,3-Diketo-5-methyl-thiopentyl-1-phosphate
S-Methyl-5-thio-D-ribulose 1-phosphate
S-Methyl-1-thio-D-xylulose 5-phosphate
Data on KEGG graph
Rendered by Pathview

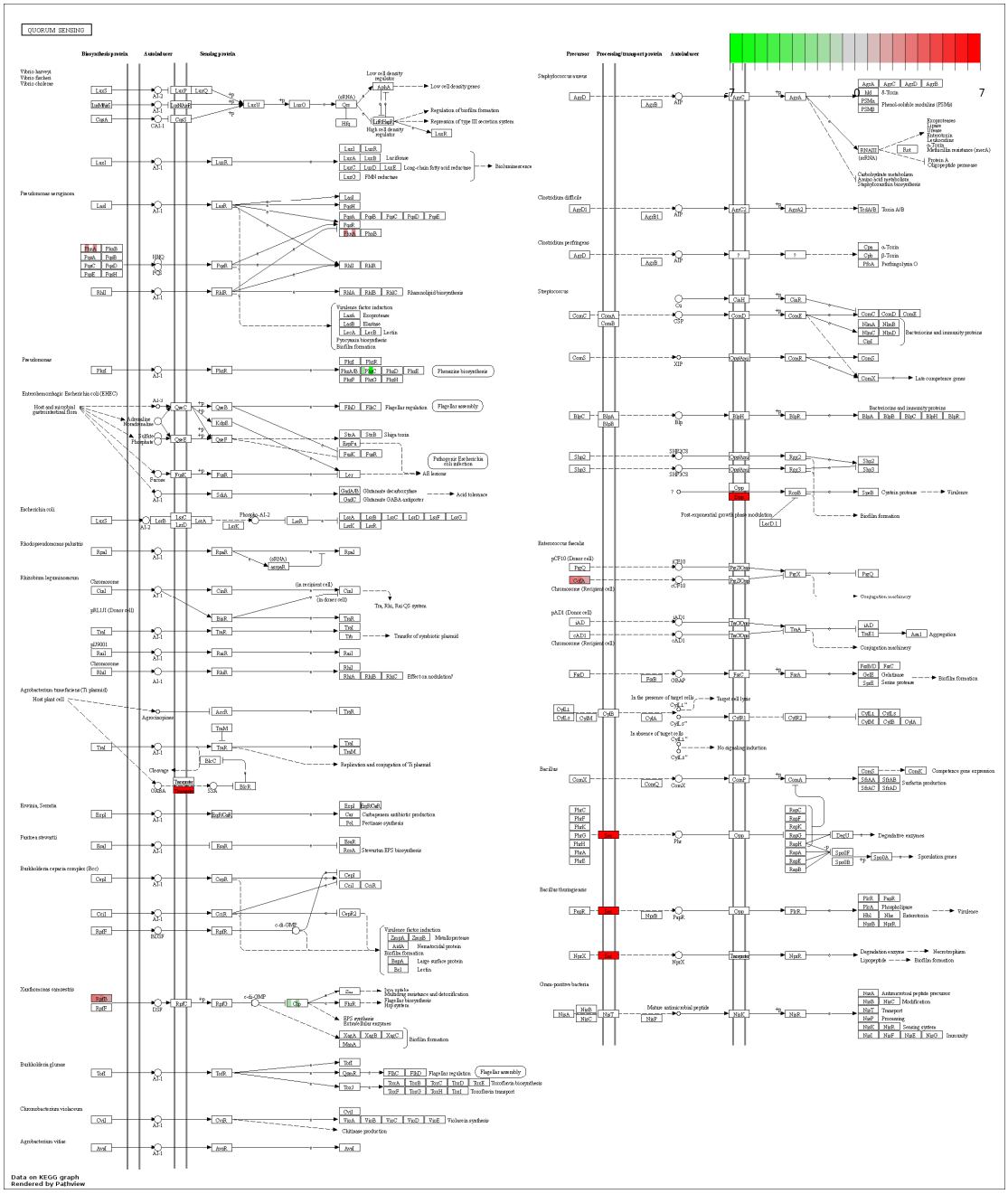
QUORUM SENSING
Biosynthesis protein
Autoinducer
Sensing protein
Precursor
Processing/transport protein
Autoinducer
Vibrio harveyi
Vibrio fischeri
Vibrio cholerae
Low cell density gene
Regulation of biofilm formation
Repression of type III secretion system
High cell density gene
Bioluminescence
Pseudomonas aeruginosa
Pseudomonas
Enterohemorrhagic Escherichia coli (EHEC)
Host and microbial gastrointestinal flora
Adrenaline Noradrenaline
Sulfate Phosphate
Pathogenic Escherichia coli infection
All factors
Flagellar regulation
Flagellar assembly
Shiga toxin
Acid tolerance
Escherichia coli
Rhodopseudomonas palustris
Rhizobium leguminosarum
Chromosome
pRLL01 (Donor cell)
pJ0001
Transfer of symbiotic plasmid
Effect on nodulation?
Agrobacterium tumefaciens (Ti plasmid)
Host plant cell
Agrocinopines
Cleavage
Replication and conjugation of Ti plasmid
Erwinia, Serratia
Carbapenem antibiotic production
Pectinase synthesis
Pantoea stewartii
Stewartan EPS biosynthesis
Burkholderia cepacia complex (Bcc)
Xanthomonas campestris
c-di-GMP
Virulence factor induction
Metalloprotease
Hemolytical protein
Biofilm formation
Large staffen protein
Lectin
EPS synthesis
Extracellular enzymes
Biofilm formation
Burkholderia glumae
Toxoflavin biosynthesis
Toxoflavin transport
Chromobacterium violaceum
Violacein synthesis
Chitinase production
Agrobacterium vitae
Staphylococcus aureus
Phenol-soluble modulins (PSMs)
Exoproteases
Lipase
Hemolysins
Enterotoxins
Exfoliative toxins
Methicillin resistance (mecA)
Protein A
Clumping factor
Carbohydrate metabolism
Amino acid metabolism
Staphylococcidin biosynthesis
Clostridium difficile
Toxin A/B
Clostridium perfringens
α-Toxin
β-Toxin
Perfringolysin O
Streptococcus
Competence and sporulation
Bacteriocins and immunity proteins
Late competence genes
Cysteine protease
Virulence
Biofilm formation
Post-exponential growth phase modulation
Enterococcus faecalis
pCF10 (Donor cell)
Chromosome (Recipient cell)
Conjugation machinery
pAD1 (Donor cell)
Aggregation
Bacillus
Competence gene expression
Surfactin production
Degradative enzymes
Sporulation genes
Bacillus thuringiensis
Phospholipase
Hemolysin
Enterotoxin
Degradation enzyme
Necrotrophism
Lipopeptide
Biofilm formation
Gram-positive bacteria
Antimicrobial peptide precursor
Modification
Transport
Processing
Sensing system
Immunity
Data on KEGG graph
Rendered by Pathview

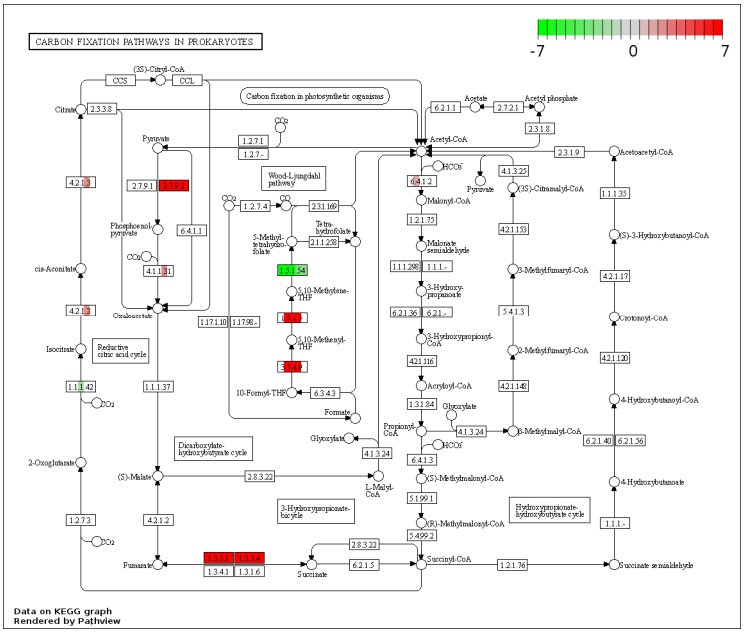
CARBON FIXATION PATHWAYS IN PROKARYOTES
-7
0
7
Data on KEGG graph
Rendered by Pathview

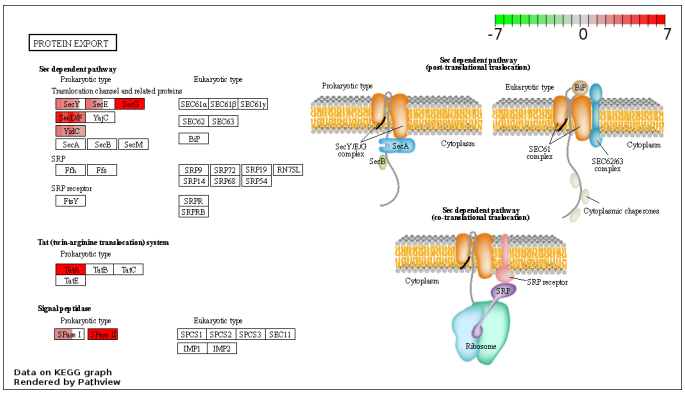
PROTEIN EXPORT
-7
0
7
Sec dependent pathway
Prokaryotic type
Eukaryotic type
Tat (twin-arginine translocation) system
Signal peptidase
Sec dependent pathway (post-translational translocation)
Sec dependent pathway (co-translational translocation)
Data on KEGG graph
Rendered by Pathview

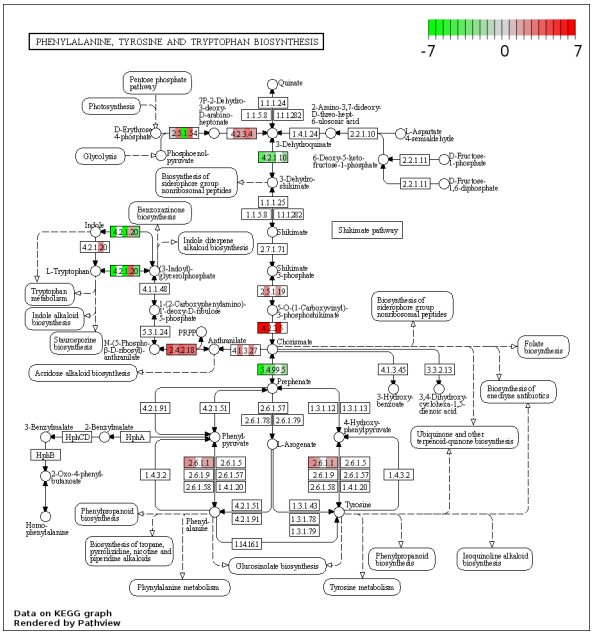
PHENYLALANINE, TYROSINE AND TRYPTOPHAN BIOSYNTHESIS
-7
0
7
Shikimate pathway
Data on KEGG graph
Rendered by Pathview

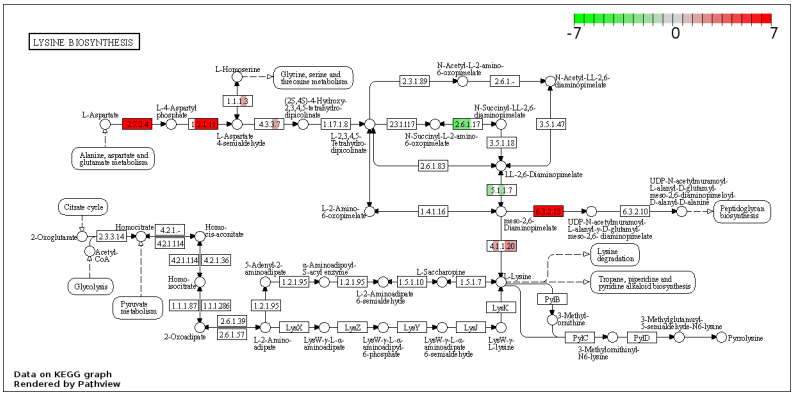
LYSINE BIOSYNTHESIS
-7
0
7
Data on KEGG graph
Rendered by Pathview

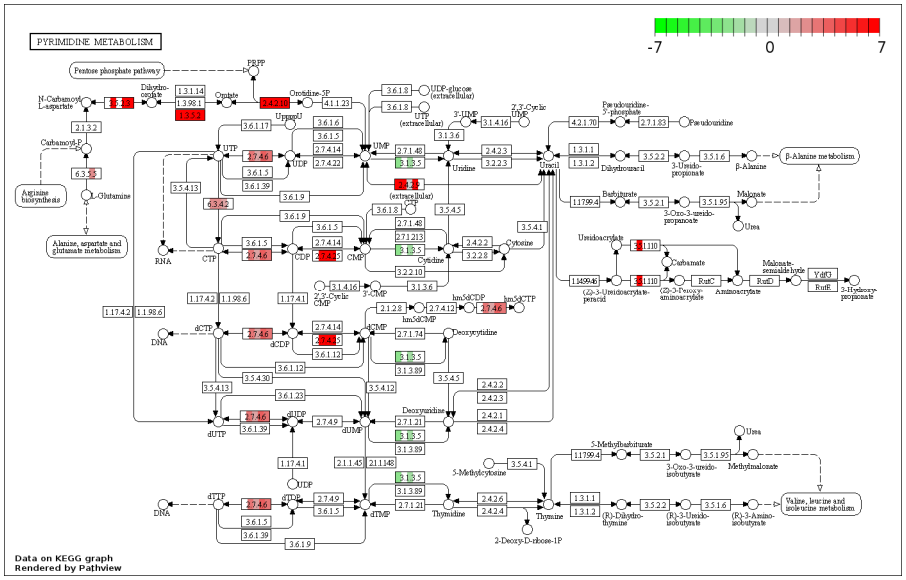
PYRIMIDINE METABOLISM
-7
0
7
Data on KEGG graph
Rendered by Pathview

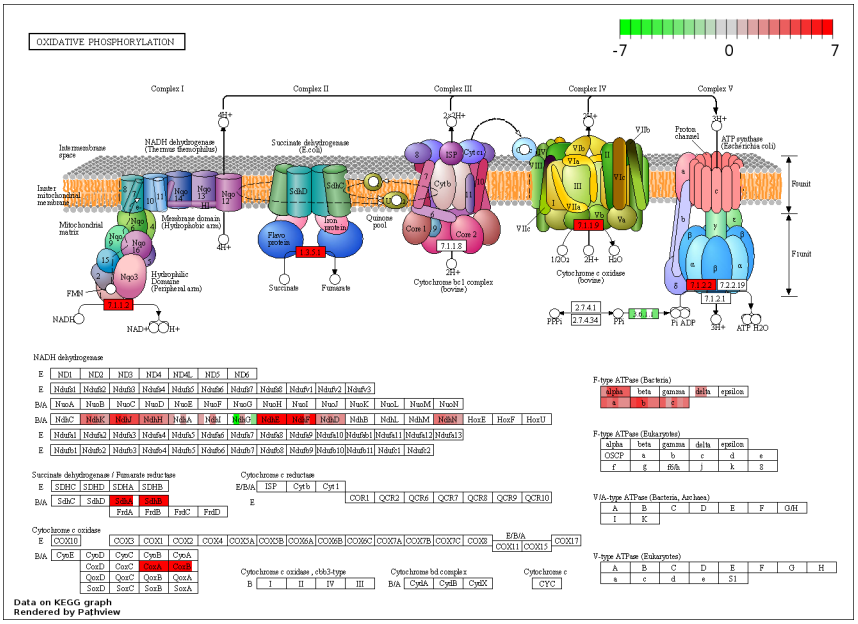
OXIDATIVE PHOSPHORYLATION
-7
0
7
Complex I
Complex II
Complex III
Complex IV
Complex V
Data on KEGG graph
Rendered by Pathview

Appendix 4.8 Schematic of enriched pathways regulated by Cs and K treatment. The results were obtained by plotting the log2 fold change of the quantified proteins identified in the KEGG database. Up-regulated proteins are shown in red colour and down-regulated proteins are shown in green colour in the boxes representing each protein. Each box was divided into 5 segments, the 5 segments from left to right correspond to the expression of proteins in the 0.5 mM Cs, 1 mM Cs, 1 mM Cs + 2.5 mM K, 2.5 mM K and 5 mM K treatments respectively.

Chapter 5 KOH versus NaOH, the inhibited effect on the growth of cyanobacteria *Pseudanabaena catenata*: Implications for control of P. catenata dominated blooms in FGMS

Kejing Zhang, Lynn Foster, Christopher Boothman, Jon K Pittman and Jonathan R Lloyd

Abstract

Microbial blooms have been reported in the First Generation Magnox Storage Pond (FGMSP) at the Sellafield Nuclear Facility where they disrupt facility operation. The dominant microorganism within the bloom is a very close relative to the cyanobacterium *Pseudanabaena catenata*. A previous study has suggested that although this organism is tolerant to the high pH values maintained within FGMSP (to prevent corrosion of the stored waste materials), this organism is sensitive to potassium ions. This study aimed, therefore, to examine the effect of potassium treatment (as KCl or KOH) versus sodium treatment (as NaCl or NaOH) on growth of a mixed inoculum dominated by *P. catenata* using batch and chemostat cultures. The addition of 5 mM KCl reduced the cell density by 80% by day 14 in the batch culture experiment, while 5 mM NaCl promoted the growth of the culture slightly. The addition of 10 mM NaCl reduced cell growth by 40%. The chemostat experiment also indicated that KOH has a strong ability of hindering the growth of the *Pseudanabaena* dominated culture, while NaOH maintained stability to the end of the experiment, when the concentration of NaOH reached 29.4 mM. Microbial community analysis demonstrated that the KOH-dependent inhibition of cell growth was organism specific in this non axenic culture of *P. catenata*. KOH treatment substantially reduced the relative abundance of *P. catenata*, and the total number of

expressed proteins of *P. catenata* were significantly reduced. In contrast, bacteria at the genus level related to *Phreatobacter (G)*, *Roseomonas (G)* and *Rhodobacteraceae (F)* increased with the KOH dosing. Both KOH and NaOH dosing enhanced the down regulation of *Pseudanabaena* protein expression. Proteins response to KOH are summarized. Collectively these data show that the alkali-tolerant bloom forming cyanobacterium *P. catenata* is sensitive to potassium ions, and the addition of KOH to nuclear storage ponds may help inhibit growth of this organism, while maintaining the high pH needed to inhibit nuclear fuel waste corrosion.

5.1 Introduction

Algal blooms are presented as the excessive growth of algae, cyanobacteria, and protists in freshwater or marine aquatic system (Deng *et al.,* 2017). The blooms can seriously affect water quality, and damage the stability of aquatic ecosystems. Some toxin-producing species in the bloom are serious threats to animal and human health (Pan et *al.,* 2011; Liu *et al.,* 2013). Microorganisms are able to adapt to a wide range of environments including extremes of salinity, pressure, temperature, pH and radiation (Billi and potts, 2002; Blanco-Rivero *et al.*, 2005; Pikuta *et al.,* 2007; Nazina *et al.,* 2007; Katz *et al.,* 2007; Foster *et al.,* 2020a). Even in an environment as extreme as Spent Nuclear Fuel Ponds (SNFPs), algal blooms have been reported (Diosi *et al.,* 2003; Chicote *et al.,* 2004; Sarró *et al.,* 2003; Dekker *et al.,* 2014; Rivasseau *et al.,* 2016; Karley *et al.,* 2017; MeGraw *et al.,* 2018; Foster *et al.,* 2020). Seasonal blooms in SNFPs have challenged facility maintenance and management, by reducing the visibility of pond water (to prevent retrievals), biofouling of pond surfaces, potentially causing microbial induced corrosion, and leading to the formation of radioactive, organic rich sludges due to bioaccumulation of radionuclides in decaying biomass (Avery *et al.,* 1992; Foster *et al.,* 2020; MeGraw *et al.,* 2018).

The First-Generation Magnox Storage Pond (FGMSP) at the Sellafield site in Cumbria, UK was constructed to accept spent Magnox fuels from the 1950s. The pond is routinely purged with deionized water to buffer the pond pH to 11.4 by NaOH to minimise the corrosion of the stored fuel cladding (Fostor *et al.,* 2020a). However, the long-term operation has resulted in a significant level of radioactive sludge accumulation in the pond. In addition, the FGMSP is open-aired facility and so animal remains, wind-blown sand and other materials have been introduced into the pond. Therefore, the access to sunlight and external nutrients from these materials will risk driving photoautotropic (and heterotrophic) growth. The microbial

community of FGMSP has been previously investigated by Foster *et al* (2020). A cyanobacterium identified as a *Pseudanabaena* sp. was shown to be the single dominant photosynthetic organism during the bloom event. Thus, developing a mitigation method for this pioneering photosynthetic bacterium is important for controlling the growth of blooms in the pond.

Algal blooms are global issues for many different aquatic environments, and many control methods have been developed. However, most of them are unsuitable for the FGMSP. For example, the effectiveness of nutrient removal is limited by the open-air nature of the pond. Halogenation and oxidation methods are not possible due to the high alkaline environment of the pond and they may cause reactions with the pond radioactive inventory materials. Other engineering approaches, for example placing a roof over the pond, is also impractical given the complex legacy infrastructure at the facility.

Potassium is an essential element for all microorganisms. It helps to maintain cell osmolarity and is an activator of many cell enzymes (Evans and Sorger, 1966; Suelter, 1970). However, high concentrations of potassium can be toxic to some microorganisms. For example, Parker et al (1997) reported that the cyanobacterium *Microcystis aeruginosa* is sensitive to K^+ ions such that 3 mM of K^+ resulted in a 50% reduction of growth. During routine FGMSP operations, NaOH is used to maintain alkaline conditions in the pond, required to prevent corrosion of the stored waste materials (Foster *et al.,* 2020). In this study the effects of KOH on growth of *Pseudanabaena sp*. was explored, to determine whether KOH can be used as an alternative to NaOH to achieve both the purpose of maintaining alkaline pH conditions and mitigation the blooms. In this study, a mixed laboratory culture dominated by *Pseudanabaena catenata* was used as a model for the pond community as it is a close relative to the cyanobacterium identified

in the FGMSP (and contained other heterotrophs known to co-colonise the pond). Low concentration of nutrients and a high pH environment were simulated by use of BG-11 medium (**Appendix 5.1**). Batch culture experiments were used first to test the effect of K^+ and Na^+ on *P. catenata* growth. A continuous flushed chemostat experiment was then used as a pond simulation to compare the inhibition effect of KOH and NaOH on *P. catenata* growth. 16S rRNA gene sequencing was used to determine the influence of KOH/NaOH on the microbial community while proteomics techniques were used to investigate the effect of KOH/NaOH on protein expression within the treated cultures.

5.2 Materials and Methods

As radiological safety limitations prevented obtaining organisms directly from water in the Spent Nuclear Fuel Pond (SNFP), a related strain of *Pseudanabaena catenata* was obtained from the NIVA Culture Collection of Algae (strain NIVA-CYA 152), Norway, and was used as a representative culture for the pond system (Foster *et al.,* 2020a). An axenic culture is not available and the culture used in this study is a mixed culture. Previous analysis has demonstrated that several key genera presented in the FGMSP were contained in this culture. Therefore this culture was highly representative of the microbial community in the pond.

5.2.1 Batch Culture Experiment

Cultures were set up by inoculating *P. catenata* into BG-11 medium to a final volume of 30 ml. The starting optical density at 600 nm (OD_{600}) was set to 0.3. Cultures were prepared with the addition of 1 mM KCl, 2.5 mM KCl, 5 mM KCl and 10 mM KCl respectively in BG-11 cultures. A treatment of NaCl spiked cultures were also set up with the same concentrations of KCl. A culture with no addition of KCl and NaCl was used as a control. Biological triplicates were prepared for all of the 9 treatments and in total 12 cultures were incubated for 2 weeks on

a shaker at 140 rpm under a white light intensity of 30 µmol m^{-2} s^{-1} on a 16:8 h light-dark cycle. The temperature of the incubator was controlled at 20 ± 1°C. Samples were taken at day 0, 3, 7, 10 and 14. Cell growth was quantified by measuring the OD_{600nm} values of 1 mL aliquots of *P. catenata* cultures using a Jenway 6700 UV/Vis spectrophotometer (Bibby Scientific Limited, Staffordshire).

5.2.2 Chemostat Experiment

P. catenata cultures were grown in 1 L Fernbach flasks containing 300 ml of BG-11 medium. Cells were grown under fluorescent lights with a 16:8 h light-dark regime on a magnetic stirrer (Fisher Scientific Isotemp, China) operating at 50 rpm. Cultures were flushed with BG-11 medium at a flow rate of 10 ml/day by using Watson Marlow 205U pumps. Three cultures were operated in the experiment, one control culture was constantly flushed with BG-11 medium. A KOH group was flushed with BG-11 medium for the first 2 weeks, then continuously flushed with BG-11 medium containing 10 mM of KOH. A NaOH group was flushed with BG-11 medium for the first 17 days, then continuously flushed with BG-11 medium containing 10 mM of NaOH. Cell growth was routinely quantified by measuring OD_{600nm} values. Concentrations of K and Na in the growth medium were quantified by inductively coupled plasma mass spectrometry (Agilent 7700 Series ICP-MS). 1 ml samples were removed at day 17, 26, 38 and 53 for microbial community analysis. 1 ml of cultures were sampled at day 17, 26 and 38 for protein expression analysis.

5.2.3 DNA extraction and 16S rRNA gene sequencing

DNA was extracted from 200 µl of sample using a DNeasy PowerSoil Pro Kit (Qiagen, Manchester, U.K). Sequencing of PCR amplicons of 16S rRNA genes were conducted with the Illumina MiSeq platform (Illumina, San Diego, CA, USA) targeting the V4 hyper variable

region (forward primer, 515F, 5′-GTGYCAGCMGCCGCGGTAA-3′; reverse primer, 806R, 5′-GGACTACHVGGGTWTCTAAT-3′) for 2 × 250-bp paired-end sequencing (Illumina). PCR amplification was performed using Roche FastStart High Fidelity PCR System (Roche Diagnostics Ltd, Burgess Hill, UK) in 50 µl reactions under the following conditions: initial denaturation at 95°C for 2 min, followed by 36 cycles of 95°C for 30 s, 55°C for 30 s, 72°C for 1 min, and a final extension step of 5 min at 72°C (Caporaso *et al.,* 2011; Caporaso *et al.,* 2012). The PCR products were purified and normalised to ~20 ng each using the SequalPrep Normalization Kit (Fisher Scientific, Loughborough, UK). The PCR amplicons from all samples were pooled in equimolar ratios. The run was performed using a 4.5 pM sample library spiked with 4.5 pM PhiX to a final concentration of 12% following the method of Kozich *et al* (2013). Raw sequences were divided into samples by barcodes (up to one mismatch was permitted) using a sequencing pipeline. Quality control and trimming was performed using Cutadapt, FastQC and Sickle (Martin, 2011; Joshi and Fass, 2011). MiSeq error correction was performed using SPADes (Nurk *et al.,* 2013). Forward and reverse reads were incorporated into full-length sequences with Pandaseq, and chimeras were removed using ChimeraSlayer. For the 16S rRNA gene sequences, OTUs were generated with UPARSE (Hass *et al.*, 2011; Masella *et al.,* 2012; Edgar, 2013). OTUs were classified by Usearch at the 97% similarity level, and singletons were removed (Edgar, 2010). Rarefaction analysis was conducted using the original detected OTUs in Qiime (Caporaso *et al.,* 2010). The taxonomic assignment was performed by the RDP naïve Bayesian classifier version 2.2, used in combination with the Silva SSU 132 ribosomal RNA gene database (Wang *et al.,* 2007; Quast *et al.,* 2013). The OTU tables were rarefied to the sample containing the lowest number of sequences, all samples having less than 5,000 sequences were removed from analyses prior to the rarefaction step. The step size used was 2000 and 10 iterations were performed at each step.

5.2.4 Protein extraction, Identification and Quantification

1 ml of samples were centrifuged at 14000 x g for 10 minutes. Supernatant was removed. Pellets were refined with 130 µl lysis buffer (5% SDS with 50 mM TEAB pH 7.5). Samples were then lysed by LE220-plus Focused-ultrasonicator with the following parameters, peak power: 500 W, duty factor: 40%, cycle/burst: 200, average power 200 W. Each sample was lysed for 600 seconds. Lysed samples were reduced and alkylated with dithiothreitol and iodoacetamide. Protein concentration were quantified by using the Millipore Direct Detect. Protein concentration were then normalized to 1 mg/l for subsequent protein extraction. 5 µl of 12% aqueous phosphoric acid was added to 50 ml (50 µg) protein lysate. 330 µl of S-Trap binding buffer (90% aqueous methanol containing a final concentration of 100 mM TEAB, pH 7.1) was added to acidified protein lysate and mixed. Protein solutions were loaded on a S-Trap column (PROTIFI) and centrifuged at 4000 RCF for 2 min, and then the S-Trap column were washed with 150 µl S-Trap binding buffer 4 times. 20 µl of digestion buffer (50 mM triethylammonium bicarbonate) and 20 µl of 0.25 µg/µl trypsin were added to the S-Trap column and incubated at 47 °C for 1 hour. 3 washes with 65 µl digestion buffer, 65 µl of 0.1% aqueous formic acid and 30 µl of 30% aqueous acetonitrile containing 0.1% formic acid were applied in order to elute peptides. For sample desalination, the digested sample solutions were moved to a Corning FiltrEX desalt filter plates and mixed them with pre-washed beads for 5 mins at 800 RPM. Liquids were removed by centrifuging at 200 g for 1 minute. The wells with beads in were then washed by using 0.1% formic acid twice. Then the peptides were extracted to by 2 washes with 50 µl 0.1% formic acid in 30% acetonitrile. 100 µl peptides solutions were transferred to sample vials and dried in Heto vacuum centrifuge. Died samples were kept in a freezer at -20 °C for subsequent analysis.

Digested samples were analyzed by liquid chromatography–mass spectrometry (LC-MS/MS) using an UltiMate® 3000 Rapid Separation LC (RSLC, Dionex Corporation, Sunnyvale, CA) coupled to a QE-HF (Thermo Fisher Scientific, Waltham, MA) mass spectrometer. Mobile phase A was 0.1% formic acid in water and mobile phase B was 0.1% formic acid in acetonitrile and the column used was a 75 mm x 250 µm i.d. 1.7 µm CSH C18, analytical column (Waters). A 1 µl aliquot of the sample was transferred to a 5 µl loop and loaded on to the column at a flow of 300 nl/min for 5 minutes at 5% mobile phase B. The loop was then taken out of line and the flow was reduced from 300 nl/min to 200 nl/min in 0.5 minute. Peptides were separated using a gradient that went from 5% to 18% mobile phase B in 34.5 minutes, then from 18% to 27% mobile phase B in 8 minutes and finally from 27% mobile phase B to 60% mobile phase B in 1 minute. The column is washed at 60% mobile phase B for 3 minutes before re-equilibration to 5% mobile phase B in 1 minute. At 55 minutes the flow is increased to 300 nl/min until the end of the run at 60 min. Mass spectrometry data were acquired in a data directed manner for 60 minutes in positive mode. Peptides were selected for fragmentation automatically by data dependent analysis on a basis of the top 12 peptides with m/z between 300 to 1750 Th and a charge state of 2, 3 or 4 with a dynamic exclusion set at 15 sec. The MS Resolution was set at 120,000 with an AGC target of 3e6 and a maximum fill time set at 20 ms. The MS2 Resolution was set to 30,000, with an AGC target of 2e5, a maximum fill time of 45 ms, isolation window of 1.3 Th and a collision energy of 28.

Proteome Discoverer software (Version 2.5.0.400) (Thermo Scientific) was used for protein identification and quantification. MS1 spectra with precursor mass between 350 Da and 5000 Da was selected. Raw data was searched against the amino acid sequence of the same culture (sequence data provided by Dr. Lynn Foster in our Manchester group) by using the Sequest HT search engine. A fragment with a peptide length between 6 and 144 was selected. Trypsin was

used as digestion enzyme. A maximum of 2 missed cleavage sites with a fixed amino acid modification through carbamidomethyl and a dynamic amino acid modification by N-terminal acetyl oxidation was accepted. The fragment mass tolerance was set to 0.02 Da and the precursor mass tolerance to 10 ppm. Highly confident peptide hits, peptide-spectrum matches (PSMs) and proteins were selected with false discovery rate (FDR) at 0.01. Precursor Ions Quantifier was used for protein quantification, intensities were used to calculate the peptide abundances. The summed abundances of connected peptide groups were used to calculate protein abundance. The protein abundances ratio was calculated as the median of all possible pairwise peptide ratios of all connected peptides. The protein file was loaded to Perseus software for further comparative analysis (Tyanova *et al.,* 2016).

5.3 Results

5.3.1 The effect of KCl and NaCl on the Growth of *P. catenata* in Batch Culture

The sensitivity of *P. catenata* to K^+ relative to Na^+ was first investigated in a batch culture experiment. The optical density of cultures supplemented with varying concentrations of KCl or NCl was measured over 14 days. The control and lower concentration K^+ cultures (1 mM and 2.5 mM) grew steadily at a similar growth rate (**Figure 5.1 A**) wherein, 1 mM of K^+ slightly promoted the growth, and 2.5 mM of K^+ slightly decreased the growth. The highest optical densities were reached at day 14, with OD_{600nm} measurments of 2.81 (0.019 SD), 2.91 (0.027 SD) and 2.60 (0.040 SD) respectively for the control, 1 mM and 2.5 mM of K^+ cultures. The culture with 5 mM K^+ grew at a much lower rate compared to the control culture, and the highest optical density of the 5 mM K^+ dosed culture (1.04, 0.038 SD) was reached at day 10, then the optical density dropped to 0.45 (0.002 SD) at day 14. 10 mM K^+ showed the strongest inhibition to cell growth. The optical density decreased from 0.31 (0.008 SD) to 0.24 (0.004

SD) after being dosed with 10 mM of K^+, then the cells grew very slowly reaching the highest optical density of 0.60 (0.014 SD) at day 14.

NaCl affected the growth of cells much less when compared to KCl (**Figure 5.1 B**). Optical density of the cultures experienced steady increases except the culture spiked with 10 mM Na^+. 1 mM, 2.5 mM and 5 mM of Na^+ only slightly affected the cell growth. The optical densities of the 2.5 mM and 5 mM Na^+ dosed cultures were slightly higher than the control cultures, while the 1 mM Na^+ dosed culture reached a slightly lower optical density. Cells in the 10 mM Na^+ spiked culture grew at a similar rate to other cultures over first week then grew slower and reached a much reduced optical density compared to the other cultures by day 14. The results evidenced that the *P. catenata* dominated cultures were more sensitive to K^+ than Na^+, and the inhibition effect increased with the increasing concentration of K^+.

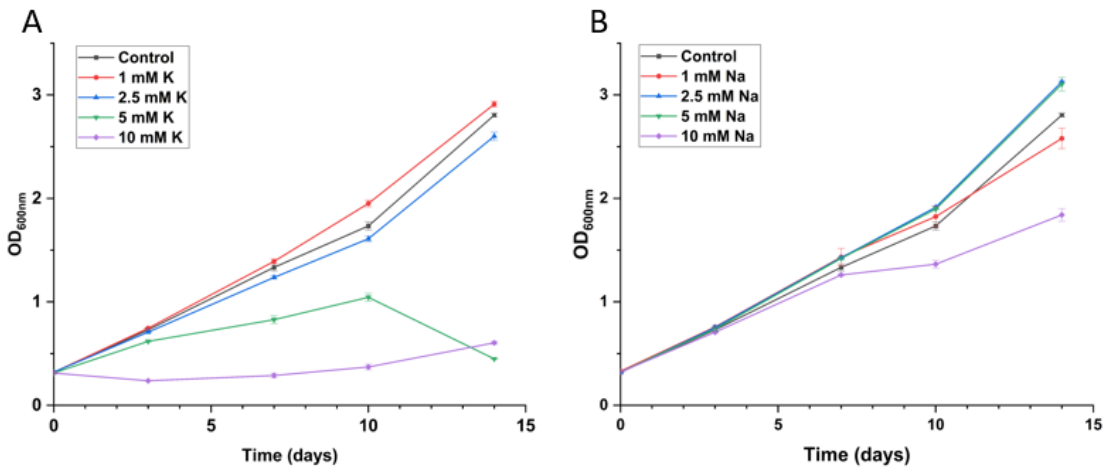

Figure 5.1. Growth curves obtained by plotting the mean value of the optical density measured at 600 nm wavelength. Error bars are defined by standard deviation. (A) OD_{600} of *P. catenata* cultures spiked with 1 mM, 2.5 mM, 5 mM and 10 mM KCl. (B) OD_{600} of *P. catenata* cultures spiked with 1 mM, 2.5 mM, 5 mM and 10 mM NaCl.

5.3.2 The effect of KOH and NaOH on the Growth of the *P. catenata* in a Chemostat System

The FGMSP pond is routinely flushed with a NaOH solution (Foster *et al.,* 2020). A chemostat was used as a simulant of the pond system to investigate and compare the effect of KOH and NaOH on the microbial growth in the pond system. Three chemostats were established, a culture flushed with standard BG-11 medium (Control culture), a culture flushed with KOH buffered BG-11 medium (KOH culture) and a culture flushed with NaOH buffered BG-11 medium (NaOH culture). The chemostats were run over a period of 94 days and the growth of the cultures were quantified by measuring the optical density at 600 nm (**Figure 5.2**). The concentration of K and Na in the culture were increased incrementally and quantified by ICP-MS (**Appendix 5.2, A and B**). The cultures were initially flushed with standard BG-11 medium. The background concentration of K^+ and Na^+ in the culture in the standard BG11 medium was around 0.45 mM and 18 mM, respectively (**Appendix 5.2**). After 17 days' steady growth, the flushing medium for the KOH and NaOH cultures was replaced by KOH and NaOH buffered BG-11 medium, respectively. Overall, KOH inhibitted growth of the cultures, while NaOH slightly promoted growth. The cutures continued growing at the first day after changing the medium. Then from day 19, when the concentration of K^+ in KOH culture reached 1.18 mM, the optical density of the culture started to decrease, while the OD_{600nm} in the control and NaOH cultures kept increasing. After 15 days of flushing with KOH/NaOH buffered medium, at day 32, the concentration of K^+ in KOH culture had increased to 5.09 mM, and the OD_{600nm} value had dropped to 0.314. By contrast, the concentration of Na^+ in the NaOH culture reached 23.7 mM and the OD_{600nm} value reached 0.634, which is slightly higher than the OD_{600nm} value of the control culture (0.597). The OD_{600nm} values of the KOH culture did not keep decreasing but instead fluctuated over time, but was always lower than the values of the control and NaOH cultures since the second day after changing the medium. These results indicated that KOH has

a better inhibition effect on this *P. catenata* dominated culture in pond simulated system compared to NaOH.

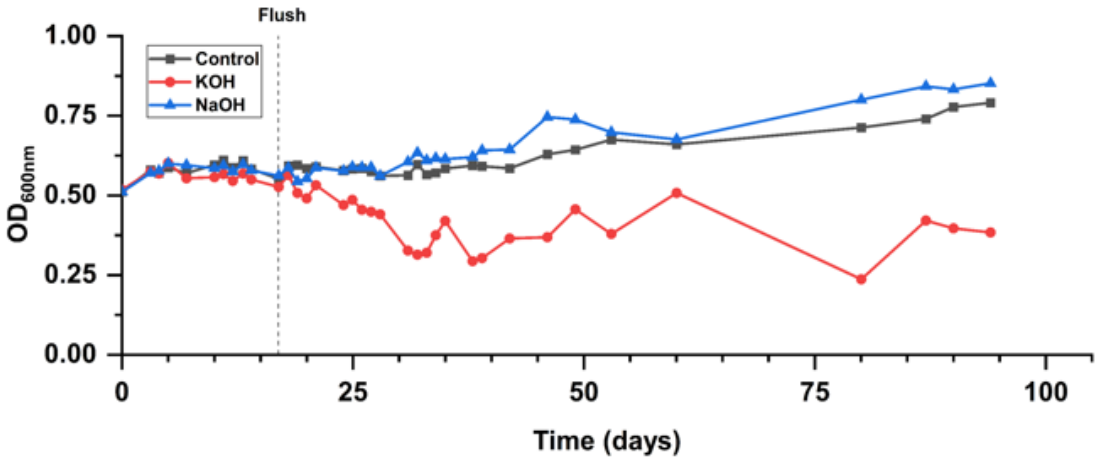

Figure 5.2 Growth curves of the chemostat cultures obtained by measuring the optical density at 600 nm wavelength. Cultures were initially flushed by standard BG-11 medium, from the time point marked "flush", 3 treatments were given to the cultures. Control culture was continuously flushed with a standard BG-11 medium. The KOH and NaOH cultures were continuously flushed with modified BG-11 medium containing either 10 mM KOH or 10 mM NaOH, respectively. The pH of the medium was adjusted to 11 with HCl.

5.3.2.1 Effects of KOH and NaOH on the microbial community composition

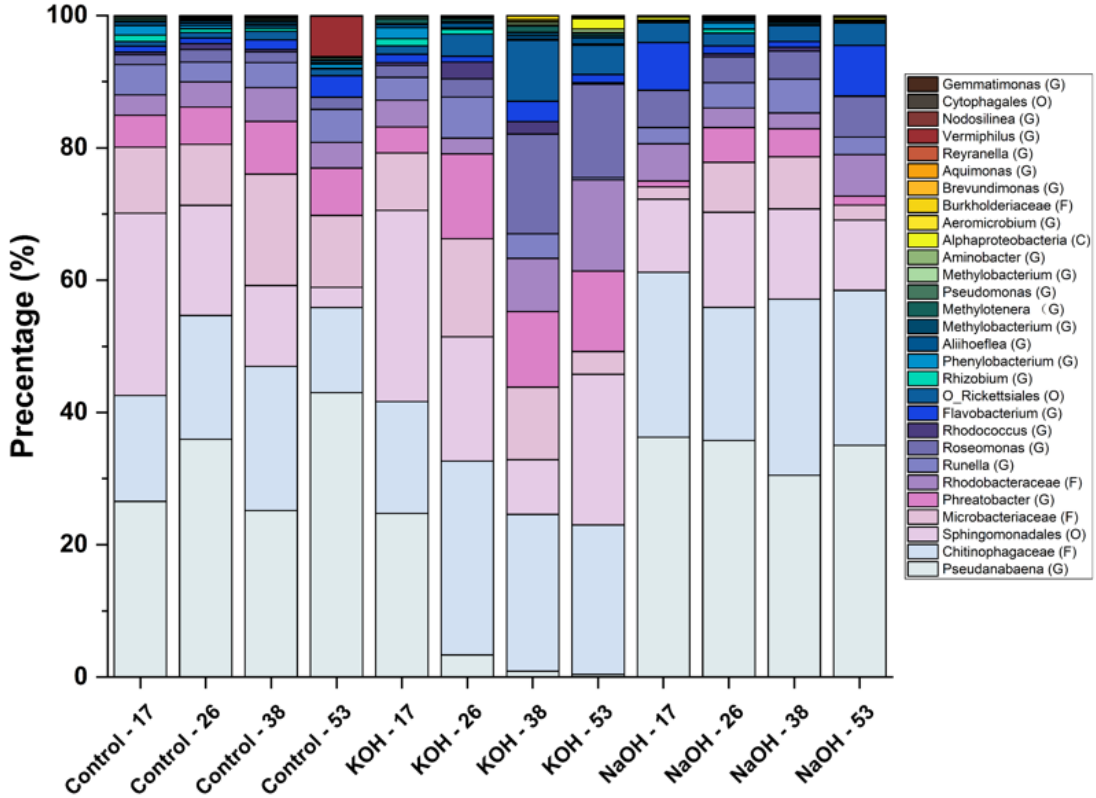

Figure 5.3 Genus-level microbial community comparison of *P. catenata* cultures flushed with standard BG-11 medium, KOH buffered BG-11 medium and NaOH buffered BG-11 medium based on 16S rRNA gene sequences. Samples were collected at day 17, 26, 38 and 53. Day 17 is the start point of changing flushing medium to KOH/NaOH buffered medium. Sequences that cannot be identified to genus level were resolved to the last matched taxonomic level of identification G- Genus, F-Family, O-orde, C-Class.

To identify whether the inhibition effect of K is organism-specific or broad-spectrum, and to compare the microbial community variation between chemostats supplied with KOH and NaOH supplementedmedium, 16S rRNA gene sequencing was performed. Samples were taken from the continuous cultures at day 17, 26, 38 and 53. The 16S rRNA gene sequencing indicated that cultures were initially dominated by operational taxonomic units (OTUs) affiliated to *Pseudanabaena* (G)(25% - 36%), *Chitinophagaceae* (F) (16% - 25%) and *Sphingomonadales* (O) (11% - 28%) (**Figure 5.3**). Flushing with NaOH buffered medium

did not affect the microbial community composition greatly, whereas continuous flushing with KOH buffered medium caused a loss of nearly all of the *Pseudanabaena* genus. For the control culture that was continuously flushed with standard BG-11 medium, the OTUs were affiliated to *Pseudanabaena* (G) (25% - 43%), while *Chitinophagaceae* (F) (12% - 21%) were relatively stable during this period. OTUs affiliated to *Sphingomonadales* (O) showed a decreasing trend, accounting for 27.5%, 16.6%, 12.2% and 3% at day 17, 26, 38 and 53 respectively in the control culture. The composition of the microbial community in the NaOH culture was more stable than the control during this time period. OTUs affiliated to *Pseudanabaena* (G), *Chitinophagaceae* (F) and *Sphingomonadales* (O) accounted for 30.5% - 36.2%, 20.1% - 26.6% and 10.6% -14.4 %, respectively. The microbial community in the KOH culture showed a different pattern. OTUs affiliated to *Pseudanabaena* (G) accounted for 24.8% of the microbial community at the beginning of the experiment then the percentage of *Pseudanabaena* decreased dramatically with the increasing concentration of K^+. At day 26, when the concentration of K^+ rose to 3.57 mM, OTUs affiliated to *Pseudanabaena* (G) dropped to 3.4%. At day 38, the concentration of K^+ reached 5.73 mM, and by then OTUs affiliated to *Pseudanabaena* decreased to 0.9%. Finally, at day 53, when the concentration of K^+ reached 8.18 mM, OTUs affiliated to *Pseudanabaena* (G) decreased to 0.4%. OTUs affiliated to *Runella* (G) showed a similar decrease in relative abundance as *Pseudanabaena* (G). OTUs affiliated to *Phreatobacter* (G) increased from 3.9% to 12.7 after 7 days flushing of KOH, then remained at around 12%. Similarly, OTUs affiliated to Rhodobacteraceae (F) and Roseomonas (G) increased with the increasing concentration of KOH in the culture. OTUs affiliated to other organisms did not show such a clear variation during the flushing, which indicated that the inhibition of KOH to cell growth was organism specific. When compared to NaOH, KOH showed a distinct ability of controlling the growth of *Pseudanabaena* (G).

The microbial diversity was also evaluated by using proteomic techniques. The ratio of total protein abundance of each organism and the total protein abundance of each culture sample isolated on a specific day were used to quantify the proportion of each organism in the sample (**Figure 5.4**). The abundance of *Pseudanabaena* proteins accounted for around 40% - 45% initially in each treatment sample at day 17. After 3 weeks flushing, the proportion in the control increased to 59.21%, and the proportion in NaOH culture slightly decreased to 37.84%. The proportion of *Pseudanabaena* proteins in the KOH group decreased from 39.98% at day 17 to 27.62% at day 26 and 9.90% at day 38. The proportions of all organisms did not show much variation across time in the control. In the KOH group, the proportion of *Chitinophagaceae* (F), *Phreatobacter* (G) and *Porphyrobacter* (G) increased across time. In the NaOH group, the proportion of *Chitinophagaceae* (F), *Runella* (G) and *Porphyrobacter* (G) slightly increased, while the proportion of *Rhodobacteraceae* (F) decreased.

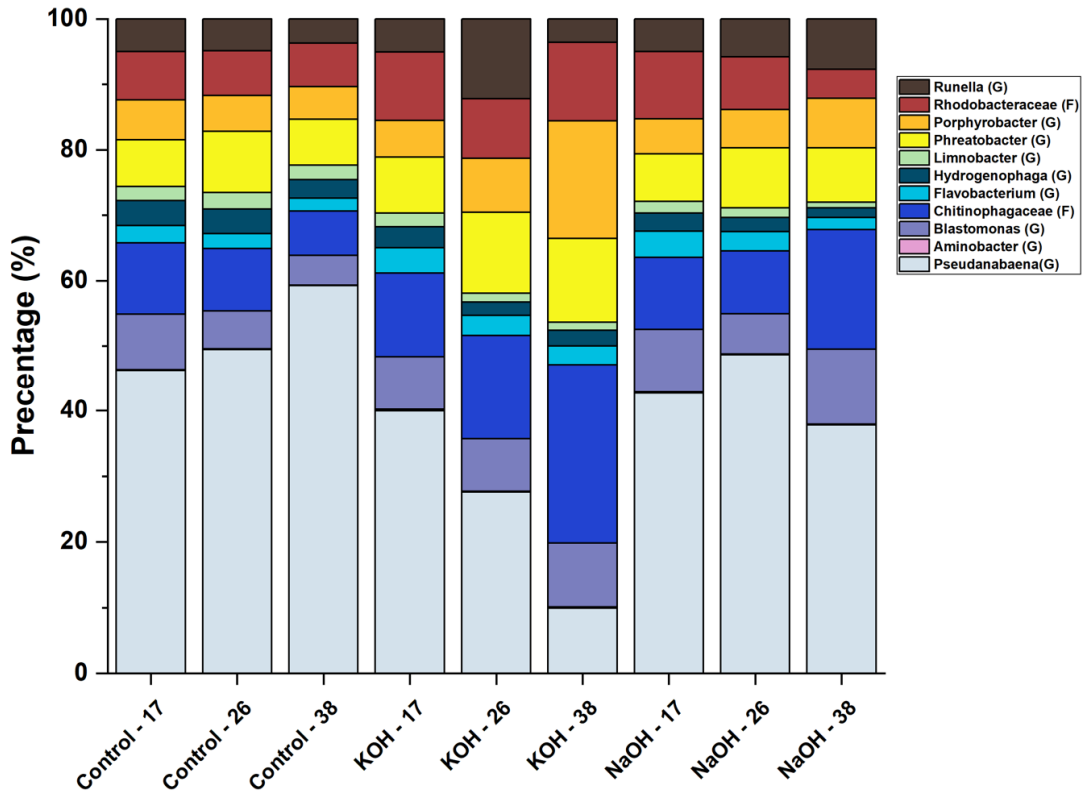

Figure 5.4 Microbial diversity comparison based on protein abundances. Percentage of each microorganism was obtained by using the total protein abundances of each organism divided by the total identified protein abundances of each sample.

5.3.2.2 Impacts of KOH/NaOH on Protein Expression

LC-MS based proteomics techniques were applied to evaluate the influences of KOH and NaOH on protein expression. A clear separation of KOH treatment was displayed according to principal component analysis (**Figure 5.5, a**). Component 1 accounted for 53.2% of the total explained variance (TEV). According to the PC1 axis, samples in the NaOH and control group clustered together. By contrast, the day 38 samples in KOH group distributed separately to the control and NaOH group, which indicated that the protein expression in the KOH group are significantly different from the NaOH and Control group. Component 2 accounted for 16.5% of the total TEV. Samples in the Control and KOH groups distributed separately across time according to the PC2 axis. However, samples in the NaOH group clustered together in both PC1 and PC2 dimensions, which indicated that protein expression in NaOH group are relatively stable when compared to control and KOH group.

The proteins in each sample were subjected to hierarchical clustering generating the heatmap in **Figure 5.5 b**. Taxonomy of the proteins were enriched at FDR 0.05 level **(Appendix 5.3)**. Protein expression was first evaluated vertically across time. Proteins in the KOH group showed obvious variances across time-course, while the Control and NaOH group were not. Cluster 1 contains 227 proteins. The KOH group showed strong up-regulation across time relative to the other samples. The enriched organisms are *Chitinophagaceae* (F), *Phreatobacter* (G) and *Blastomonas* (G). Cluster 2 contains 167 organisms, and proteins in the control and NaOH groups were slightly down regulated across time, while the proteins in the KOH group

were slightly up regulated at day 26, then down regulated at day 38. The enriched organisms are *Runella* (G) and *Flavobacterium* (G). Cluster 3 contains 631 proteins, of which the proteins in the KOH group showed down regulation and the only enriched organism is *Pseudanabaena* (G). Cluster 4 contains 214 proteins and showed a similar pattern to cluster1, the day 38 sample in the KOH group showed mostly up-regulation while proteins in other samples were relatively stable. The enriched organisms were *Porphyrobacter* (G) and *Rhodobacteraceae* (F). Cluster 5 contains 118 proteins, in which proteins in the KOH and NaOH groups were down regulated relative to the control. Enriched organisms are *Limnobacter* (G), *Hydrogenophaga* (G) and *Pseudanabaena* (G). The results indicated that KOH had a distinct impact on protein expression and the impact is organism specific.

The regulation of protein expression was then evaluated horizontally across diffenent treatments. The protein abundance ratio values of the KOH and NaOH groups relative to the Control were used to evaluate the change (up- or down-regulation) of protein expression in the KOH and NaOH groups. The ratio value was then converted to log2 based normalization. Proteins with log2 fold change >2 or <-2 were classified as up or down regulated. Proteins of *Pseudanabaena* showed significant down regulation during the KOH suspended medium flush (**Figure 5.6, a and b**). The number of down regulated proteins increased from 118 to 386 from day 17 to 38. The number of up regulated *Pseudanabaena* proteins slightly decreased with time. *Pseudanabaena* was the only organism in which proteins were obviously down regulated with the increasing concentration of KOH in the culture. By contrast, proteins of many organisms such as *Blastomonas* (G), *Porphyrobacter* (G), *Rhodobacteraceae* (F) and *Chitinophagaceae* (F) were up regulated in response to increasing concentration of KOH. When the culture was flushed with NaOH medium, the protein expression profile of *Pseudanabaena* (G) was affected more than other organisms (**Figure 5.6, c and d**). Around 86 down regulated *Pseudanabaena*

(G) proteins were identified, and the number increased to 237 by day 38. The number of up regulated *Pseudanabaena* (G) proteins were kept to around 30. Apart from *Pseudanabaena* (G), down regulated proteins of *Rhodobacteraceae* (F) slightly increased from 9 to 27 by day 38. Up regulated proteins of *Chitinophagaceae* (F), *Blastomonas* (G) and *Porphyrobacter* (G) increased during the NaOH flush.

Pseudanabaena cells were depleted due to the increasing concentration of K^+ in the culture. The down regulation of proteins might have partly resulted from the reduction of *Pseudanabaena* cell density. Thus, identifying the down regulated proteins caused by KOH is difficult. However, the up regulated proteins presented were clearly due to the high concentration of KOH. Up regulated proteins covered metabolism, genetic information processing and signalling and cellular processes (**Appendix 5.4**). Proteins related to metabolism are mainly enzymes. These include, glutathione peroxidase (gpx1), which functions as a defence against organic peroxides and hydrogen peroxide (Brenot *et al*., 2004), chorismate mutase (aroH), which is related to the biosynthesis of phenylalanine, tyrosine and tryptophan (Chook *et al.,* 1994), and N-acetylmuramic acid 6-phosphate etherase (murQ), which converts N-acetylmuramic acid-phosphate (MurNAc-P) to N-acetylglucosamine-phosphate and is essential for growth on MurNAc as the source of carbon (Uehara *et al.,* 2006). Another up-regulated enzyme was uridylate kinase (pyrH), which is the first enzyme in pyrimidine nucleotide biosynthesis and responsible for microbial UMP phosphorylation (Marco-Marin *et al.,* 2005). Other up-regulated proteins included ispF, which is involved in the biosynthesis of secondary metabolites (Herz *et al.,* 2000). Up-regulated proteins related to genetic information processing include, deoxyuridine 5'-triphosphate nucleotidohydrolase (dut) (Mol *et al.,* 1996), recombination protein (recA) (Hintz *et al.,* 1995), pyruvate kinase (pyk) (Mazurek, 2011) and ribosomal proteins, large subunit ribosomal protein L28 (rpmB) (Maguire,

2011), large subunit ribosomal protein L16 (rplP) (Arnold, 1996), small subunit ribosomal protein S1 (rpsA) (Skorski *et al.,* 2006), and the concentrative nucleoside transporter (TC.CNT).

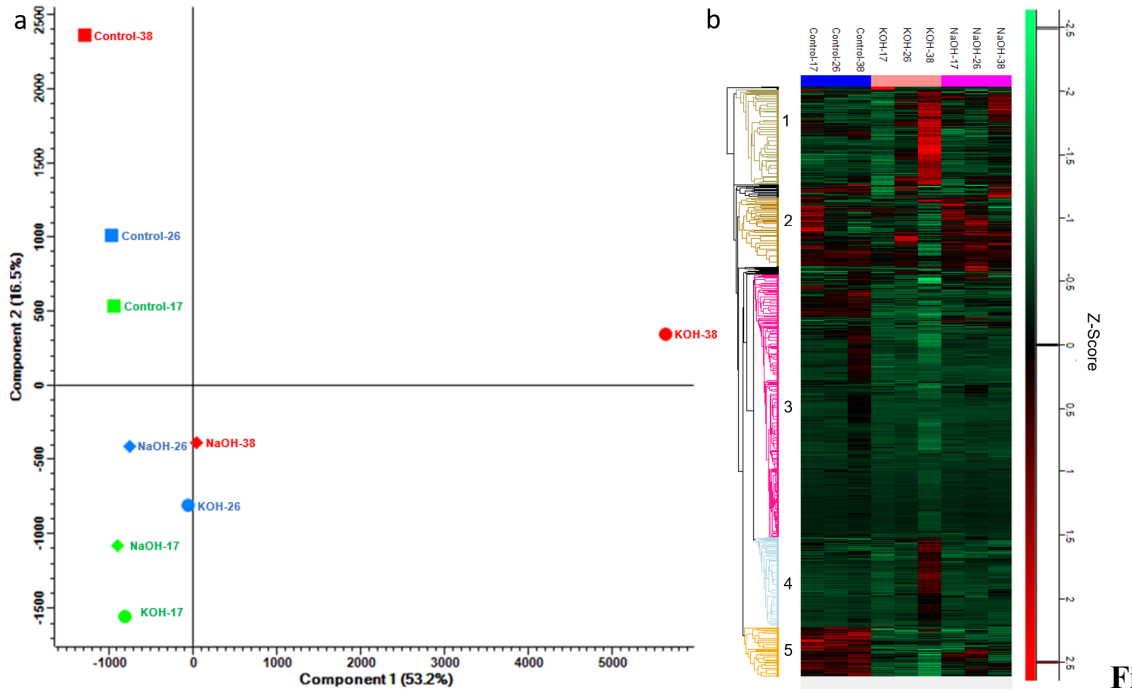

Figure 5.5. Comparison of dynamic proteomic changes across time points. (a) Principal component analysis plot based on the abundance values of all identified proteins. Results were cut off by Benjamini-Hochberg FDR 0.05. Squares represents control samples. Circles represents KOH buffered medium flushed samples. Diamonds represents NaOH buffered medium flushed samples. Colour code: Green- day 17, Blue- day 26, Red- day 38. (b) Hierarchical clustering showing the changes in abundances of the identified proteins. Missing values were imputed from normal distribution. The protein abundances were normalized by z-score (the mean of each protein was subtracted; the results were then divided by the standard deviation). Z-scores were used for hierarchical clustering into heat map. The nearness of two items was defined by Euclidean distance. The distance between 2 clusters was defined by average distances between 2 single items.

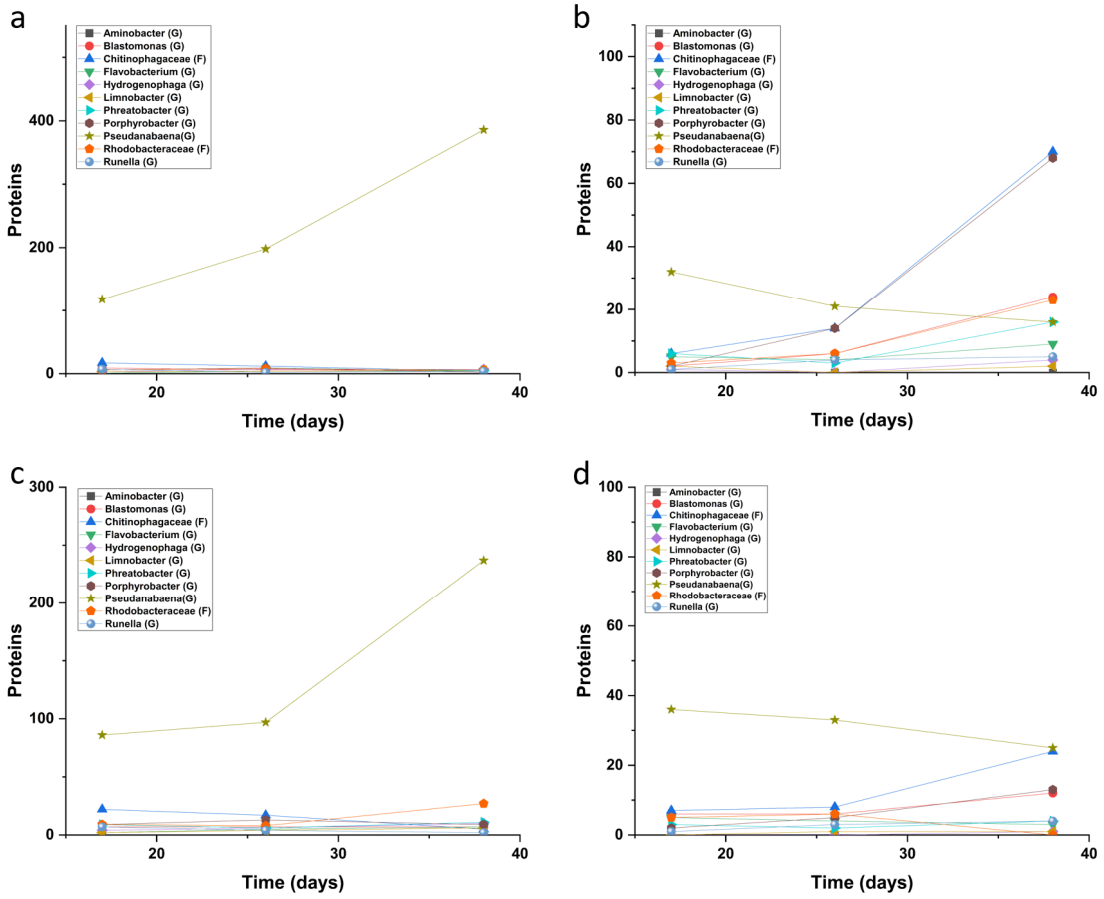

Figure 5.6 Numbers of up-regulated or down-regulated proteins in the KOH and NaOH group relative to the Control group. Abundance ratios of the KOH and NaOH group to the Control group at selected time points were used to evaluate the regulation of protein expression (e.g., regulation of a specific proteins in the KOH group at day 26 was evaluated by the ratio of protein abundance of this protein in the KOH group to its abundance in the control group at day 26). The ratios were log2 transformed. Proteins with log2 fold change values > 2 or < -2 were classified into up-regulated or down regulated proteins. (a) Down-regulated proteins in KOH group. (b) Up-regulated proteins in KOH group. (c) Down-regulated proteins in NaOH group. (d) Up-regulated proteins in NaOH group.

5.4 Discussion

Seasonal blooms have been regularly reported at the FGMSP located at the Sellafield nuclear processing site. A cyanobacterium belonging to the genus *Pseudanabaena* was identified to be the dominant microorganism in the community during the microbial bloom in August 2016, and it was the only photosynthetic organism present in the bloom event (*Foster et al*, 2020). Thus, controlling the growth of *Pseudanabaena* is thought to be the key to control the seasonal bloom in this pond. This study tested the use of KOH instead of NaOH in the pond simulated system to achieve the purpose of maintaining an alkaline environment and controlling the growth of *Pseudanabaena* simultaneously.

Initial batch culture experiments compared K versus Na response through the addition of chloride salts, and 5 mM of KCl started to show a strong ability of inhibiting the growth of the *Pseudanabaena* dominated culture, which decreased by around 80% of the optical density compared to the control. By contrast, cultures dosed with 5 mM NaCl achieved a relatively higher OD value at the end of the experiment. 10 mM of NaCl started to inhibit the growth of the culture, but the reduction of OD was moderate when compared to the KCl treatment. The FGMSP at Sellafield site is routinely purged with deionised water dosed with NaOH to minimise the rate of corrosion of the fuel and fuel cladding (*Foster et al,* 2020). A chemostat experiment were therefore designed to simulate the pond system. Cultures were continuously flushed with KOH or NaOH dosed medium. The concentration of K^+ or Na^+ ions were continuously increaed during the experiment. However, even at the end of the experiment, when the concentration of Na^+ ions reached nearly 28 mM, the OD value was higher than for the control and the KOH dosed culture. Microbial community analysis and protein expression analysis also showed that the microbial community and protein expression in the NaOH dosed culture were more stable than the control and KOH dosed culture. By contrast, the OD of the

KOH flushed culture showed an obvious reduction once the culture had been flushed with KOH supplemented medium for 3 days. Furthermore, the culture was physically changed from dark brown to transparent at the end of the experiment (**Appendix 5**).

The KCl used in the batch culture experiment and KOH used in the chemostat experiment both showed a strong ability to inhibit the growth of the culture, which indicated that K^+ ions, added either as chlorides or hydroxide, inhibit the growth of *Pseudanabaena.* The microbial community analysis showed that KOH flushing removed nearly all of the *P.catenata* and reduced the abundance of *Pseudanabaena* proteins significantly with the increased concentration of KOH in the culture. However, genera closely related to *Phreatobacter* (G), *Roseomonas* (G) and *Rhodobacteraceae* (F) increased in abundance while some organisms did not change with the KOH dosing, which indicated that the inhibition effect of K^+ ions on cell growth is specific to *Pseudanabaena*. K^+ is an essential nutrient for all organisms, involved in many cellular functions, such as controlling cell osmotic activity, transport activity, enzyme activity and gene expression (Alexandrowicz, 1962; Kundig *et al.,* 1966; Perlin and Lerner, 1981; Sutherland *et al.*, 1986; Epstein, 1986, Wood, 1999; Gralla and Vargas, 2005). Studies related to the inhibition of microorganism growth by excess K^+ are limited. Other cyanobacteria which were shown to be sensitive to K^+ were *Microcystis* spp. Reducing the concentration of K^+ in modified Fitzgerald medium achieved a better yield of *M. aeruginosa* NRC-1. By contrast, partly replacing $NaNO_3$ by KNO_3 inhibited the growth of *M. aeruginosa* NRC-1 (Zehnder and Gorham, 1960). Parker *et al.* (1997) reported that both *M. aeruginosa* and *Microcystis flos-aquae* were sensitive to K^+, such that 1 mM KCl in DP medium caused a 50% reduction in the 10-day yield. By contrast, 2 – 30 mM of NaCl had no effect on *M. flos-aquae* growth. Later, a mixed culture of *M. aeruginosa* and *Wolffia arrhizal* was initially dominated by *M. aeruginosa,* but the dominant species changed to *W. arrhizal* after dosing with 4.8 mM of KCl (Parker *et*

al., 1997). Thus, there are similarities between the response of *Microcystis* spp. to K^+ ions, and the response presented here for *Pseudanabena*.

The impacts of KOH and NaOH on protein expression were evaluated, and KOH caused up regulation of *Blastomonas* (G), *Porphyrobacter* (G), *Rhodobacteraceae* (F) and *Chitinophagaceae* (F) proteins. Both KOH and NaOH dosing caused down regulation of *Pseudanbaena* proteins. However, as the population of *Pseudanbaena* cells were significantly decreased due to the increasing concentration of K^+ in the culture, the observed down regulation might be partly due to the reduction of total *Pseudanbaena* population. However, the up regulated proteins in these reduced population cells are thought to be stimulated by KOH dosing.

The condition of FGMSP in Sellafield is unique. The pond is open to the air, filled with alkaline water and spent nuclear fuels were stored in the pond. Commonly used bloom control methods should be considered carefully in such a situation. For example, the effectiveness of nutrient removal methods will be limited by the open-air nature of the pond. Induction of halogenation and oxidation reactions may not work due to the alkaline pH of the pond water, and the nuclear inventory may react with the halogens and oxidants. Foster *et al.* (2020a) reported that the formation of the onset of microbial blooms occurred when the water purge rate was reduced (residence time of the purge water increased), and suggested that the increase of the water purge rate could be a method for controlling the microbial bloom. The pond is purged with reused water from the Fuel Handling Plant (FHP) and Independent Pond Purge (IPP), and the shortest residence time that can be reached in the pond is around 10 days. Whether the facility can meet the required purging regime should be considered. In addition, increasing the purge rate will also increase the effluent discharged from the pond which would increase the load of

downstream processes. KOH has been evidenced in this study as a treatment to effectively inhibit *Pseudanabaena* yields. However, there could be other consequences to Sellafied operations by using KOH instead of NaOH. The purged pond water is sent to the Sellafield Iox eXchange Effluent Plant (SIXEP) to remove Sr-90 and Cs-137 by using ion exchangers. The impact of changing NaOH to KOH on SIXEP operation and/or to other downstream processes should be evaluated.

At the end of the chemostat experiment, the concentration of K^+ in the KOH culture reached 9.02 mM, while the concentration of Na^+ in the NaOH culture reached 29.36 mM. The K^+ concentration which could dramatically reduce the growth of the culture was much lower than Na^+. The maximum concentration of Na^+ in the FGMSP was about 4 mM, which was much lower than the concentration of Na^+ in our experiment (Konovalovaite, 2019). Based on the results from the chemostat experiment, 4 mM of K^+ was capable to reduce the OD to 0.365. A previous study indicated that the inhibition effect of K^+ to cells may be a result of the altered ratio of K^+ to Na^+ (Parker *et al., 1997*). The effect of K^+ and Na^+ ratio was not tested here. A further study can try to identify whether the absolute concentration of K^+ or the relative concentration of K^+ and Na^+ are important to inhibit the growth of *Pseudanabaena.* If the inhibition effect is driven by the ratio of K^+ and Na^+, changing NaOH to KOH might be a very effective way to control the bloom, and the concentration of K^+ required can be much lower than that determined in this study. Thus, the impact of changing NaOH to KOH on the downstream Sellafield processes may be further decreased.

In our study, KOH reduced the growth of *Pseudanabaena*, meanwhile organisms such as *Phreatobacter* (G), *Roseomonas* (G) and *Rhodobacteraceae* (F) were stimulated. As the stimulation of other organisms are weaker relative to the inhibition to *Pseudanabaena* growth, the OD of the whole culture presented a decreasing trend. The composition of the culture

used in this experiment was not exactly the same as the Sellafield Pond system, and so it is possible that organisms that can be stimulated by KOH exists in the pond system. Therefore, future work should test KOH on actual pond samples to evaluate the inhibition effect.

5.5 Conclusion

Pseudanabaena cells are sensitive to K^+ ions. Both our batch culture experiment and chemostat experiment evidenced that high concentration of K^+ can significantly inhibit the growth of *Pseudanabaena* dominated cultures. The inhibition effect of K^+ is organism specific. In our experiment, only *Pseudanabaena* was inhibited by K^+ ions and organisms such as *Phreatobacter* (G), *Roseomonas* (G) and *Rhodobacteraceae* (F) were slightly stimulated. KOH mainly down regulated *Pseudanabaena* proteins, the down regulation increased with the increasing concentration of K^+. However, the decreascing cell numbers may contribute to the down-reglation in KOH dosed culture Up regulated proteins were identified, but the up regulated proteins decreased with the increasing concentration of K^+. Proteins related to metabolism, genetic and information processing and signalling and cellular processes were stimulated. KOH is more capable of controlling the growth of a *Pseudanabaena* dominated culture compared to NaOH. If applying KOH as a bloom control method in FGMSP, the influence of KOH on the downstream facility should be considered and the possibility of causing other organisms to become dominant in a bloom should be evaluated.

5.6 References.

Alexandrowicz, Z. (1962). Osmotic and Donnan equilibria in polyacrylic acid–sodium bromide solutions. Journal of Polymer Science, 56(163), 115-132.

Arnold, R. J., & Reilly, J. P. (1999). Observation of *Escherichia coli* Ribosomal Proteins and Their Posttranslational Modifications by Mass Spectrometry. Analytical biochemistry, 269(1), 105-112.

Billi, D., & Potts, M. (2002). Life and death of dried prokaryotes. Research in microbiology, 153(1), 7-12.

Blanco-Rivero, A., Leganes, F., Fernandez-Valiente, E., Calle, P., & Fernandez-Pinas, F. (2005). mrpA, a gene with roles in resistance to Na+ and adaptation to alkaline pH in the cyanobacterium *Anabaena sp. PCC7120*. Microbiology, 151(5), 1671-1682.

Brenot, A., King, K. Y., Janowiak, B., Griffith, O., & Caparon, M. G. (2004). Contribution of glutathione peroxidase to the virulence of *Streptococcus pyogenes*. Infection and immunity, 72(1), 408-413.

Caporaso, J. G., et al. (2010). "QIIME allows analysis of high-throughput community sequencing data." Nat Meth 7(5): 335-336.

Caporaso, J. G., Lauber, C. L., Walters, W. A., Berg-Lyons, D., Lozupone, C. A., Turnbaugh, P. J., ... & Knight, R. (2011). Global patterns of 16S rRNA diversity at a depth of millions of sequences per sample. Proceedings of the national academy of sciences, 108(Supplement 1), 4516-4522.

Caporaso, J. G., Lauber, C. L., Walters, W. A., Berg-Lyons, D., Huntley, J., Fierer, N., ... & Knight, R. (2012). Ultra-high-throughput microbial community analysis on the Illumina HiSeq and MiSeq platforms. The ISME journal, 6(8), 1621-1624.

Chicote, E., Moreno, D. A., Garcia, A. M., Sarro, M. I., Lorenzo, P. I., & Montero, F. (2004). Biofouling on the walls of a spent nuclear fuel pool with radioactive ultrapure water. Biofouling, 20(1), 35-42.

Chook, Y. M., Gray, J. V., Ke, H., & Lipscomb, W. N. (1994). The monofunctional chorismate mutase from *Bacillus subtilis*: structure determination of chorismate mutase and its complexes with a transition state analog and prephenate, and implications for the mechanism of the enzymatic reaction. Journal of molecular biology, 240(5), 476-500.

Dekker, L., Osborne, T. H., & Santini, J. M. (2014). Isolation and identification of cobalt-and caesium-resistant bacteria from a nuclear fuel storage pond. FEMS microbiology letters, 359(1), 81-84.

Deng, Y., Wu, M., Zhang, H., Zheng, L., Acosta, Y., & Hsu, T. T. D. (2017). Addressing harmful algal blooms (HABs) impacts with ferrate (VI): Simultaneous removal of algal cells and toxins for drinking water treatment. Chemosphere, 186, 757-761.

Diosi, G., Telegdi, J., Farkas, G., Gazso, L. G., & Bokori, E. (2003). Corrosion influenced by biofilms during wet nuclear waste storage. International biodeterioration & biodegradation, 51(2), 151-156.

Edgar, R. C. (2013). UPARSE: highly accurate OTU sequences from microbial amplicon reads. Nature methods, 10(10), 996-998.

Edgar, R. C. (2010). Search and clustering orders of magnitude faster than BLAST. Bioinformatics, 26(19), 2460-2461.

Epstein, W. (1986). Osmoregulation by potassium transport in *Escherichia coli*. FEMS microbiology reviews, 2(1-2), 73-78.

Evans, H. J., & Sorger, G. J. (1966). Role of mineral elements with emphasis on the univalent cations. Annual review of plant physiology, 17(1), 47-76.

Foster, L., Boothman, C., Ruiz-Lopez, S., Boshoff, G., Jenkinson, P., Sigee, D., ... & Lloyd, J. R. (2020a). Microbial bloom formation in a high pH spent nuclear fuel pond. Science of The Total Environment, 720, 137515.

Foster, L., Muhamadali, H., Boothman, C., Sigee, D., Pittman, J. K., Goodacre, R., ... & Lloyd, J. R. (2020b). Radiation tolerance of *Pseudanabaena catenata*, a cyanobacterium relevant to the first generation magnox storage pond. Frontiers in microbiology, 11, 515.

Gralla, J. D., & Vargas, D. R. (2006). Potassium glutamate as a transcriptional inhibitor during bacterial osmoregulation. The EMBO journal, 25(7), 1515-1521.

Gregson, C. R., Goddard, D. T., Sarsfield, M. J., & Taylor, R. J. (2011). Combined electron microscopy and vibrational spectroscopy study of corroded Magnox sludge from a legacy spent nuclear fuel storage pond. Journal of nuclear materials, 412(1), 145-156.

Haas, B. J., et al. (2011). "Chimeric 16S rRNA sequence formation and detection in Sanger and 454-pyrosequenced PCR amplicons." Genome Research 21(3): 494-504.

Herz, S., Wungsintaweekul, J., Schuhr, C. A., Hecht, S., Lüttgen, H., Sagner, S., ... & Rohdich, F. (2000). Biosynthesis of terpenoids: YgbB protein converts 4-diphosphocytidyl-2C-methyl-D-erythritol 2-phosphate to 2C-methyl-D-erythritol 2, 4-cyclodiphosphate. Proceedings of the National Academy of Sciences, 97(6), 2486-2490.

Hintz, N. J., Ennis, D. G., Liu, W. F., & Larsen, S. H. (1995). The recA gene of Chlamydia trachomatis: cloning, sequence, and characterization in Escherichia coli. FEMS microbiology letters, 127(3), 175-179.

Jackson, S. F., Monk, S. D., & Riaz, Z. (2014). An investigation towards real time dose rate monitoring, and fuel rod detection in a First Generation Magnox Storage Pond (FGMSP). Applied Radiation and Isotopes, 94, 254-259.

Katz, A., Waridel, P., Shevchenko, A., & Pick, U. (2007). Salt-induced changes in the plasma membrane proteome of the halotolerant alga *Dunaliella salina* as revealed by blue native gel electrophoresis and nano-LC-MS/MS analysis. Molecular & Cellular Proteomics, 6(9), 1459-1472.

Karley, D., Shukla, S. K., & Rao, T. S. (2018). Isolation and characterization of culturable bacteria present in the spent nuclear fuel pool water. Environmental Science and Pollution Research, 25(21), 20518-20526.

Konovalovaite, J. (2019). Control of algae in fuel storage ponds (Doctoral dissertation, University of Manchester).

Kozich, J. J., Westcott, S. L., Baxter, N. T., Highlander, S. K., & Schloss, P. D. (2013). Development of a dual-index sequencing strategy and curation pipeline for analyzing amplicon sequence data on the MiSeq Illumina sequencing platform. Applied and environmental microbiology, 79(17), 5112-5120.

Kundig, W., Kundig, F. D., Anderson, B., & Roseman, S. (1966). Restoration of active transport of glycosides in *Escherichia coli* by a component of a phosphotransferase system. Journal of Biological Chemistry, 241(13), 3243-3246.

Liu, D., Wang, P., Wei, G., Dong, W., & Hui, F. (2013). Removal of algal blooms from freshwater by the coagulation–magnetic separation method. Environmental Science and Pollution Research, 20(1), 60-65.

Maguire, B. A., & Wild, D. G. (1997). The effects of mutations in the rpmB, G operon of *Escherichia coli* on ribosome assembly and ribosomal protein synthesis. Biochimica et Biophysica Acta (BBA)-Gene Structure and Expression, 1353(2), 137-147.

Masella, A. P., Bartram, A. K., Truszkowski, J. M., Brown, D. G., & Neufeld, J. D. (2012). PANDAseq: paired-end assembler for illumina sequences. BMC bioinformatics, 13(1), 1-7.

Marco-Marín, C., Gil-Ortiz, F., & Rubio, V. (2005). The crystal structure of *Pyrococcus furiosus* UMP kinase provides insight into catalysis and regulation in microbial pyrimidine nucleotide biosynthesis. Journal of molecular biology, 352(2), 438-454.

Martin, M. (2011). Cutadapt removes adapter sequences from high-throughput sequencing reads. EMBnet. journal, 17(1), 10-12.

Mazurek, S. (2011). Pyruvate kinase type M2: a key regulator of the metabolic budget system in tumor cells. The international journal of biochemistry & cell biology, 43(7), 969-980.

MeGraw, V. E., Brown, A. R., Boothman, C., Goodacre, R., Morris, K., Sigee, D., ... & Lloyd, J. R. (2018). A novel adaptation mechanism underpinning algal colonization of a nuclear fuel storage pond. MBio, 9(3), e02395-17.

Mol, C. D., Harris, J. M., McIntosh, E. M., & Tainer, J. A. (1996). Human dUTP pyrophosphatase: uracil recognition by a β hairpin and active sites formed by three separate subunits. Structure, 4(9), 1077-1092.

Nazina, T. N., Shestakova, N. M., Grigor'yan, A. A., Mikhailova, E. M., Tourova, T. P., Poltaraus, A. B., ... & Belyaev, S. S. (2006). Phylogenetic diversity and activity of anaerobic microorganisms of high-temperature horizons of the Dagang oil field (PR China). Microbiology, 75(1), 55-65.

Nurk, S., Bankevich, A., Antipov, D., Gurevich, A., Korobeynikov, A., Lapidus, A., ... & Pevzner, P. A. (2013, April). Assembling genomes and mini-metagenomes from highly chimeric reads. In Annual International Conference on Research in Computational Molecular Biology (pp. 158-170). Springer, Berlin, Heidelberg.

Pan, G., Chen, J., & Anderson, D. M. (2011). Modified local sands for the mitigation of harmful algal blooms. Harmful algae, 10(4), 381-387.

Parker, D. L., Kumar, H. D., Rai, L. C., & Singh, J. B. (1997). Potassium salts inhibit growth of the cyanobacteria *Microcystis spp*. in pond water and defined media: implications for control of microcystin-producing aquatic blooms. Applied and Environmental Microbiology, 63(6), 2324-2329.

Perlin, M. H., & Lerner, S. A. (1981). Localization of an amikacin 3′-phosphotransferase in *Escherichia coli*. Journal of bacteriology, 147(2), 320-325.

Pikuta, E. V., Hoover, R. B., & Tang, J. (2007). Microbial extremophiles at the limits of life. Critical reviews in microbiology, 33(3), 183-209.

Quast, C., Pruesse, E., Yilmaz, P., Gerken, J., Schweer, T., Yarza, P., ... & Glöckner, F. O. (2012). The SILVA ribosomal RNA gene database project: improved data processing and web-based tools. Nucleic acids research, 41(D1), D590-D596.

Rivasseau, C., Farhi, E., Compagnon, E., de Gouvion Saint Cyr, D., van Lis, R., Falconet, D., ... & Couté, A. (2016). *Coccomyxa actinabiotis sp. nov.*(*Trebouxiophyceae, Chlorophyta*), a new green microalga living in the spent fuel cooling pool of a nuclear reactor. Journal of phycology, 52(5), 689-703.

Sarró, M. I., Moreno, D. A., Chicote, E., Lorenzo, P. I., García, A. M., & Montero, F. (2003). Biofouling on austenitic stainless steels in spent nuclear fuel pools. Materials and Corrosion, 54(7), 535-540.

Skorski, P., Leroy, P., Fayet, O., Dreyfus, M., & Hermann-Le Denmat, S. (2006). The highly efficient translation initiation region from the *Escherichia coli* rpsA gene lacks a Shine-Dalgarno element. Journal of bacteriology, 188(17), 6277-6285.

Suelter, C. H. (1970). Enzymes activated by monovalent cations. Science, 168(3933), 789-795.

Sutherland, L., Cairney, J., Elmore, M. J., Booth, I. R., & Higgins, C. F. (1986). Osmotic regulation of transcription: induction of the proU betaine transport gene is dependent on accumulation of intracellular potassium. Journal of Bacteriology, 168(2), 805-814.

Tyanova, S., Temu, T., Sinitcyn, P., Carlson, A., Hein, M. Y., Geiger, T., ... & Cox, J. (2016). The Perseus computational platform for comprehensive analysis of (prote) omics data. Nature methods, 13(9), 731-740.

Uehara, T., Suefuji, K., Jaeger, T., Mayer, C., & Park, J. T. (2006). MurQ etherase is required by *Escherichia coli* in order to metabolize anhydro-N-acetylmuramic acid obtained either from the environment or from its own cell wall. Journal of bacteriology, 188(4), 1660-1662.

Walderhuang, M. O., Dosch, D. C., & Epstein, W. (1987). Potassium transport in bacteria. In Ion transport in prokaryotes (pp. 85-130). Academic Press.

Wang, Q., Garrity, G. M., Tiedje, J. M., & Cole, J. R. (2007). Naive Bayesian classifier for rapid assignment of rRNA sequences into the new bacterial taxonomy. Applied and environmental microbiology, 73(16), 5261-5267.

Wood, J. M. (1999). Osmosensing by bacteria: signals and membrane-based sensors. Microbiology and molecular biology reviews, 63(1), 230-262.

Zehnder, A., & Gorham, P. R. (1960). Factors influencing the growth of *Microcystis aeruginosa Kütz. Emend. Elenkin*. Canadian Journal of Microbiology, 6(6), 645-660.

5.7 Appendix

Appendix 5.1 Chemical composition of BG-11 medium

Chemical	Concentration in BG11 (mM)
NaNO3	17.64913519
K2HPO4	0.229647491
MgSO4.7H2O	0.304296669
CaCl2.2H2O	0.244881301
CITRIC ACID (C6H8O7)	0.031230481
FeC6H11NO7	0.022641509
EDTANa2	0.002974332
Na2CO3	0.188697047
H3BO3	0.046255863
MnCl2.4H2O	0.009145571
ZnSO4.7H2O	0.000765058
Na2MoO4.2H2O	0.001611903
CuSO4.5H2O	0.000320397
Co(NO3)2.6H2O	0.000171804

a

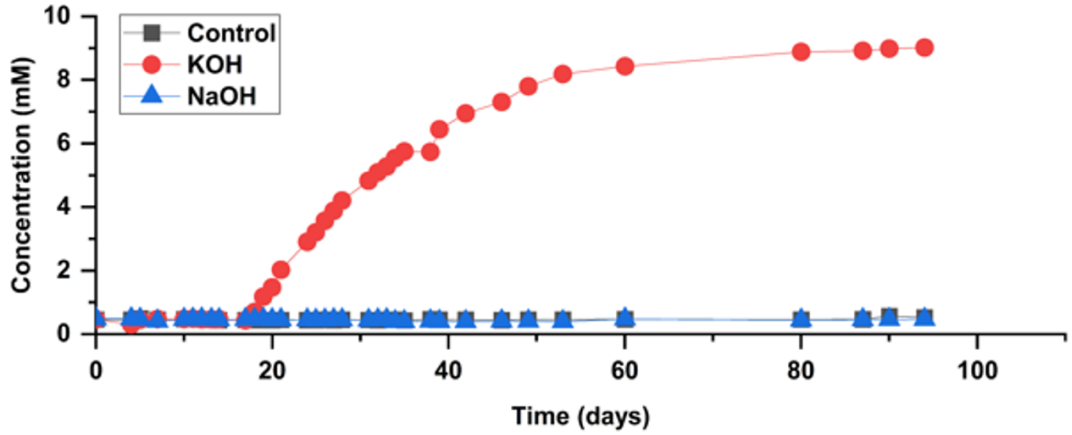

b

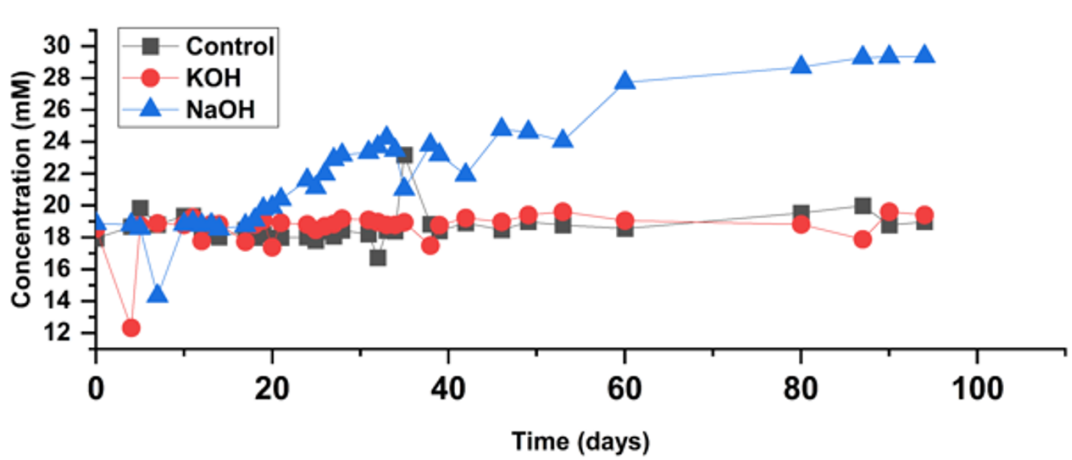

Appendix 5.2 Concentration of K/Na in the culture measured by ICP-MS. 1 mM samples were taken routinely, samples were centrifuged and the supernatant were using for quantification of the K/Na concentrations in the culture (a) Concentration of potassium in culture across time (mM), (b) Concentration of sodium in culture across time (mM)

Appendix 5.3 Enrichment results, FDR 0.05

Type	Name	P value	Enrichment Score	Total identified proteins	Proteins In cluster	Cluster size	Benj. Hoch. FDR
Cluster 1	Chitinophagaceae (F)	6.7747E-41	3.7539	151	91	227	3.7261E-40
Cluster 1	Phreatobacter (G)	1.9962E-28	4.3367	79	55	227	7.3193E-28
Cluster 1	Blastomonas (G)	5.9852E-10	2.7597	79	35	227	1.6459E-09
Cluster 2	Runella (G)	1.9791E-10	4.2335	44	22	167	2.177E-09
Cluster 2	Flavobacterium (G)	0.0011136	2.6611	35	11	167	0.0061245
Cluster 3	pseudanabaena(G)	3.103E-133	1.6776	728	545	631	3.413E-132
Cluster 4	Porphyrobacter (G)	6.6974E-40	3.993	139	84	214	3.6836E-39
Cluster 4	Rhodobacteraceae (F)	1.8416E-21	3.332	117	59	214	6.7525E-21
Cluster 5	Limnobacter (G)	0.0014868	4.2293	17	6	118	0.016355
Cluster 5	Hydrogenophaga (G)	0.0089967	2.9958	24	6	118	0.032988
Cluster 5	pseudanabaena(G)	0.015831	1.1522	728	70	118	0.043534

Appendix 5.4 Up-regulated proteins in KOH group. Protein classification was based on KEGG. Proteins were filtered by Log2 folder change > 2

Metabolism	Function	Log2 Folder Change (Day 26)	Log2 Folder Change (Day 38)
Glutathione peroxidase	Enzymes	6.64	4.76
Chorismate mutase AroH	Enzymes	6.64	
N-acetylmuramic acid 6-phosphate etherase	Enzymes	6.64	
Uridylate kinase	Enzymes	6.64	2.53
2-C-methyl-D-erythritol 2,4-cyclodiphosphate synthase	Enzymes		3.33
Genetic Information Processing			
Deoxyuridine 5'-triphosphate nucleotidohydrolase	DNA repair and recombination proteins	6.64	
Recombination protein	DNA repair and recombination proteins		6.64
Pyruvate kinase	Membrane trafficking	6.64	
50S ribosomal protein L28	Ribosome	6.64	
30S ribosomal protein S1	Ribosome	6.64	3.9
50S ribosomal protein L16	Ribosome		6.64
Signaling and Cellular Processes			
Pyruvate kinase	Exosome	6.64	
concentrative nucleoside transporter	Transport		6.64

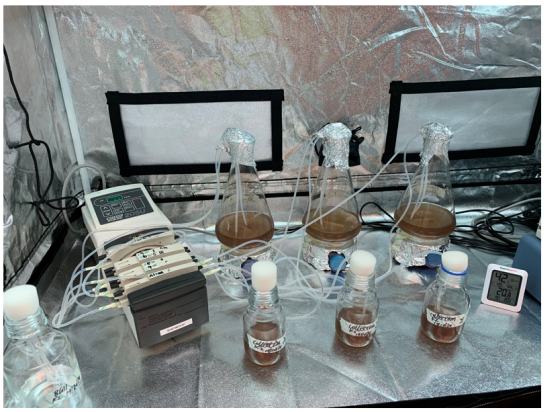

Day 17

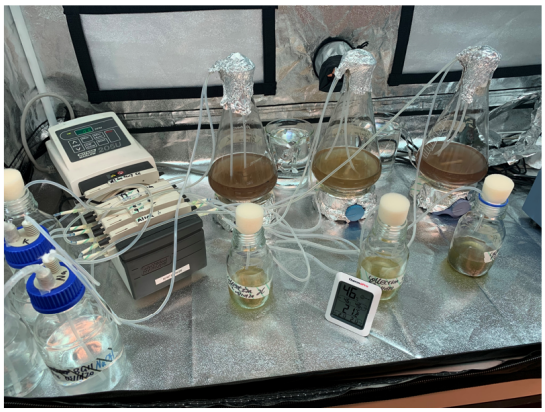

Day 24

Day 38

Day 80

Appendix 5.5 cultures were flushed with standard BG-11 medium, KOH suspended BG-11 medium, NaOH suspended BG-11 medium from left to right

Chapter 6 Discussion

Seasonal blooms have been reported regularly at the FGMSP located at the Sellafield nuclear processing site. A cyanobacterium belonging to the genus *Pseudanabaena* was identified to be the dominant microorganism in the community during the microbial bloom in August 2016, and it was the only photosynthetic organism present in the bloom event (Foster et al, 2020). Thus, controlling the growth of *Pseudanabaena* is thought to be the key to control the seasonal bloom in this pond. The pond is open to the air, maintained at a high pH, radioactive and rich in radionuclides such as strontium and caesium. Due to the complex conditions of the pond and aging infrastructures, developing bloom control methods for the FGMSP is challenging. Understanding interplays between the microorganisms and radionuclides present in the ponds and the physiology of microorganisms in such environment is essential for developing bloom control methods. Because of the radiological safety limitations prevented obtaining organisms directly from water in the Spent Nuclear Fuel Pond (SNFP), a mixed culture dominated by *Pseudanabaena catenate* were selected as a representative of the microbial community in the pond for our study. Previous studies tested the resistance of *P. catenata* to X-ray irradiation and studied the interactions between *P. catenate* and strontium (Foster *et al.,* 2020a; Foster et al., 2020b). The main aim of this project was to improve our understanding of the interactions between *P. catenate* and Cs, and also to develop bloom control methods for the *P. catenate* dominated bloom.

In **chapter 4,** the impact of Cs to *P. catenate* growth was identified. Low concentrations of Cs to some extent promotes the yields of *P. catenate* dominated culture. When the concentration of Cs reached up to 1 mM, the growth was stayed at the same level as the control culture. This suggests that the entire culture was able to tolerate the dose of Cs. Previous study showed that

Sr and radiation levels similar to those in the pond did not significantly affect the growth of *P. catenate* either. I also found that the *P. catenate* dominated culture would self-buffer the pH of the growth medium to around 10.5. This explained the reason that microbial blooms occurred in the "extreme" condition in FGMSP. The microscopy images showed that 1 mM Cs caused morphological change of cells. Analysing the protein expression file gave the results that Cs switched off the Kdp-ATPase K transport system, but stimulated the Trk high velocity K transport system. In addition, Cs additions dramatically up-regulated a range of cellular proteins. These included a battery of common stress response and nutrients limitation response systems. Previous studies reported that for some microbes, K and Cs might share a same transport by a series of kinetics experiments. In this study, the regulation of K transport system proteins were uncovered, which directly proved that for *P.catenata* cell, Cs acted as a competitor for K in K transport. The results from growth kinetics, cell morphology and protein expression profile gave fundamental knowledge of the behaviour and mechanism that *P.catenata* cells adapted to Cs abundant environment. To the nuclear industry, the findings explained the basis that the *P.catenata* colonised the FGMSP, which gained detailed information that could be considered in pond management strategies.

The fate of Cs in *P. catenate* active culture has been identified in the project by using ICP-MS and STXM. This was the first attempt of imaging Cs in a cyanobacteria cell. The findings evidenced that *P.catenata* could uptake Cs and accumulate them in discrete zones. Despite the amount of accumulated Cs was hint, understanding the mechanisms by which the Cs is concentrated in discrete zones may help uncover detoxification processes for this metal, and also has implications for Cs retention in biomass within FGMSP and other radioactive environments.

Finally, 5 mM K presented a surprising and profound inhibitory effect on culture yields in this study, which provided a possible way for controlling the growth of *P. catenate*. NaOH dosing is used to maintain an alkaline environment in pond (Konovalovaite, 2019), and the use of KOH could offer a biocontrol strategy while maintaining the high pH required to prevent fuel corrosion in the pond.

In **chapter 5,** I compared the inhibitory effect of KOH and NaOH to *P. catenate*. First, I compared K to Na in both batch cultures and in a chemostat system which simulated the pond purging system. The results from both experiments showed that *P. catenate* was sensitive to K, and that K can be used for controlling the growth of the organism. Microbial community profiles of the *P. catenate*-dominated culture were collected by 16S rRNA gene analysis, alongside changes in community protein expression profiles. Overall, the community analysis demonstrated that the sensitivity to K is organism specific, leading to enrichment to organisms such *Phreatobacter (G)*, *Roseomonas* (G) and *Rhodobacteraceae (F)*. However, despite the increase in relative abundance of these organisms, the overall biomass levels in the experiment declined significantly, suggesting that KOH dosing may offer a bloom control strategy, through inhibition of the primary photosynthetic pioneering colonizer within the FGMSP pond. The findings gave nuclear industry a biocontrol option for *P.catenata* dominated microbial bloom. However, before applying KOH to the FGMSP for bloom control, the methods should be tested on actual pond samples to evaluate the inhibitory effect, as the composition of the culture used in this experiment was not exactly the same as the Sellafield Pond system, and so it is possible that organisms that can be stimulated by KOH exists in the pond system ecosystem. In addition, the impact of changing Na to K to downstream processes at the plant should be evaluated (e.g. radionuclide treatment of pond effluents using SIXEP ion exchange systems). Previous studies indicated that the inhibitory effect of K+ to cells may be a result of the altered ratio of K+ to

Na+ (Parker et al., 1997). The effect of K+ and Na+ ratios was not tested in this study. A further study could also try to identify whether the absolute concentration of K+ or the relative concentration of K+ and Na+ are important to inhibit the growth of *Pseudanabaena*. If the inhibition effect is driven by the ratio of K+ and Na+, changing NaOH to KOH might be a very effective way to control the bloom, and the concentration of K+ required can be much lower than that determined in this study. Thus, the impact of changing NaOH to KOH on the downstream Sellafield processes may be further decreased. In addition to the nuclear industry. the findings can be explored to other high pH aquatic system as a bloom control strategy. Consistent with the loss of in *P. catenate* in the KOH-treated cultures, was a decline in proteins from the *P. catenate* proteome. However, the increase in abundance of proteins such as gpx1, suggested up-regulation stress-response proteins, when exposed to K. Which demonstrated the impact of high concentration of K to *P.catenata* cells in cellular level.

Appendices

A1 The fate of Sr in alkaline cultures of the cyanobacterium *Pseudanabaena catenata*

Lynn Foster, Adrian Cleary, Heath Bagshaw, David Sigee, Jon K Pittman, Katherine Morris, Kejing Zhang, Kurt F Smith, and Jonathan R Lloyd*

Abstract

A non-axenic culture of *Pseudanabaena catenata*, a close relative of the bloom-forming cyanobacterium found in the high pH First Generation Magnox Storage Pond (FGMSP) at the Sellafield Nuclear Facility, was supplemented with 1 mM of $SrCl_2$, to determine its effect on the fate of Sr. The addition of 1 mM Sr to the *P. catenata* culture resulted in ~16 % reduction in the overall growth of the culture (OD_{600nm}) and a 21 % reduction in the concentration of chlorophyll-a (Chl-a) compared to those without Sr. The fate of Sr was assessed using a multi-technique approach. Inductively coupled plasma atomic emission spectroscopy (ICP-AES) showed that virtually all of the Sr was removed from solution, while extracellular biomineral precipitates were analysed using TEM analysis, and were shown to contain Sr, Ca and S using energy-dispersive X-ray spectroscopy (EDS) analysis. In addition, intracellular P-containing electron-dense features, likely to be polyphosphate bodies, were associated with the *P. catenata* cells and contained lower levels of Sr. Bulk analysis of the cultures by X-ray diffraction (XRD) showed the presence of Ca-containing strontianite ($Sr(Ca)CO_3$), whilst EXAFS analysis showed the presence of $SrPO_4$ minerals. The presence of Sr associated with intracellular polyphosphate was unexpected, and contrasts with other model photosynthetic systems in the literature that have highlighted carbonate biominerals as the dominant sink for Sr. Understanding the fate of Sr within microorganisms associated with SNFPs is crucial to

understanding the fate of radioactive ^{90}Sr in such extreme environments, and could also suggest a potential remediation strategy for treatment of ^{90}Sr contaminated waters from SNFPs and in contaminated aquatic systems.

A1.1 Introduction

The generation of energy and the development of weapons by the nuclear industry has resulted in the production of significant levels of radioactive material (Crossland, 2012; Wilson, 1996). Despite efforts to contain these radioactive materials, accidental releases have occurred, for example the accidents associated with the nuclear reactors at the Chernobyl (Ukraine) and Fukushima (Japan) sites (Fukuda et al., 2014; Krejci et al., 2011). The release of radionuclides into the environment requires effective remediation strategies to be employed to minimize their transport and any harmful effects. There has been a lot of interest in the potential use of microorganisms in cost-effective and efficient remediation strategies, since they are ubiquitous in the environment and have a diverse range of metabolic capabilities (Blanco-Rivero et al., 2005; Pikuta et al., 2007). A wide range of microorganisms, including bacteria, cyanobacteria, eukaryotic algae and fungi are known to influence the speciation and fate of radionuclides by either metabolism-independent or dependent mechanisms (Gadd, 1990).

Of particular interest is the removal of fission products, such as ^{137}Cs and ^{90}Sr from aquatic environments, since they are not only radioactive but also bioavailable, as analogues for K^+ and Ca^{2+}, respectively (Brookshaw et al., 2012; Fukuda et al., 2014; Simonoff et al., 2007). The ability of microorganisms to influence the fate of these high yield and key fission products has been demonstrated, for example with high levels of ^{137}Cs uptake by the eukaryotic microalgal species *Coccomyxa actinabiotis* (Rivasseau et al., 2013). The fate of ^{90}Sr appears to be strongly linked to Ca behaviour with, for example, co-association with carbonate minerals

that can precipitate out of solution or adsorb to surfaces (Fukuda et al., 2014; Kang et al., 2014; Lauchnor et al., 2013). In addition Sr is known to interact with phosphate, for example it can interact with biologically precipitated hydroxyapatite [$Ca_5(PO_4)_3(OH)$] which can be formed by microbial communities supplied with glycerol 2-phosphate (Handley-Sidhu et al., 2014). The majority of carbonate mineral formation is thought to occur as extracellular precipitates that can adsorb to a variety of surfaces including clays and extracellular features of microorganisms (Chiang et al., 2010; Gadd, 1990; Schultze-Lam and Beveridge, 1994). Strontium carbonate formation has recently been shown to occur intracellularly in a small number of microorganisms including the desmid green algae *Closterium moniliferum*, and more recently some cyanobacterial species, e.g. *Candidatus Gleomargarita lithophora* (Cam et al., 2015, 2016; Couradeau et al., 2012; Krejci et al., 2011). Li *et al*., (Li et al., 2016) observed that traditional electron microscopy methods used to prepare microbial cells for examination of ultrastructure and sites of metal accumulation, can result in the removal or distortion of such features, and therefore give a false account of intracellular carbonate biomineralisation. Indeed, the number of microbial species which are identified as being capable of forming such intracellular carbonate minerals may increase with improvements in preparation techniques.

In the UK, legacy waste from early Magnox gas-cooled nuclear reactors has been stored in the First Generation Magnox Storage Pond (FGMSP). The FGMSP is an open air spent nuclear fuel pond (SNFP) on the Sellafield nuclear complex (Cumbria, UK), in operation since the late 1950s (Sellafield, 2014; Wilson, 1996). Magnox reactor fuel consisted of unenriched uranium metal clad in a magnesium non-oxide (MAGNOX) alloy, which both have low chemical stabilities in water (Gregson et al., 2011a; Jackson et al., 2014). The MAGNOX fuel was originally intended for reprocessing, but in some cases has been stored in the Spent Nuclear Fuel Pond (SNFP) for considerably longer than anticipated, which has led to extensive corrosion of the MAGNOX cladding and fuel (Jackson et al., 2014). As a result of fuel

corrosion, the pond has significant levels of radioactivity including ^{90}Sr and ^{137}Cs associated with the corroded spent nuclear fuel (NDA, 2016), pond effluent, and radioactive sludge (Gregson et al., 2011a, 2011b; Jackson et al., 2014), of which a major constituent is brucite ($Mg(OH)_2$) (Ashworth et al., 2018). In addition to the radioactive inventory, the pond is open to the air and so it is subject to an influx of carbon, nitrogen and environmental debris (Gregson et al., 2011a, 2011b; Jackson et al., 2014). The pond is continuously purged with alkaline dosed demineralised water at alkaline pH (~11.4), which provides thermal cooling whilst minimizing any further corrosion to the fuel (Foster et al., 2020a; Gregson et al., 2011a, 2011b; Jackson et al., 2014).

Despite the elevated pH and radionuclide inventory in the pond, microorganisms are known to colonise the pond, with extensive growth periods observed and reported as algal blooms (Foster et al., 2020a; Gregson et al., 2011a, 2011b). Recently the microbial community of the pond has been investigated using DNA-based tools over a three year period including during a bloom event in August 2016 (Foster et al., 2020a). The pond community of background water samples taken in non-bloom periods was shown to be dominated by *Proteobacteria*, with photosynthetic or hydrogen-metabolising capabilities present in abundant members of the population (Foster et al., 2020a). During the August 2016 bloom event, the cyanobacterium, *Pseudanabaena catenata* (Foster et al., 2020a) was the most abundant organism detected, making up ~30 % of the 16S rRNA genes sequenced in water samples. Despite its presence in a range of other environments and in algal blooms (Acinas et al., 2009; Zhu et al., 2015), there is little information in the scientific literature about the ecology of this filamentous cyanobacterium, and its impact on radionuclide speciation and fate.

The FGMSP is currently undergoing decommissioning as a high priority. This includes planning for waste retrieval operations over 10 year plus timescales and more recently has involved the start of removal of the radioactive sludge inventory (Sellafield, 2014). It is important to understand the potential fate of key radionuclides in the pond during plant operations, to ensure predictable and safe management. While stable Sr is present in pond waters at low levels, ^{90}Sr is present at significant levels by activity and is potentially very soluble, and thus needs to be considered carefully during effluent processing to minimise discharges to the environment (Ashworth et al., 2018). The purpose of this investigation was to determine the fate of Sr in the presence of microorganisms representative of those in the FGMSP system, namely a mixed laboratory culture dominated by *P. catenata*, a good model for the pond community (Foster et al., 2020b). This study also aimed to determine whether under the conditions of study, intracellular Sr-containing minerals could be formed by this species of cyanobacterium. Here we demonstrate that in the presence of an actively growing *P. catenata* culture, both $(Sr,Ca)CO_3$ and $SrPO_4$ biominerals are formed. Interestingly, Sr could be observed by TEM and EDS analysis in association with the electron dense intracellular features containing P, thought to be polyphosphate bodies. Understanding the interactions between Sr and the *P. catenata* culture provides insight into the fate of Sr in the pond and may provide pathways towards potential remediation strategies in other ^{90}Sr contaminated aquatic sites.

A1.2 Methods

A.1.2.1 Culturing of *Pseudanabaena catenata* with Sr

Experiments were set up to investigate the interaction and fate of Sr with a cyanobacterium, *P. catenata,* which has been identified in the FGMSP on the Sellafield site (Foster et al., 2020a). Radiological control measures in place at the Sellafield site for the legacy SNFP prevented the

isolation and culturing of microorganisms directly from pond water. A photosynthetic culture dominated by *P. catenata*, which is a close match to the species identified in the FGMSP, was obtained from the NIVA Culture Collection of Algae (NIVA-CYA 152), Norway. Whilst it was not possible to source an axenic culture, previous 16S rRNA gene sequencing revealed that of the 9 operational taxonomic units (OTUs) identified in the NIVA-CYA 152 culture, 5 were affiliated with genera identified in the FGMSP (Foster et al., 2020b). The *P. catenata* culture used in the current work was therefore considered representative of the pond community.

Cultures were set up by inoculating the *P. catenata* culture into 30 mL of unbuffered BG11 medium (Culture Collection of Algae and Protozoa) to a starting optical density (600 nm) of 0.2. Three biological replicates were spiked with $SrCl_2$ (Sigma-Aldrich) solution to a final concentration of approximately 1 mM. A further three identical cultures were set up with sterile deionised water used to adjust the total volume in line with the Sr-containing cultures, to assess the impact of Sr on the growth of the culture. All cultures were incubated at 25 ±1 °C, and shaken at 100 rpm in a light incubator with a photon flux density of 150 μmol m^{-2} s^{-1}, with a 16:8 h light-dark cycle (supplied by cool fluorescent daylight lamps). Sterile controls were also set up using 30 mL BG11 medium with 1 mM $SrCl_2$ to determine the effect of abiotic versus biotic processes.

A1.2.2 Optical density, chlorophyll-a concentration, and pH measurements

In order to determine whether the addition of Sr affected the growth of *P. catenata*, optical density, chlorophyll-a (Chl-a) concentration and pH measurements were taken at selected time points throughout the experiment. All absorbance measurements were carried out on 1 mL samples using a Jenway 6700 UV/Vis spectrophotometer (Bibby Scientific Ltd, Staffordshire,

UK). The growth of the *P. catenata* culture was assessed by measuring optical density at 600 nm (OD_{600nm}) to indicate the total biomass present in the cultures. The concentration of Chl-a was determined using the same samples as used for the OD_{600nm} measurements, as described in Foster *et al*. (Foster et al., 2020b). Briefly, the cells from a 1 mL sample were pelleted by centrifuging at 14,000 *g* for 10 min and the supernatant was discarded. The cells were re-suspended in 1 mL 70 % ethanol and left in the dark at room temperature for 2 h. The samples were centrifuged for a further 10 min at 14,000 *g*, and the absorbance of the supernatant was recorded at 665 nm (Chl-a) and 750 nm (turbidity correction). The concentration of Chl-a was calculated using the formula as set out by Jespersen and Christoffersen (Jespersen and Christoffersen, 1987). All pH measurements were made using a calibrated FiveEasyPlus pH Meter (Mettler Toledo Ltd, Leicestershire, UK).

A1.2.3 Assessment of Sr behaviour

The fate of Sr in the presence of the *P. catenata* culture was determined using a range of analytical techniques.

Inductively coupled plasma atomic emission spectroscopy (ICP-AES). The concentration of soluble Sr in the culture medium was measured by inductively coupled plasma atomic emission spectrometry (ICP-AES, Perkin-Elmer Optima 5300 dual view) using a matrix-matched serially diluted Specpure multielement plasma standard solution 4 (Alfa Aesar) for calibration. Briefly, a 600 µL sample was centrifuged at 14,000 *g* for 10 min, 500 µL of supernatant was then added to 9.5 mL of 2 % nitric acid prior to analysis.

Electron Microscopy. In order to image any Sr minerals formed during the experiment and their potential interactions with *P. catenata,* (and other associated microorganisms present in

the culture (Foster et al., 2020b)) electron microscopy was carried out on non-fixed samples. Samples (1 mL) were taken after 20 days of incubation for analysis by transmission electron microscopy (TEM). The samples were washed twice in sterile demineralised water (centrifuged 10 min at 14,000 *g*). For TEM analysis, 2 µL of the washed cell suspension was dropped onto a copper TEM grid with a carbon film (Agar Scientific, Essex, UK) and allowed to dry at room temperature. The samples were assessed using a FEI Tecnai T20 LaB6 Transmission Electron Microscope operating at 200 kV equipped with an Oxford XMax EDS detector. The images were captured with Gatan Digital Micrograph whilst the EDS data analysis was performed using Oxford INCA software.

X-Ray Diffraction (XRD). An aliquot of culture containing Sr was centrifuged to pellet the cells, the supernatant was discarded, and the cell pellet was spread evenly over a glass slide and allowed to dry. The sample was then analysed by XRD to identify any crystalline Sr-containing minerals present. Measurements were carried out on a Bruker D8 Advance diffractometer, equipped with a Göbel Mirror a Lynxeye detector. The X-ray tube had a Cu source, providing Cu $K_{\alpha 1}$ X-rays with a wavelength of 1.540 Å. The sample was scanned from 5-70 °2θ, with a step size of 0.01 ° and a count time of 1.5 s per step. The resultant patterns were evaluated using EVA version 4, which compares experimental data to standards from the ICDD (International Centre for Diffraction Data) Database.

Extended X-ray absorption fine structure (EXAFS). The coordination environment of Sr in the bulk solid phase was analysed using X-ray absorption spectroscopy (XAS). Samples were prepared for XAS by removing the solid phase after 20 days from the culture media by vacuum filtration and then diluting with cellulose to form a pellet with approximately 1 % Sr loading. Sr K-edge spectra (16115.26 keV) were collected in transmission mode on Beamline B18 at

the Diamond Light Source, Harwell, using a liquid nitrogen cooled cryostat. Multiple scans were averaged, calibrated, background subtracted and normalised using ATHENA (Ravel and Newville, 2005). ARTEMIS was then used to fit extended X-ray absorption fine structure (EXAFS) spectra to determine the average coordination environment of Sr in the solid phase (Ravel and Newville, 2005). Shells were only included in the fit if they made a statistically significant improvement to the model fit as determined by the F-test (Downward et al., 2007).

A 1.2.4 PHREEQC modelling

All speciation and saturation thermodynamic calculations were performed using the United States Geological Survey thermodynamic speciation code PHREEQC (3.3.7) using the Andra specific interaction theory database (ThermoChimie v.9.b0 August 2015).

A1.3 Results

A1.3.1 The effect of Sr on the growth of the *P. catenata* culture

In order to determine whether the addition of Sr had any effect on the growth of the *P. catenata* culture, the optical density and the concentration of Chl-a of the cultures were measured. Measurements were taken over a period of 20 days. When inoculated with an actively growing culture, both the control and Sr-containing cultures showed a steady increase in optical density over the 20-day sampling period as expected. (Figure A1.1.1a). The two sets of treatments started with approximately the same OD_{600nm} measurements of 0.22 (0.01 standard deviation (SD)) for the Sr-free controls compared to 0.21 (0.01 SD) in the Sr-containing cultures. The culture containing Sr grew at the same rate as the control until day 12, indicating that the addition of the Sr did not inhibit growth during initial growth. The cultures reached their highest optical densities at day 20; 2.49 (0.11 SD) and 2.10 (0.14 SD) for the Sr-free control and Sr-containing cultures respectfully. Assessment of the OD_{600nm} measurements at day 20,

using a one-way ANOVA test, shows that there was a significant difference between these measurements (P-value 0.01, F-ratio 15.3). This indicates that at the end of the sampling period the 1 mM Sr had an inhibitory effect on the final growth yields of the *P. catenata* culture compared to the control. In addition to the OD_{600nm} measurements, the concentration of Chl-a was measured to give an indication of the photosynthetic biomass of the cultures (Figure A1.1.1b). The cultures started off with Chl-a concentrations of 0.66 mg L^{-1} (0.04 SD) and 0.60 mg L^{-1} (0.04 SD) for the control and Sr-containing cultures respectfully. Both sets of cultures showed a continuous increase in the concentration of Chl-a, which was not significantly different for the first 12 days of the experiment. At day 20 the concentrations recorded were 7.95 mg L^{-1} (0.82 SD) in the control and 6.23 mg L^{-1} (0.52 SD) in the Sr-containing cultures, which represents a 21 % reduction in Chl-a levels between the two treatments. The differences seen between the two treatments at day 20 are significant according to a one-way ANOVA test (P-value 0.04, F-ratio 9.4). The reduction in the Chl-a concentrations are consistent with the reduction seen in the OD_{600nm} measurements indicating that this is likely to be a consequence of reduced biomass. The pH of the cultures was not controlled by acid or base additions during the course of the experiment, allowing for pH buffering as a result of the photosynthetic activity of *P. catenata*. The pH started at 7.5 (0.1 SD) and 7.6 (0.1 SD) in the control and Sr-containing cultures respectfully (Figure A1.1.1c). By day 5 the pH of the control cultures had risen to 9.3 (0.01 SD) and the Sr-containing cultures pH was 9.7 (<0.01 SD) experiments and remained elevated over the remaining sampling period. The pH of sterile BG11 medium with Sr remained stable over the same experimental period (data not shown), which confirms that that observed increase in the pH is driven by photosynthesis (Jin et al., 2005; López-Archilla et al., 2004).

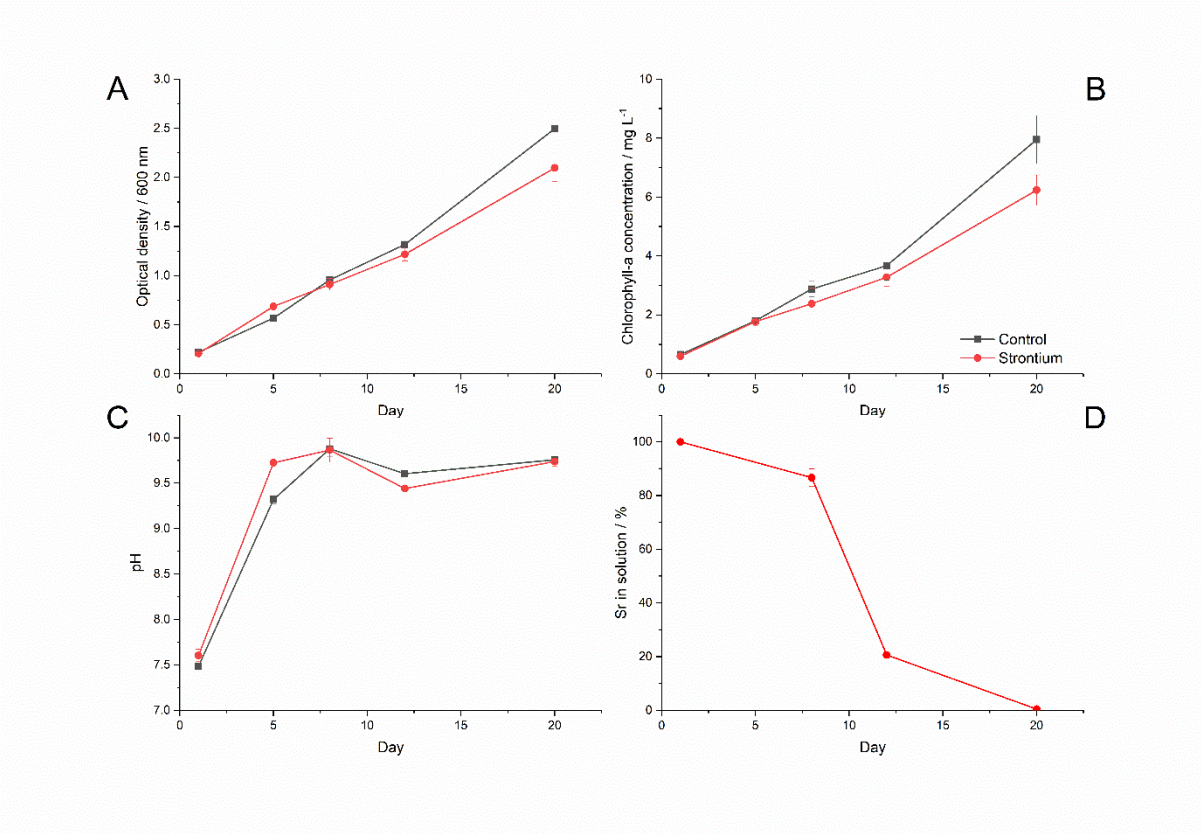

Figure A1.1: Growth curves of *P. catenata* with and without the addition of Sr: a) optical density at 600 nm; b) Chl-a concentrations (µgL^{-1}); c) pH; d) percentage of Sr in solution measured by ICP-AES. Error bars are the standard deviation of 3 replicates.

A1.3.2 Sr removal from solution

ICP-AES was used to determine the amount of Sr in solution throughout the experiment (Figure A1.1d). At day 8, 13.5 % Sr was removed from solution with the biomass. In the next 4 days a further 65.3 % was removed from solution, and by day 20 >99.5 % of the total Sr added had been removed. The largest reduction in soluble Sr concentrations coincided with the maximum pH measurements recorded. In contrast a maximum of 20 % of Sr was insoluble in sterile BG11 medium controls at pH 7.5 (Supplementary Figure 1), indicating the large-scale removal seen in this study was pH driven by photosynthesis.

A1.3.3 Sr saturation calculations

Thermodynamic modelling of 1 mM Sr in BG11 medium was carried out to identify the products that could precipitate with Sr under representative experimental conditions (Supplementary Table 1). The concentration of PO_4^{3-} and CO_3^{2-} in BG11 medium was 0.23 mM and 0.19 mM, respectively. The modelling indicated when the BG11 medium was at pH 7.2, calcium and strontium phosphate phases were over saturated, suggesting phosphate induced precipitation was possible. When the modelling was repeated at pH 10 (representative of the upper limit of pH in the experiments), the saturation indices (log_{10}(ion activity/solubility product)) for the metal phosphates phases increased, indicating that precipitation was more favourable. Here, thermodynamic calculations at the elevated pH (10) suggested that carbonates such as strontianite ($SrCO_3$) were oversaturated.

A1.3.4 Determining the fate of Sr in the *P. catenata* culture

Electron Microscopy analysis. TEM was used to analyse samples from both the Sr-containing (and control cultures) to assess where the Sr was located and if it was associated with the microorganisms. The samples were washed twice with sterile demineralised water and air dried prior to analysis. Cells were clearly visible in both sets of samples, with the distinctive *P. catenata* filaments clearly visible (~ 1 μm x 5 μm) alongside other smaller heterotrophic microorganisms (Foster et al., 2020b). In both sets of samples *P. catenata* cells displayed circular electron dense features, which frequently occurred in the centre of and down the length of the filaments (Figure A1.2 a and Supplementary Figure 2). EDS analysis of these features commonly identified the presence of phosphorus, and this suggested that these features could be polyphosphate bodies. In addition, low levels of calcium could also be detected in association with these features. Sr could also be detected with these phosphorus-containing structures, indicating that the Sr detected could be intracellular (Figure A1.2). Significant Sr

concentrations could not be detected in other regions of the cells (Supplementary Figure 3), offering further support that Sr taken up by the cells was localised with the phosphorus-containing features. The micrographs also showed the presence of Sr-containing deposits which appeared to be extracellular but were still associated with the microorganisms (Figure A1.2: b4 and c5). EDS analysis of the extracellular deposits showed the presence of Sr, Ca and S in different proportions.

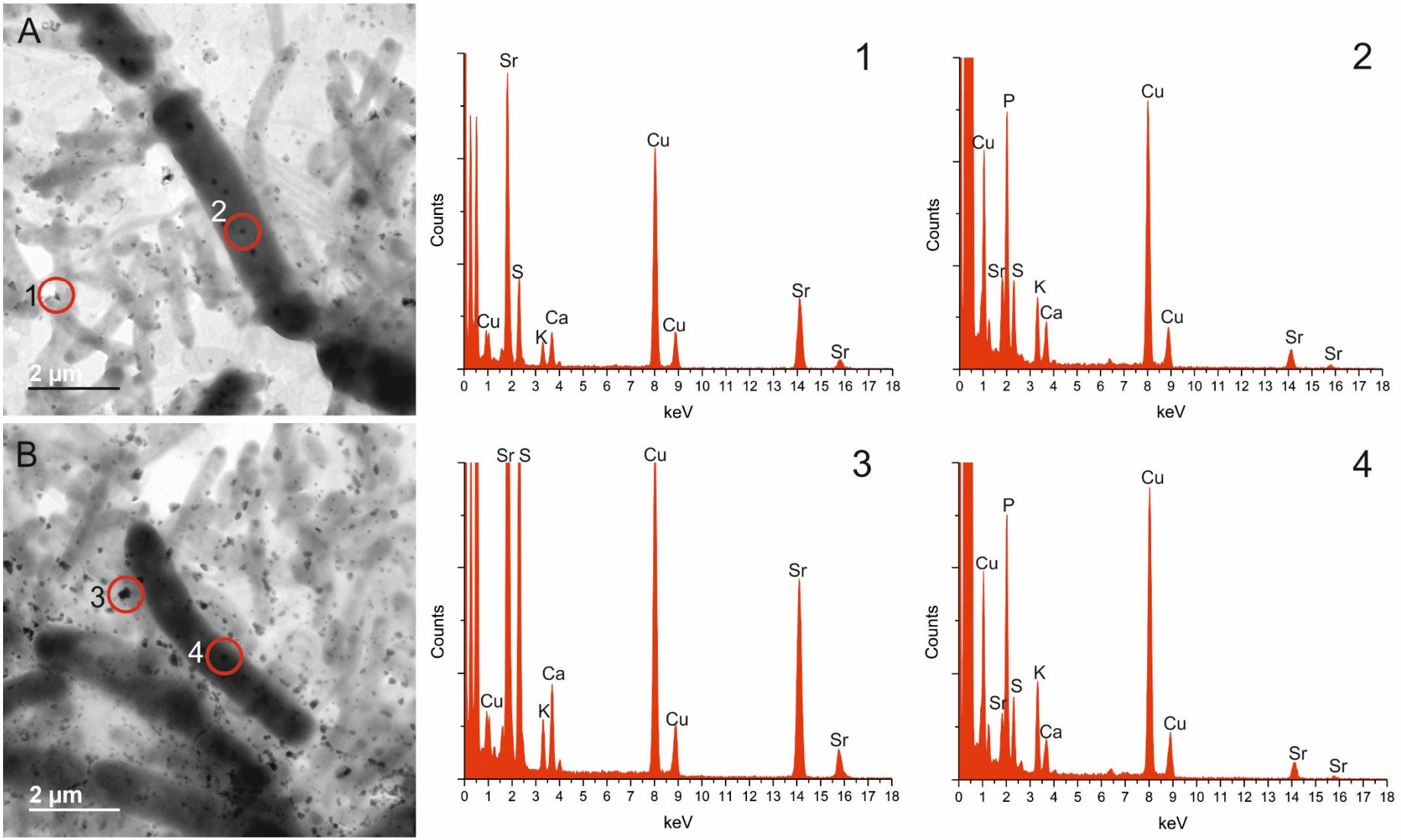
A
1
2
2 µm
B
3
4
2 µm
1
Counts
keV
Sr
Cu
S
Ca
K
2
P
3
4

Figure A1.2: TEM images and EDS data taken from samples of *P. catenata* cultures incubated with $SrCl_2$ at day 20, washed twice. EDS data corresponds to the numbers on TEM images, site of scans indicated by red circle. All scale bars represent 2 µm.

X-ray diffraction (XRD) characterisation of Sr biominerals. An additional sample of the *P. catenata* precipitate that contained Sr was analysed using XRD to identify any crystalline minerals that had been formed during the course of the study. The results of the scan indicated the presence a carbonate mineral which was comprised of Sr and Ca in a ratio of 0.85 : 0.15 (Figure A1.3).

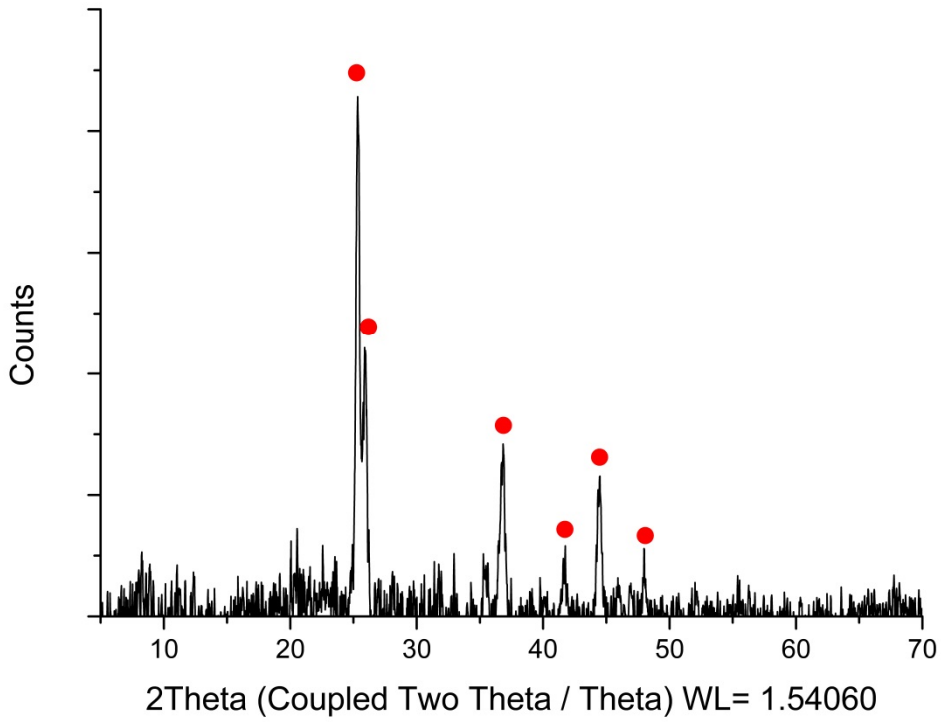

Figure A1.3: XRD analysis of a bulk sample of *P. catenata* culture incubated with Sr. Red dots indicate the presence of calcian strontianite [(Sr 0.85, Ca 0.15) (CO_3)]

EXAFS analysis of Sr minerals. The average speciation and coordination environment of the Sr in the microbial cultures was further analysed using X-ray absorption spectroscopy. K-edge XANES and EXAFS spectra were collected on Sr in the solid phase. XANES spectra for all samples showed a single peak consistent with a

9 fold coordination environment (Thorpe et al., 2012b, 2012a). Modelling of the EXAFS as outer sphere sorbed Sr with a single shell of 9 oxygen atoms at a distance of 2.6 Å provided a satisfactory first fit, however there were features between 3.2 and 3.6 Å in the Fourier Transform that were not resolved with this simple model (Figure A1.4). Further refinement of the the EXAFS modelling was informed by the relevant literature on Sr bio-mineral formation (Bazin et al., 2014; Handley-Sidhu et al., 2014; Thorpe et al., 2012b). Here, the best fit was obtained when Sr was coordinated to P with a shell of 1.8 P backscatterers at 3.2 Å and 1 Sr backscattering path at 3.48 Å. These bond lengths are consistent with Sr substituted into nanoparticulate hydroxyapatite-like phases seen in past work (Bazin et al., 2014; Handley-Sidhu et al., 2014). Interestingly, as XRD data suggested the measurable crystalline fraction of the Sr was present in a crystalline strontianite phase, the EXAFS data were also modelled as $SrCO_3$, however this did not yield a realistic fit. This suggests the bulk of the Sr is associated with nano-crystalline hydroxyapatite-like phases, consistent with observations from TEM that the polyphosphate structures had Ca, Sr and P co-located.

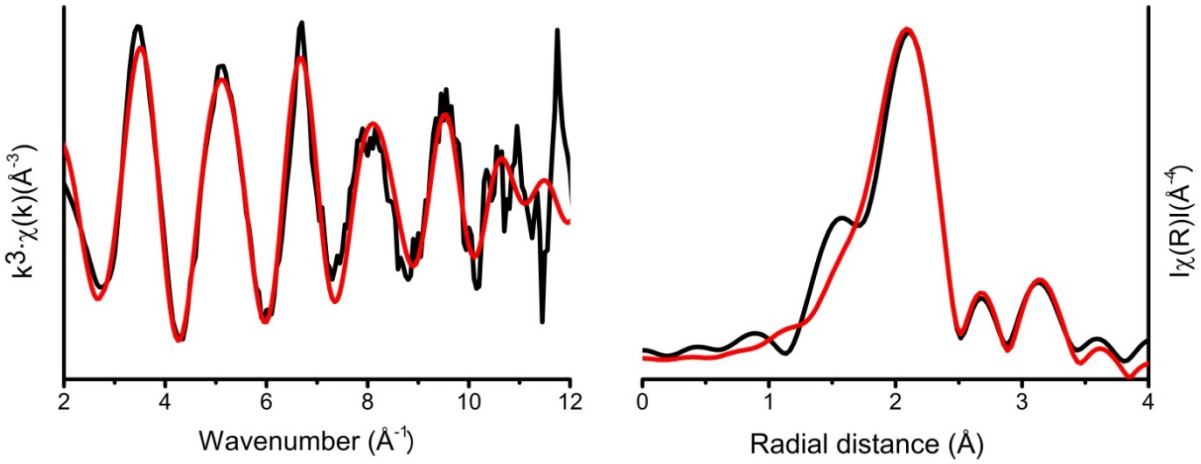

Figure A1.4: Sr K-edge EXAFS experimental data (black line). Theoretical best fit (red line) calculated using Artemis (Ravel and Newville, 2007)

A1.4 Discussion

The FGMSP situated on the Sellafield site contains a significant inventory of radioactive fission products, including ^{90}Sr. This current study investigated the fate of Sr when incubated with non-axenic culture of *P. catenata*, representative of the microbial community detected in a microbial bloom in the pond on August 2016 (Foster et al., 2020a, 2020b). This is the first study to our knowledge, which investigates the fate of Sr on a mixed microbial community relevant to the microbial ecology of a high pH legacy SNFP.

Collectively our experiments show that the presence of Sr in the culture medium does not prevent the growth of the microorganisms in this mixed culture, although the total biomass at the end of the study period was lower when Sr was present, presumably due to toxicity of the added metal. Analysis of the Sr in the culture using EXAFS showed that Sr most likely formed hydroxyapatite like nanoparticulate phases consistent with thermodynamic modelling predictions suggesting oversaturation of phosphate phases. The TEM data provides evidence that *P. catenata* cells are capable of taking up a small proportion of the Sr in solution, which can become co-localised with polyphosphate type features in the cells. Significant quantities of small extracellular Sr-containing minerals were also visible using the TEM, which varied in their composition, with P

not always present. The extracellular minerals appeared to be associated with the outer surfaces of the microorganisms. The extracellular minerals lacking a P peak, are likely to be carbonate minerals, as indicated by XRD analysis. The XRD analysis was not able to confirm the presence of PO_4 minerals in the bulk sample, presumably due to the amorphous character of Sr-Ca-PO_4, hydroxyapatite-like phases observed through EXAFS analyses on the bulk cell precipitates.

Polyphosphate bodies are made up of many orthophosphate residues that are linked by phosphoanhydride bonds to form linear polymers, and can be found in many organisms (Achbergerová and Nahálka, 2011; Albi and Serrano, 2016). Previous studies have shown that polyphosphate bodies can have a variety of metals associated with them, with the most commonly studied metals including Cd, Pb, and Ca (Albi and Serrano, 2016; Baxter and Jensen, 1980; Jensen et al., 1982). Evidence for Sr interactions with polyphosphate bodies is, however, limited. A study by Baxter and Jensen (Baxter and Jensen, 1980) showed variable uptake of Sr by the cyanobacterium *Plectonema boryanum*. Intracellular Sr, as shown by TEM analysis, was associated with two types of electron dense clusters, the first being polyphosphate bodies whilst the second was devoid of any detectable P. The authors noted the presence of K in both of the Sr containing electron dense clusters, with the addition of S and Ca features when P was absent. Interestingly in the current work K, S, and Ca were also observed in the minerals formed in the *P. catenata* culture, including those associated with the polyphosphate type bodies. The Sr containing electron dense bodies seen in the past work with *P.*

boryanum, could potentially be carbonate minerals, incorporating both Sr and Ca. Such intracellular Sr carbonates have been the focus of more recent studies using *Candidatus Gleomargarita lithophora* and *Cyanothece* sp. PCC7425, which show selective uptake and carbonate mineral formation with Sr (Benzerara et al., 2014; Cam et al., 2015, 2016; Couradeau et al., 2012). The ability to form intracellular carbonate minerals does not appear to be ubiquitous, with *P. catenata* appearing to be incapable of such intracellular mineral formation.

The uptake of small amounts of Sr in *P. catenata,* which are localised at distinct features including polyphosphate, is potentially significant, particularly during microbial bloom periods. There are multiple functions associated with polyphosphate in organisms, including the detoxification of heavy metals (Albi and Serrano, 2016; Keasling, 1997). The level of polyphosphate in microorganisms has been linked to metal tolerance, with higher levels resulting in increased tolerance (Albi and Serrano, 2016) and there is evidence that polyphosphate play a role in adaptation strategies in extreme environments (Achbergerová and Nahálka, 2011). In addition, efflux systems have been identified in other microorganisms that have been proposed to remove the metals as PO_4 minerals via the Pit transport system, following the enzymatic degradation of the polyphosphate (Albi and Serrano, 2016; van Veen et al., 1994). Whilst this mechanism has not been observed previously with Sr systems, it is plausible that the microorganisms in the FGMSP could utilise a similar mechanism to protect themselves against the toxicity of ^{90}Sr.

Interactions between the microorganisms in the FGMSP and ^{90}Sr are as yet unknown, however this study provides information about the potential fate of ^{90}Sr in such systems. In pond effluents ^{90}Sr is present in the water column, suggesting that at least a proportion of the Sr is mobile in the pond. Given the low levels of PO_4 in the pond, which are below the limits of detection (Foster et al., 2020a), it is more likely that the majority of microbial induced precipitation would be comprised of carbonate minerals in contrast to the observations in this laboratory study. The ability of microorganisms to adjust the pH of their surrounding environments and to influence the precipitation and the potential uptake of Sr is of wider interest in contaminated environments, such as the Fukushima site in Japan. Here, it is clear that naturally occurring microbial populations could potentially facilitate a first step in the removal of fission products such as ^{90}Sr from aquatic systems.

A1.5 References

Achbergerová, L., and Nahálka, J. (2011). Polyphosphate - an ancient energy source and active metabolic regulator. *Microb. Cell Fact.* 10, 1–14.

Acinas, S. G., Haverkamp, T. H., Huisman, J., and Stal, L. J. (2009). Phenotypic and genetic diversification of *Pseudanabaena* spp. (cyanobacteria). *ISME J.* 378, 31–46.

Albi, T., and Serrano, A. (2016). Inorganic polyphosphate in the microbial world. Emerging roles for a multifaceted biopolymer. *World J. Microbiol. Biotechnol.* 32, 1–12.

Ashworth, H., Abrahamsen, L., Bryan, N., Foster, L., Lloyd, J. R., Kellet, S., et al. (2018). Effect of humic acid and bacterial exudates on sorption-desorption interactions of ^{90}Sr with brucite. *Environ. Sci. Process. Impacts* 20, 956–964.

Baxter, M., and Jensen, T. (1980). Uptake of magnesium, strontium, barium, and manganese by *Plectonema boryanum* (*Cyanophyceae*) with special reference to polyphosphate bodies. *Protoplasma* 104, 81–89.

Bazin, D., Dessombz, A., Nguyen, C., Ea, K., Lioté, F., Rehr, J., et al. (2014). research papers The status of strontium in biological apatites : an XANES / EXAFS investigation research papers. *J. Synchrotron Radiat.* 21, 136–142.

Benzerara, K., Skouri-Panet, F., Li, J., Férard, C., Gugger, M., Laurent, T., et al. (2014). Intracellular Ca-carbonate biomineralization is widespread in cyanobacteria. *Proc. Natl. Acad. Sci.*, 1–6.

Blanco-Rivero, A., Leganés, F., Fernández-Valiente, E., Calle, P., and Fernández-Piñas, F. (2005). *mrpA*, a gene with roles in resistance to Na^+ and adaptation to alkaline pH in the cyanobacterium *Anabaena* sp. PCC7120. *Microbiology* 151, 1671–1682.

Brookshaw, D. R., Pattrick, R. A. D., Lloyd, J. R., and Vaughan, D. J. (2012). Microbial effects on mineral-radionuclide interactions and radionuclide solid-phase capture processes. *Mineral. Mag.* 76, 777–806.

Cam, N., Benzerara, K., Georgelin, T., Jaber, M., Lambert, J. F., Poinsot, M., et al. (2016). Selective uptake of alkaline earth metals by cyanobacteria forming intracellular carbonates. *Environ. Sci. Technol.* 50, 11654–11662.

Cam, N., Georgelin, T., Jaber, M., Lambert, J. F., and Benzerara, K. (2015). In vitro synthesis of amorphous Mg-, Ca-, Sr- and Ba-carbonates: What do we learn about intracellular calcification by cyanobacteria? *Geochim. Cosmochim. Acta* 161, 36–49.

Chiang, P. N., Wang, M. K., Huang, P. M., Wang, J. J., and Chiu, C. Y. (2010). Cesium and strontium sorption by selected tropical and subtropical soils around nuclear facilities. *J. Environ. Radioact.* 101, 472–481.

Couradeau, E., Benzerara, K., Gérard, E., Moreira, D., Bernard, S., Brown, G. E., et al. (2012). An early-branching microbialite cyanobacterium forms intracellular carbonates. *Science (80-.).* 336, 459–462.

Crossland, I. (2012). *Nuclear fuel cycle science and engineering*. 1st ed. , ed. I.

Crossland Philadelphia: Woodhead Publishing.

Downward, L., Booth, C. H., Lukens, W. W., and Bridges, F. (2007). A variation of the F-test for determining statistical relevance of particular parameters in EXAFS fits. *AIP Conf. Proc.* 882, 129–131.

Foster, L., Boothman, C., Ruiz-Lopez, S., Boshoff, G., Jenkinson, P., Sigee, D., et al. (2020a). Microbial bloom formation in a high pH spent nuclear fuel pond. *Sci. Total Environ.* 720, 137515.

Foster, L., Muhamadali, H., Boothman, C., Sigee, D., Pittman, J. K., Goodacre, R., et al. (2020b). Radiation tolerance of *Pseudanabeana catenata*, a cyanobacterium relevant to the First Generation Magnox Storage Pond. *Front. Microbiol.* Provisiona, 1–13.

Fukuda, S. ya, Iwamoto, K., Atsumi, M., Yokoyama, A., Nakayama, T., Ishida, K. ichiro, et al. (2014). Global searches for microalgae and aquatic plants that can eliminate radioactive cesium, iodine and strontium from the radio-polluted aquatic environment: A bioremediation strategy. *J. Plant Res.* 127, 79–89.

Gadd, G. M. (1990). Heavy metal accumulation by bacteria and other microorganisms. *Experientia* 46, 834–840.

Gregson, C. R., Goddard, D. T., Sarsfield, M. J., and Taylor, R. J. (2011a). Combined electron microscopy and vibrational spectroscopy study of corroded Magnox sludge from a legacy spent nuclear fuel storage pond. *J. Nucl. Mater.* 412, 145–156.

Gregson, C. R., Hastings, J. J., Sims, H. E., Steele, H. M., and Taylor, R. J. (2011b). Characterisation of plutonium species in alkaline liquors sampled from a UK legacy nuclear fuel storage pond. *Anal. Methods* 3, 1957.

Handley-Sidhu, S., Hriljac, J. A., Cuthbert, M. O., Renshaw, J. C., Pattrick, R. A. D., Charnock, J. M., et al. (2014). Bacterially produced calcium phosphate nanobiominerals: sorption capacity, site preferences, and stability of captured radionuclides. *Environ. Sci. Technol.* 48, 6891–6898.

Jackson, S. F., Monk, S. D., and Riaz, Z. (2014). An investigation towards real time dose rate monitoring, and fuel rod detection in a First Generation Magnox Storage Pond (FGMSP). *Appl. Radiat. Isot.* 94, 254–259.

Jensen, T. E., Baxter, M., Rachlin, J. W., and Jani, V. (1982). Uptake of heavy metals by *Plectonema boryanum* (Cyanophyceae) into cellular components, especially polyphosphate bodies: An X-ray energy dispersive study. 27, 119–127.

Jespersen, A.-M., and Christoffersen, K. (1987). Measurements of chlorophyll-a from phytoplankton using ethanol as extraction solvent. *Arch. Hydrobiol.* 109, 445–454.

Jin, X., Chu, Z., Yi, W., and Hu, X. (2005). Influence of phosphorus on Microcystis growth and the changes of other environmental factors. *J. Environ. Sci.* 17, 937–941.

Kang, C. H., Choi, J. H., Noh, J. G., Kwak, D. Y., Han, S. H., and So, J. S. (2014). Microbially induced calcite precipitation-based sequestration of strontium by

Sporosarcina pasteurii WJ-2. *Appl. Biochem. Biotechnol.* 174, 2482–2491.

Keasling, J. D. (1997). Regulation of intracellular toxic metals and other cations by hydrolysis of polyphosphate. *Ann. N. Y. Acad. Sci.* 829, 242–249.

Krejci, M. R., Finney, L., Vogt, S., and Joester, D. (2011). Selective sequestration of strontium in desmid green algae by biogenic co-precipitation with barite. *ChemSusChem* 4, 470–473.

Lauchnor, E. G., Schultz, L. N., Bugni, S., Mitchell, A. C., Cunningham, A. B., and Gerlach, R. (2013). Bacterially induced calcium carbonate precipitation and strontium coprecipitation in a porous media flow system. *Environ. Sci. Technol.* 47, 1557–1564.

Li, J., Margaret Oliver, I., Cam, N., Boudier, T., Blondeau, M., Leroy, E., et al. (2016). Biomineralization patterns of intracellular carbonatogenesis in cyanobacteria: Molecular hypotheses. *Minerals* 6, 10.

López-Archilla, A. I., Moreira, D., López-García, P., and Guerrero, C. (2004). Phytoplankton diversity and cyanobacterial dominance in a hypereutrophic shallow lake with biologically produced alkaline pH. *Extremophiles* 8, 109–115.

NDA (2016). Nuclear Decommissioning Authority: Business plan 2017 to 2020. *Gov.uk*. Available at: https://www.gov.uk/government/consultations/nuclear-decommissioning-authority-business-plan-2017-to-2020 [Accessed May 4, 2018].

Pikuta, E. V., Hoover, R. B., and Tang, J. (2007). Microbial extremophiles at the limits of life. *Crit. Rev. Microbiol.* 33, 183–209.

Ravel, B., and Newville, M. (2005). *ATHENA, ARTEMIS, HEPHAESTUS*: Data analysis for X-ray absorption spectroscopy using *IFEFFIT*. *J. Synchrotron Radiat.* 12, 537–541.

Rivasseau, C., Farhi, E., Atteia, A., Couté, A., Gromova, M., de Gouvion Saint Cyr, D., et al. (2013). An extremely radioresistant green eukaryote for radionuclide bio-decontamination in the nuclear industry. *Energy Environ. Sci.* 6, 1230–1239.

Schultze-Lam, S., and Beveridge, T. J. (1994). Nucleation of celestite and strontianite on a cyanobacterial S-layer. *Appl. Environ. Microbiol.* 60, 447–453.

Sellafield (2014). Sellafield magazine. 20–29. Available at: https://www.gov.uk/government/publications/sellafield-magazine-issue-4 [Accessed May 30, 2018].

Simonoff, M., Sergeant, C., Poulain, S., and Pravikoff, M. S. (2007). Microorganisms and migration of radionuclides in environment. *Comptes Rendus Chim.* 10,

Thorpe, C. L., Lloyd, J. R., Law, G. T. W., Burke, I. T., Shaw, S., Bryan, N. D., et al. (2012a). Strontium sorption and precipitation behaviour during bioreduction in nitrate impacted sediments. *Chem. Geol.* 306–307, 114–122.

Thorpe, C. L., Morris, K., Boothman, C., and Lloyd, J. R. (2012b). Alkaline Fe(III) reduction by a novel alkali-tolerant *Serratia* sp. isolated from surface sediments

close to Sellafield nuclear facility, UK. *FEMS Microbiol. Lett.* 327, 87–92.

van Veen, H. W., Abee, T., Kortstee, G. J. J., Konings, W. N., and Zehnder, A. J. B. (1994). Translocation of metal phosphate via the phosphate inorganic transport system of *Escherichia coli*. *Biochemistry* 33, 1766–1770.

Wilson, P. D. (1996). *The nuclear fuel cycle from ore to waste*. , ed. P. D. Wilson Oxford: Oxford University Press.

Zhu, M., Yu, G., Song, G., Chang, J., Wan, C., and Li, R. (2015). Molecular specificity and detection for *Pseudanabaena* (cyanobacteria) species based on *rbcLX* sequences. *Biochem. Syst. Ecol.* 60, 110–115.

A1.6 Supplementary material

Supplementary Table 1: PHREEQC thermodynamic calculations of Sr (1 mM) saturation in BG11 medium at pH 7.2 and pH 10.

Complex	Saturation index / pH 7.2	Saturation index / pH 10.0
$Sr_5(PO_4)_3(OH)$ (s)	13.75	21.25
$Sr_5(PO_4)_3$ (s)	0.03	3.55
$MnPO_4$ (s)	3.32	0.84
Hydroxyapitite $[Ca_5(OH)(PO_4)_3]$	4.17	10.84
Chloroapitite $[Ca_5Cl(PO_4)_3]$	3.46	8.35
$Ca_3(PO4)_2$ (alfa)	-1.46	1.85
Strontianite $[SrCO_3]$	-1.06	2.42
Sphaerocobaltite $[CoCO_3]$	-2.73	0.17
Magnesite $[MgCO_3]$ (nat)	-2.00	1.47
Magnesite $[MgCO_3]$ (syn)	*2.82	0.64
Vaterite $[CaCO_3]$	-3.08	0.32
Dolomite $[CaMg(CO_3)_2]$	-4.76	2.11
$CaCO_3.H_2O$ (s)	-3.36	0.05
Calcite $[CaCO_3]$	-2.46	0.91
$CaMg_3(CO_3)_4$ (s)	-12.96	0.84
Argonite $[CaCO_3]$	-2.66	0.74

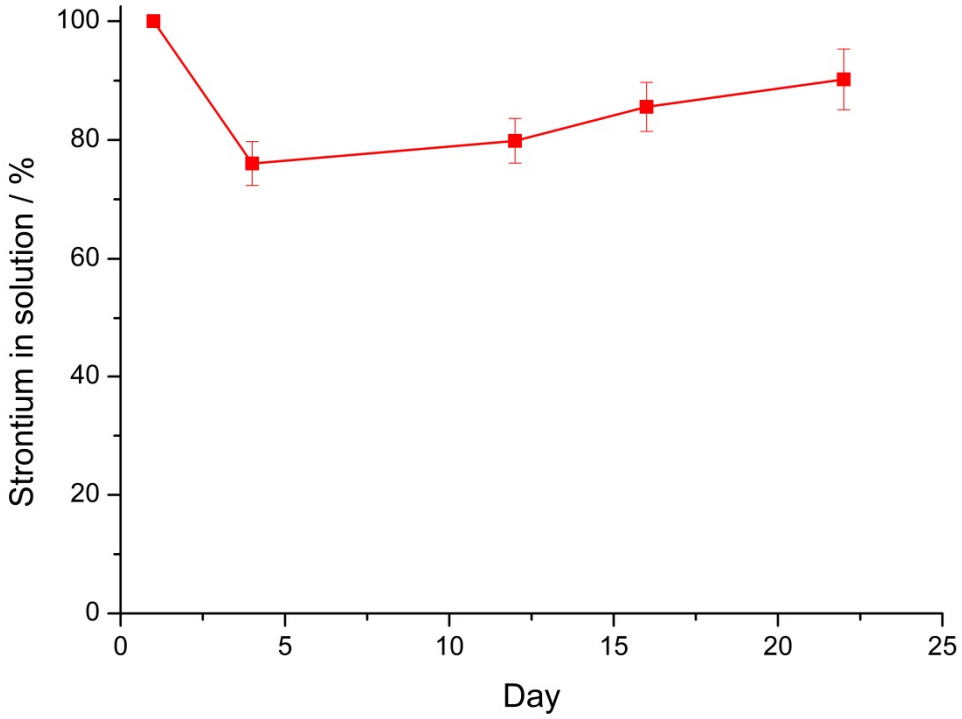

Supplementary Figure 1: Percentage of Sr in solution of sterile BG11 medium. Error bars denote standard deviation of three replicates.

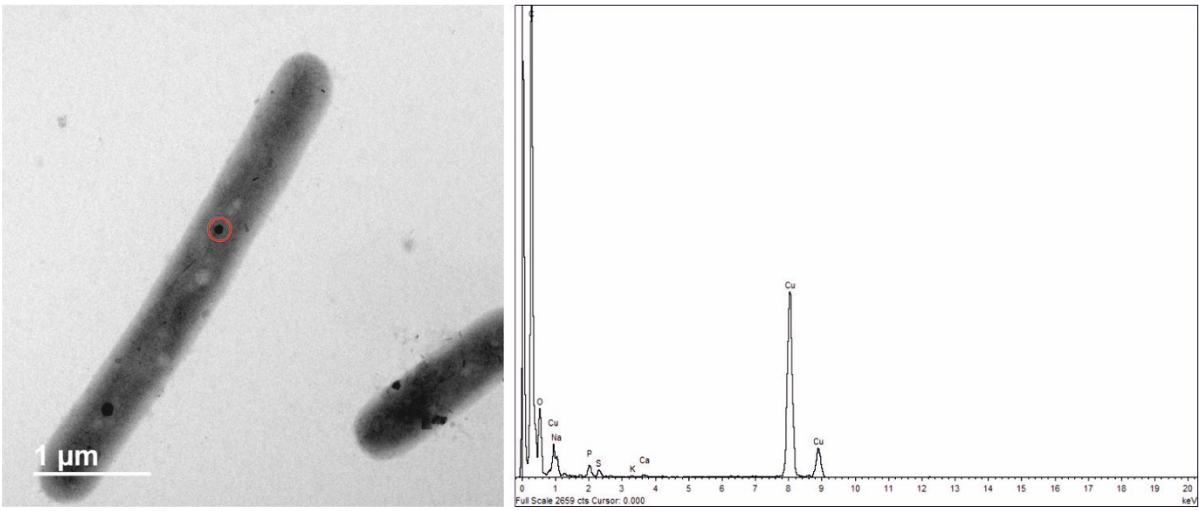

Supplementary Figure 2: TEM image and EDS data taken from a sample of *P. catenata* culture day 20, washed twice. EDS data taken from the electron dense feature of highlighted with the red circle. Peaks indicate the presence of P; the Cu peaks are due to the Cu-TEM grids.

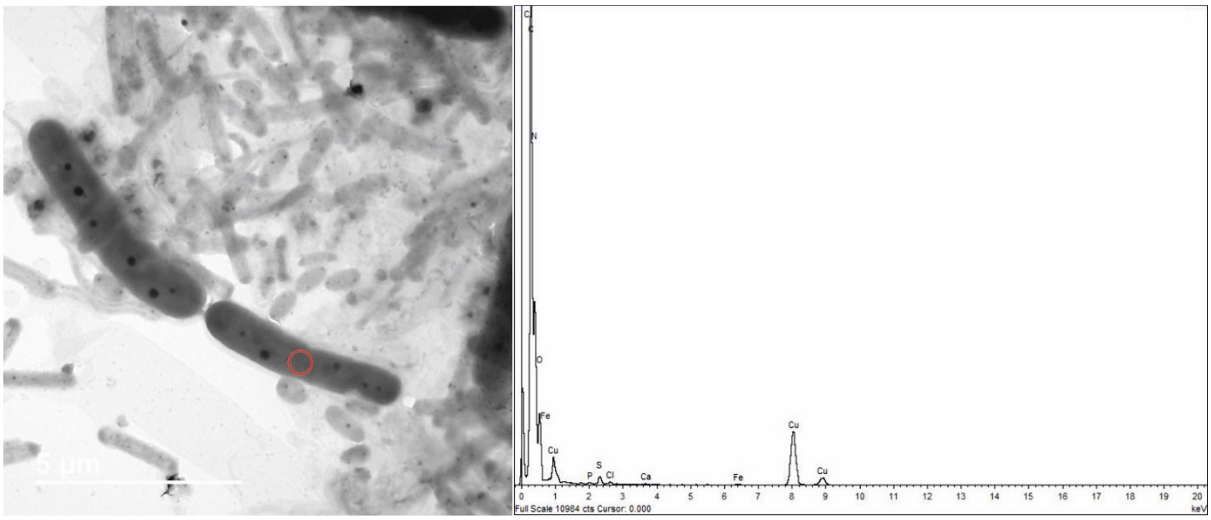

Supplementary Figure 3: TEM image and EDS data taken from a sample of *P. catenata* culture incubated with $SrCl_2$ at day 20, washed twice. EDS data collected from within the region indicated by red circle. The peaks do not show the presence of Sr associated with the cell (away from the polyphosphate features), the Cu peaks are due to the Cu-TEM grid.